Graduate School of Sciences and Technology for Innovation

Yamaguchi University

Cell Surface and Intracellular Metabolism of *Gluconobacter* spp.

（グルコノバクター属酢酸菌の細胞表層および細胞内代謝）

A DISSERTATION

Submitted by

NGUYEN MINH THUY

in Partial Fulfillment of the Requirement for the Degree of

DOCTOR OF LIFE SCIENCE

March 2021

DECLARATION

I hereby declare that the work reported in this research project report has been carried out by the undersigned. I also declare that where reference has been made to the results of other workers, appropriate acknowledgment of the source of information has been made.

March, 2021 Yamaguchi University Author

NGUYEN MINH THUY

PREFACE

Our laboratory (Applied microorganism) has been keen on acetic acid bacteria research for a long history. Based on this background, this dissertation was contributed to the understanding of acetic acid bacteria, specifically *Gluconobacter* sp.. It discusses the metabolism of intermediate oxidation products (Chapter 2 and 4) and characterization of cryptic membrane bound dehydrogenase enzyme (Chapter 3) of *Gluconobacter* sp..

The first study on characterization of 5-keto-D-fructose reductase enzyme. This enzyme is one of KFR enzyme in reducing 5-keto-D-fructose with the coenzyme NADPH to fructose and $NADP^+$ in the cytoplasm. Furthermore, the disruption of *kfr* in genome can be a promising strain for producing 5KF.

The second study was about PQQ-DH9, a cryptic membrane bound enzyme that the expression of it in the genome was under detected level. This study brings a new PQQ-DH enzyme information that seem no research has done before.

The third study focus on the three DHA kinase enymes in DHA metabolism. It clarified the function of three enzyme that involved in utilization of DHA. Moreover, the disruption of three DHA kinase enzymes can be a promising strategy for DHA producing.

This dissertation is organized in five main sections. The first section is general introduction whereby I described fundamental understanding about *Gluconobacter* sp, and expressed rationale of carrying out this research. The three following sections are corresponding with three studies respectively.

I believed this research would be interesting for all readers who are interested in bacteriology, biochemistry, genetics as well as molecular biology.

ACKNOWLEDGMENTS

This research was conducted in the Laboratory of Applied Microbiology, Biochemistry Department, Agriculture Faculty Yamaguchi University, Japan since I was a research student until nearly finishing my PhD course between October 2015 and March 2021.

First of all, I would like to express my deep gratitude to my main supervisor Prof. Dr. Toshiharu Yakushi who wholeheartedly guided, advised and inspired me throughout my Master and PhD student life. It is my honor to be his student. He is patience and kindly teaching me even I did not own any good background. Furthermore, I am sure that I could not learn many knowledge and technique regarding to biochemistry, microbiology, molecular biology as well as making a good presentation, writing a scientific paper and also many of life lessons without his supervision. After 5 and a half years being his student, I feel confident to access to wherever I will work in the future. Once again, I would like to say thank you from the bottom of my heart for all of things that you did during my student life.

I would like to express my sincere thanks to Prof. Dr. Kazunobu Matsushita who gave me a chance to apply scholarship and introduced me to my supervisor. During my study, his advanced comments greatly contributed to my research.

I am deeply indebted to Prof. Dr. Osao Adachi who carefully teaching and helping me when I had trouble in experiments. I have learned a lot of knowledge and techniques from him. Moreover, his warmly care help me overcome all difficult day of missing my home.

I am deeply grateful to Dr. Naoya Kataoka who patiently and tirelessly help me in HPLC experiments. My research never completed without his excellent HPLC analysis. During my study, his comments and advices contributed to make my research much better.

I am deeply grateful to Prof. Dr. Mamoru Yamada and Dr. Tomoyuki Kosaka for all advanced comments and helpful advices for my research.

I would like to express my sincere thanks to Dr. Minenosuke Matsutani and Nami Matsumoto who response for excellent bioinformatic analysis, support. Moreover, they are always kindly help and teach me whenever I faced with problems.

I am deeply indebted to Ms. Miyaji, Ms. Nakashima, Ms. Okamoto, Ms. Takeshita They help to prepare all of my documents not only in school but also in life. My life in Japan was smooth, wonderful and all troubles were solved thanks to their professional work.

I would like to acknowledge all Obi laboratory members (being enrolled or exchanged from 2015 to 2021), especially special thanks to Kaori Hirata, my tutor for the first time I started to do experiment in laboratory. We have a happy moment together and thank you for all things.

I am deeply thankful to the Ministry of Education, Culture, Sports, Science and Technology (Monbukagakusho) of Japan for financial support and giving me an opportunity to study and research in Yamaguchi University during my Master and PhD's life.

I am deeply indebted to Yamaguchi University to all staffs and teachers for support, dedicated teaching me. One of wonderful university that I had an opportunity to study.

I am deeply grateful to Vietnamese friends, International friends in Yamaguchi and all of my friends who always support, give advices, help me during my student life.

Save the best for the last, I would like to express the deepest gratitude to my grandmothers, parents, all of my family members who tirelessly supported me and encouraged me to overcome difficulties to obtain the highest achievements throughout my study journey.

TABLE OF CONTENTS

LIST OF ABBREVIATIONS

5KF	5-keto-D-fructose
AGE	Agarose gel electrophoresis
Ap	Ampicillin
β-ME	β-mercaptoethanol
Km	Kanamycine
BPB	Bromophenol blue
DHA	Dihydroxyacetone
FAD	flavin adenin dinucleotide
FDH	Fructose dehydrogenase
GLDH	Glycerol dehydrogenase
HPLC	high-performance liquid chromatography
RI	refraction index
PDA	photodiode array
IPTG	Isopropyl β-D-1-thiogalactopyranoside
KFR	5-keto-fructose reductase
KPB	Potassium phosphate buffer
rpm	Round per minute
SDH	shikimate dehydrogenase
NADH	Nicotinamide adenine dinucleotide
NADPH	Nicotinamide adenine dinucleotide phosphate
Ni-NTA	nickel-nitrilotriacetic
DCIP	Dichlorophenolindophenol
PMS	phenazinemethosulfate
DHAP	Dihydroxyacetone phosphate
DHAK	Dihydroxyacetone kinase
PEP	Phosphoenolpyruvate

CHAPTER ONE

General Introduction

1.1. Acetic acid bacteria

Acetic acid bacteria (AAB) play an important role in oxidative fermentation of food and beverage industries. AAB are obligate aerobes and well known to have a strong ability to oxidize ethanol, sugars, and sugar alcohols to produce the corresponding sugar acids or ketones for intermediates for industrial applications. The unique oxidative fermentation of AAB is briefly described as follows, the subtrates are oxidized by primary dehydrogenases of the respiratory chain and the oxidized products are then released to the culture medium. AAB are classified in 17 genera, of which many species have been reported in the genera *Acetobacter*, *Gluconobacter*, *Gluconacetobacter*, and *Komagataeibacter*. Other genera are *Acidomonas*, *Kozakia*, *Swaminathania*, *Saccharibacter*, *Neoasaia*, *Granulibacter*, *Tanticharoenia*, *Ameyamaea*, *Endobacter*, *Nguyeni- bacter*, *Swingsia*, *Neokomagataea* and *Gammaproteobacteria* {Matsushita et al., 1994, 2016}.

1.2. *Gluconobater* sp.

Strains of *Gluconobacter* are isolated from fruits, flowers, and other sugar-rich materials. *Gluconobacter* is a strict aerobe, Gram negative alpha-proteobacterium. It is able to oxidize various sugars and sugar alcohols incompletely to accumulate the oxidation products in the culture medium without complete oxidation to water and carbon dioxide. This unique characteristic comes from it has an incomplete citrate cycle lacking succinate dehydrogenase {Prust et al., 2005}. By this property, *Gluconobacter* catalyzes many membrane-bound, dehydrogenase-dependent oxidative fermentation reactions resulting in valuable industrial products, such as L-sorbose from D-sorbitol, dihydroxyacetone from glycerol, and 2- or 5-keto- D -gluconate from gluconate {Matsushita et al., 2003}. One of the key factors of strong ability to oxidize alcohols and sugars is primary membrane-bound dehydrogenases in the cytoplasmic membrane and other is NAD(P)H-dependent dehydrogenase in the cytosolic soluble fraction {Matsushita, 1994}. These dehydrogenases are distinguished by their cofactors: pyrroloquinoline quinone (PQQ), flavin adenine dinucleotide (FAD, and molybdopterin. Based on the genomic data, PQQ-dependent proteins (quinoproteins) can be categorized into six groups according to the compositions of their subunits and their primary sequences in acetic acid bacteria {Matsutani and Yakushi, 2018}.

1.2.1. *Gluconobacter frateurii* CHM43

Gluconobacter frateurii CHM43 was first isolated and characterized from fruit in Thailand by Moonmangmee et al. (2000) and known as a thermotolerant *Gluconobacter* strain. So that the screening method was not only growing well at 37 ºC but also oxidized D-sorbitol and D-mannitol to L-sorbose and D-fructose, and identified based on comparison with the reference strain *G.*

frateurii Mason & Claus IRO 3264^{T}. This CHM43 strain has a strong capacity for producing of L-sorbose even at high temperature {Hattori et al., 2012}. A previous research has reported that a single-nucleotide insertion in a drug transporter gene causing the metabolic flux to generate more NADPH and enhance thermotolerance {Matsumoto et al., 2018}.

Based on the genomic data {Matsutani and Yakushi, 2018}, *G. frateurii* CHM43 strain tend to possess a variety of dehydrogenases on the cytoplasmic membrane. However, a significant number of orphan quinoproteins remain uncharacterized. This strain has the membrane bound, FAD-dependent fructose dehydrogenase (FDH) while this enzyme is absent in *G. thailandicus* NBRC 3255 and *G. oxydans* 621H. The FDH is the key enzyme in oxidation of fructose to 5-keto-D-fructose {Ameyama, 1981b} {Kawai, 2013}. From these points above, I chose CHM43 strain for further research on the 5KF metabolism and characterize the orphan PQQ-dependent dehydrogenase 9 (PQQ-DH9) in CHM43 strain in chapters two and three.

1.2.2. *Gluconobacter thailandicus* NBRC 3255

Gluconobacter thailandicus strain NBRC3255 (formerly *Gluconobacter suboxydans*) was isolated from a strawberry in Japan, the draft genome sequence was reported {Matsutani et al., 2013}. This strain was reported as dihydroxyacetone (DHA) producing strain because the membrane-bound alcohol dehydrogenase is absent {Charoenyingcharoen et al., 2015; Matsushita et al., 1991}. However, the NBRC 3255 strain has ability to degrade DHA {Adachi et al., 2008}. Therefore, DHA metabolize is needed for further disruption of the genes which response in DHA consumption. Chapter four of this dissertation examined three ATP-dependent phosphorylating enzymes in DHA metabolism in *G. thailandicus* NBRC 3255.

CHAPTER TWO

5-keto-D-fructose production from mannitol and the 5-keto-D-fructose reductase of *Gluconobacter frateurii* CHM43 is a novel class in the shikimate dehydrogenase family

ABSTRACT

Gluconobacter frateurii CHM43 has mannitol dehydrogenase (quinoprotein glycerol dehydrogenase)(GLDH) and flavoprotein fructose dehydrogenase (FDH) in the membranes. In the periplasmic space, GLDH oxidize mannitol to fructose and then FDH does fructose to 5-keto-D-fructose (5KF). When the strain was cultured in mannitol, mannitol is converted to 5KF with 65 % yield. 5KF production with almost 100 % yield was realized with the resting cells.

Since NADPH-dependent 5KF reductase was found in the soluble fraction of *Gluconobacter* spp., 5KF might be transported into the cytoplasm and metabolized. Here we identified the *GLF_2050* gene as the kfr gene encoding 5KF reductase (KFR). A mutant strain devoid of the *kfr* gene showed lower KFR activity and less 5KF consumption than the wild-type strain. The crystal structure revealed that KFR is similar to NADP -dependent shikimate dehydrogenase (SDH), which catalyzes the reversible $NADP^+$-dependent oxidation of shikimate to 3-dehydroshikimate. We found that several amino acid residues in the putative substrate-binding site of KFR were different from those of SDH. Phylogenetic analyses revealed that only a subclass in the SDH family containing KFR conserved such a unique substrate-binding site. We constructed KFR derivatives with amino acid substitutions, including replacement of Asn21 in the substrate-binding site with Ser that is found in SDH. The KFR-N21S derivative showed a strong increase in the K_M value for 5KF, but a higher shikimate oxidation activity than wild-type KFR, suggesting that Asn21 is important for 5KF binding. In addition, the conserved catalytic dyad Lys72 and Asp108 were individually substituted for Asn. The K72N and D108N derivatives showed only negligible activities without a dramatic change in the K_M value for 5KF, suggesting a similar catalytic mechanism to that of SDH. Taken together, we suggest that KFR is a new member of the SDH family.

2.1. INTRODUCTION

Regarding to 5-keto-D-fructose (D-threo-2,5-hexodiulose, 5KF) production by acetic acid bacteria, the first report was done in 1961 by Terada et al. {Terada, 1961}. They identified the unknown substance from D-fructose oxidation to be 5KF. Formation and utilization of 5KF were reported with *Gluconobacter cerinus* IFO 3267 {Mowshowitz, 1974}. Thereafter, a membrane-bound D-fructose dehydrogenase (FDH, EC 1.1.99.11) catalyzing 5KF formation from fructose was purified and characterized as a flavoprotein dehydrogenase-cytochrome complex from the membrane fraction of *Gluconobacter industrius* IFO 3260 (renamed as *Gluconobacter japonicus* NBRC 3260) {Ameyama, 1981a}. Later, the genes encoding FDH of NBRC 3260 was identified as fdhSCL and its high expression strain was also constructed {Kawai, 2013}. Since the first description of 5KF production by acetic acid bacteria, many efforts have been done to create a strain for better 5KF production {Siemen, 2018}{Herweg, 2018}{Hoffman, 2020}{Battling, 2020}. 5KF has been evaluated as a natural sweetener with low calorie{Terada, 1961}{Blasi, 2020}{Wyrobnik, 2009} that can be substituted with D-glucose preventing metabolic diseases caused by high blood glucose level. Deppenmiere's group reported 5KF production from fructose with genetically modified *Gluconobacter oxydans* strains where they used plasmid-based fdh of *G. japonicus* NBRC 3260 {Siemen, 2018} or *G. japonicus* LMG 1281 {Herweg, 2018} Later, Battling et al.{Battling, 2020} reported 5KF production from fructose with a novel plasmid-free strain of *G. oxydans*. The two groups of German scientists elaborated bacterial strains for 5KF production but the principle has remained within the same scope of Terada et al. {Terada, 1961#96} who used fructose as the starting material for 5KF formation. Deppenmiere's group also reported 5KF production from sucrose, instead of fructose, with *G. oxydans* strain having chromo- some-integrated fdh of *G. japonicus* NBRC 3260 and invertase gene of *G. japonicus* LMG 1417 {Hoffman, 2020}. In this case, sucrose was efficiently converted to fructose and D-glucose, then the fructose to 5KF efficiently, but the glucose remained in the culture medium. We tried to look for alternative convenient substrates for 5KF production as well as a better 5KF producing strain among isolated wild strains. Mannitol was chosen as the most promising substrates. Mannitol is one of the best compounds to support growth of *Gluconobacter* spp. {Richhardt, 2012}, a member of acetic acid bacteria. *G. frateurii* CHM43 {Moonmangmee, 2000} oxidizes mannitol to fructose by membrane-bound, pyrroloquinoline quinone dependent glycerol dehydrogenase {Matsushita, 2003} and does fructose to 5KF further by membrane-bound, FAD-dependent fructose dehydrogenase (FDH; Fig. 2.1) {Ameyama, 1981b}{Kawai, 2013}. Such the periplasmic oxidation is a unique process in several aerobic microorganisms including acetic acid bacteria such as *Gluconobacter* spp. and produces proton motive force across the cytoplasmic membrane to contribute energy metabolism in these microorganisms

{Matsushita, 1994}. Oxidative biotransformation of mannitol to 5KF takes place in a nearly stoichiometric manner.

On the other hand, 5KF metabolism in *Gluconobacter* spp. is not fully understood. Here, we examined 5KF metabolism in *G. frateurii* CHM43, which we reasonably expect the metabolic pathway for 5KF in. The previous studies reported the function of 5KF reductase (KFR) in vitro, which catalyzes the reduction of 5KF to fructose with NADPH {Aida, 1964}{Avigad, 1966}{Ameyama, 1981b}. Occurrence of this enzyme implies a metabolic pathway for 5KF in *Gluconobacter* cell, i.e. 5KF would be incorporated into the cell via an unidentified transporter and reduced by KFR with NADPH, then produced fructose would be phosphorylated (Fig. 2.1). Fructose-6-phosphate would enter into the glycolytic pathway, i.e. pentose phosphate pathway or Entner Doudoroff pathway in *Gluconobacter* {Prust, 2005}{Richhardt, 2012}.

5KF is a unique substance produced from mannitol or fructose by *Gluconobacter* strains {Terada, 1961}. 5KF is considered as a low calories sweetener, because it cannot be metabolized in human body {Wyrobnik, 2009}. It is found in noble rot wine, a kind of white wine {Barbe, 2001}. Thus, 5KF has received attention as a promising natural but low-calories sweetener. The economic and human health values of 5KF encourage elucidating a 5KF metabolism in *Gluconobacter* sp. Here, we identified the *GLF_2050* gene of the CHM43 strain as the gene for KFR. The crystal structure of KFR was similar to that of $NADP^+$-dependent shikimate dehydrogenase (SDH), and bioinformatics studies suggested that KFR is in a sub-class in the SDH family. Amino acid replacement experiment on KFR suggested an important amino acid residue for the substrate binding in KFR.

2.2. MATERIALS AND METHODS

2.2.1. Chemicals

5KF was supplied by Kyowa-Hakko Bio (Tokyo, Japan). 5-Fluorocytosine was purchased from Fluorochem (Glossop, UK). 3-Dehydroshikimate was prepared from quinate as described previously {Adachi, 2006}. All other materials used were of analytical grade and obtained from commercial sources.

2.2.2. Bacterial strains and culture condition

Escherichia coli strains DH5α was used for plasmid construction {Hanahan, 1983}. The BL21 and BL21(DE3)/pLys strains were used for protein expression {Studier, 1986}{Studier, 1991}. The *Gluconobacter* strains and plasmids used in this study are listed in Table 2.3. *Gluconobacter frateurii* CHM43 and its derivatives were cultivated routinely at 30°C with shaking (200 rpm) in mannitol medium consisting of 50 g of D-mannitol, 3 g of yeast extract (Oriental Yeast, Tokyo, Japan) and 3 g of Hipolypepton (Nihon Pharmaceuticals, Osaka, Japan) per litre. For the strain construction, the CHM43 strain was cultivated on sorbitol medium

consisting of 50 g of D- sorbitol, 3 g of yeast extract and 3 g of Hipolypepton per litre. *Escherichia coli* strains were cultivated in Luria Bertani (LB) medium at 30°C. Ampicillin was used at final concentrations of 50 and 500 μg mL^{-1} for *E. coli* and *Gluconobacter*, respectively. Kanamycin and tetracycline were used at final concentrations of 50 μg mL^{-1} and 10 μg mL^{-1}, respectively.

2.2.3. Construction of plasmids

The genomic DNA of *Gluconobacter frateurii* CHM43 was isolated by the method of Marmur {Marmur, 1961} with some modifications {Kawai, 2013}. The *GLF_2050* gene was amplified by PCR with the Herculase II fusion DNA polymerase (Stratagene, CA, USA), the CHM43 genome DNA, and a pair of oligonucleotide: ex-GLF_2050-5-Hin(+) and ex-GLF_2050-3-Xba(-) (Table 4). The PCR product was inserted into the HindIII and XbaI site of pJY19 {Yorimitsu, 2003}, pCM62 {Marx, 2001}， and pSHO8 {Kawai, 2013}, a derivative of the broad host range vector pBBR1MCS-4 {Kovach, 1995}, to construct pNMT4, p9KX6264, and pNMT72, respectively.

To delete the *GLF_2050* gene in the CHM43 strain, the homologous arms in the 5' and 3' regions of the *GLF_2050* gene were amplified using two sets of oligonucleotides ΔGLF_2050-5-Kpn(+) and ΔGLF_2050-5-RI(-) for 5' region and ΔGLF_2050-3-RI(+) and ΔGLF_2050-3-Xba(-) for 3' region. The two PCR products was inserted into the KpnI and XbaI site of the suicide vector pKOS6b {Kostner, 2013} to construct pNMT91.

The N-terminally hexahistidine-tagged GLF_2050 was constructed by PCR with the oligonucleotide RI-His6-3C-kfr(+). The PCR product was inserted into the HindIII and XbaI site of pTTQ18 to construct pbqNK1. The amino acid replacements in the *GLF_2050* gene were constructed by PCR with the pairs of oligonucleotides listed in Table 4, followed by DpnI treatment. PCR was performed by using the chromosomal, 5'-phosphorylated and 3'-phosphorylated primers, Herculase DNA polymerase (Stratagene).

The *GOX1959* gene was amplified by PCR using the genome DNA of *Gluconobacter oxydans* ATCC621H and a pair of oligonucleotide: GOX1959-5-Eco(+) and GOX1959-3-SphBgl(-). The PCR product was inserted into NdeI and BamHI sites of pET3a (Novagen, Darmstadt, Germany) to construct pJ808. Nucleotide sequences of all DNA fragments inserted into the plasmids were confirmed by Sanger method (BigDye Terminator v3.1 Cycle Sequencing Kit, Applied Biosystems, Foster City, CA, USA).

2.2.4. Transformation of *Gluconobacter frateurii* CHM43 and the construction of gene deletion variant

The CHM43 strain was transformed with the plasmids constructed in this study via electroporation and selected on sorbitol agar medium with appropriate antibiotics as described previously {Yakushi, 2018a}. In the case of construction of gene deletion variant, the first

recombinant strain was inoculated on sorbitol agar medium containing 60 μg mL^{-1} 5-fluorocytosine to select the second recombinants as described previously {Kostner, 2013}{Yakushi, 2018b}.

2.3.5. Determination of mannitol, fructose and 5KF in the culture medium

The bacterial culture was taken and centrifuged at 10,000 × g for 5 min at 4°C to remove the cells. The supernatant was filtered with a filter with 0.4-μm-size pore (Merck Millipore, Burlington, MA, USA). The filtered supernatant was analyzed using a high-performance liquid chromatography (HPLC) system equipped with a refraction index (RI) detector and photodiode array (PDA). Mannitol was separated on a Pb^{2+}-loaded cation-exchange column (SUGAR SP0810, 8.0 mm inside diameter × 300 mm length, Shodex, Showa Denko KK, Kawasaki, Japan) at 80°C by using distilled and deionized water as a mobile phase at a flow rate of 0.5 mL min^{-1}. Fructose and 5KF were separated on an ion-exclusion column (RSpak KC-811, 8.0 mm inside diameter × 300 mm length, Shodex, Showa Denko KK, Kawasaki, Japan) at 60°C using 0.1% (w/v) phosphoric acid as a mobile phase at flow rate 0.4 mL min^{-1}. Mannitol and fructose were detected by RI, while 5KF was detected by PDA at 210 nm. The retention times on mannitol, fructose and 5KF were 35.1, 20.8, and 19.0 min, respectively. Mannitol, fructose, and 5KF were determined by the calibration curves based on the peak heights of the compounds on the chromatograms.

2.2.6. Purification of native KFR

G. frateurii CHM43 harboring pNMT72 was cultured in 500 mL mannitol medium containing 500 μg mL^{-1} ampicillin with shaking at 30°C until late exponential phase of growth. Cells were harvested by centrifugation at 10,000 × g for 10 min at 4°C, followed by washing with 10 mM K^+- phosphate (pH 6.0) containing 1 mM β-mercaptoethanol (β-ME). The cells were suspended in the same buffer and passed through French pressure cell press (1,100 kg cm^{-2}) twice. Intact cells and cell debris were removed by centrifugation at 10,000 × g for 10 min at 4°C, and the membranes were removed from the supernatant by ultracentrifugation at 100,000 × g for 1 h at 4°C. The soluble fraction was applied to a DEAE-cellulose column equilibrated with 10 mM K^+- phosphate (pH 6.0) containing 1 mM β-ME. After washing the column with the same buffer, KFR was eluted by a linear gradient system that consisted of 10 and 200 mM K^+- phosphate (pH 6.0) containing 1 mM β-ME. The collected active fractions were dialyzed to 10 mM K^+-phosphate (pH 6.0) containing 1 mM β-ME. The dialyzate was applied to a ceramic hydroxyapatite (Bio-Rad) column, which had been equilibrated with the same buffer. The enzyme was eluted with the linear gradient system consisted of 100 and 300 mM K^+- phosphate (pH 6.0) containing 1 mM β-ME. In order to concentrate protein, the collected active fractions were dialyzed and applied to a small DEAE-cellulose column and eluted by 200 mM K^+- phosphate (pH 6.0) containing 1 mM β-ME. The fraction with the highest activity was dialyzed to 10 mM K^+-phosphate (pH 6.0) containing 1 mM β-ME was used for crystallization and other enzyme characterization.

2.2.7. Gel filtration column chromatography

The purified enzyme was loaded on the Superdex 200 column that had been equilibrated with 10 mM K^+-phosphate (pH 6.0) containing 0.1 M NaCl and 1 mM β-ME. Molecular mass of KFR was determined by a calibration curve of the standard marker protein (Oriental Yeast, Tokyo, Japan), which consist of yeast glutamate dehydrogenase (290 kDa), pig heart lactate dehydrogenase (142 kDa), yeast enolase (67 kDa), yeast myokinase (32 kDa), and horse heart cytochrome *c* (12.4 kDa).

2.2.8. Purification of the KFR derivatives

The N-terminally hexahistidine-tagged KFR and its amino acid replacements were expressed in *E. coli* BL21 grown in 100 mL of LB medium containing 50 μg mL^{-1} ampicillin. The recombinant *E. coli* cells were cultivated at 30°C for 12 h, and then isopropyl β-D-thiogalactopyranoside (IPTG) was added to the final concentration of 1 mM to induce His-tagged KFR by additional cultivation at 30°C for 12 h. Cells were collected by centrifugation at 10,000 × g for 10 min at 4°C and washed twice with 20 mM Na^+-phosphate (pH 7.8) containing 500 mM NaCl. Cells were disrupted by French pressure cell press, and then the soluble fraction was obtained by ultracentrifugation as described above. The soluble fraction (1 mL) was mixed with 40 μL of nickel-nitrilotriacetic (Ni-NTA) affinity beads (Toyobo, Tokyo, Japan). The beads were washed twice with 20 mM sodium phosphate (pH 6.0) containing 500 mM NaCl and 10 mM of imidazole. The His-tagged KFR was eluted with 20 mM sodium phosphate (pH 6.0) containing 500 mM NaCl and 75 mM of imidazole.

2.2.9. Enzyme assay and kinetics

KFR activity was measured by monitoring the oxidation of 0.1 mM NADPH at 340 nm with 5 mM 5KF in 50 mM K^+-phosphate (pH 7.5) in a total reaction volume of 1 mL at 25°C. The oxidation reactions were measured by monitoring the reduction of 0.25 mM $NADP^+$ at 340 nm with 10 mM fructose or 100 mM shikimate in 50 mM Na^+-glycine buffer (pH 10) in a total reaction volume of 1 mL at 25°C. The background activity without substrate (5KF, fructose and shikimate) was monitored, which was subtracted from the activity with substrate to calculate the net activity. The V_{max} and K_M values were determined on KaleidaGraph ver. 4.5 (Synergy Software, Reading, PA, USA).

2.2.10. Sequence data retrieval and phylogenetic tree construction

The 1964 genome sequences (one genus per one genome) were downloaded from the NCBI Reference Sequence (RefSeq) FTP website at ftp.ncbi.nlm.nih.gov/genomes/refseq/. For phylogenetic analysis, we performed a BLASTP search against all protein-coding sequences from the 1964 genomes using amino acid sequences of six functionally validated protein sequences, *GLF_2050*, AroE-like protein of *Pseudomonas putida* (Pp_Ael1) {Singh, 2008}{Peek, 2011}, aminoshikimate dehydrogenase of *Pseudomonas putida* (Pp_Rifl2){Peek, 2013}, SDH of

Thermus thermophilus (Tt_AroE), SDH-like protein of *Haemophilus influenzae* (Hi_SdhL) {Singh, 2005}, SDH of *Corynebacterium glutamicum* (Cg_AroE){Kubota, 2013}, and quinate dehydrogenase of *C. glutamicum* (Cg_QDH){Höppner, 2013} as the query {Altschul, 1997}. The homologous set was selected with a BLASTP filtering expectation value (e-value) $\leq 10^{-10}$ and sequence overlap $\geq 70\%$. All homologous hits from each query were collected, and the merged unique sequence data set was used for phylogenetic tree construction. Input sequence was aligned using MUSCLE v.3.8.31 with amino acid sequence level, and used for phylogenetic construction {Edgar, 2004}. The MEGAX 10.1.8 package was used to generate the phylogenetic tree to study the phylogenetic relationships using the neighbor-joining (NJ) approach {Tamura, 2007}{Stecher, 2020}. Functionally validated protein sequences used as the query for BLASTP searches were also included in the phylogenetic analysis.

2.3.11. Visualization of consensus sequences in active sites from each phylogenetic clade

The active site sequences from each phylogenetic clade were used as input into WebLogo to assess the common consensus sequence. The sequences were illustrated by WebLogo using stacks of symbols, one stack for each position in the sequence. The size of symbols within the stack indicates the relative frequency of each base at that position {Crooks, 2004}.

2.3.12. Crystallization, data collection, and structural determination of KFR

For crystallization, a purified KFR from the recombinant *G. frateurii* CHM43 was used. Initial sparse matrix crystallization screening was performed at 295 K, by hanging-drop vapor diffusion, with 4 μL drops of enzyme against reservoir solution, using HAMPTON PEG/ION screen kit. Native (ligand-free) KFR was crystallized using 7.6 mg/mL enzyme solution and 18% (w/v) PEG3350, 0.95 M HEPES-Na, pH 8.0, 140 mM calcium acetate, 4.5% (v/v) ethylene glycol, 5% (v/v) 1,4-butanediol as the reservoir solution. For crystallization of the KFR·NADPH complex, drops were prepared by mixing 2 μL of enzyme solution (17 mg / mL) with 1 μL of 20 mM NADPH and 2 μL of reservoir and equilibrated against 100 μL of reservoir at room temperature. Crystals were obtained in 16% (w/v) PEG3350, 45 mM HEPES-Na, pH 7.5, 180 mM ammonium fluoride, 19% (v/v) MPD. The crystals under both conditions appeared after 1 week and grew to the size used for the measurement in 2 weeks. The crystal size used for the X-ray diffraction were approximately $0.13 \times 0.07 \times 0.02$ mm^3.

The X-ray diffraction data sets for the native KFR crystal and KFR·NADPH complex crystal were collected from the Synchrotron Radiation Source at the PF beam line BL1A and the PF-AR beam line NW12A (Tsukuba, Japan). Prior to measurement, the KFR crystals were dipped in a cryoprotectant with 15% glycerol and flash-cooled in a stream of cool nitrogen gas at 95~100 K. As to the KFR·NADPH complex, since the reservoir contained MPD, the crystals were used without cryoprotectant. The native KFR crystal diffracted to 1.50 Å in cell dimensions of a = 41.53, b = 63.47, c = 93.92 Å, β = 93.42 ° with the space group of $P\ 2_1$. The KFR·NADPH

complex crystal diffracted to 1.95 Å in cell dimensions of a = 40.50, b = 61.53, c = 96.86 Å, β = 96.82 ° with the space group of $P\ 2_1$. Processing and scaling were performed with the program XDS {Kabsch, 2010} scaling with POINTLESS {Evans, 2006}{Evans, 2011} and SCALA {Evans, 2006} of CCP4 {Winn, 2011}. The parameters of data collection and processing are summarized in Table 5. The structure was solved by molecular replacement using MOLREP {Vagin, 1997} with an initial model of Shikimate Dehydrogenase from Methanocaldococcus jannaschii (PDB entry 1NVT, {Padyana, 2003}). The structure was manually built in COOT {Emsley, 2010} and refined with REFMAC5 {Murshudov, 2011} with subsequent rounds of model building, refinement, and structural analysis until R_{work} and R_{free} of native KFR stabilized to 0.23 and 0.25, respectively. The structure of KFR-NADPH complex was refinement until R_{work} and R_{free} stabilized to 0.21 and 0.26, respectively (Table 2.7). Electron density for NADPH could be clearly seen in the NADPH-binding pocket. The final structural coordinates and electron density maps were deposited with the Protein Data Bank (PDB codes: 7COK and 7COL for the ligand-free and NADPH-complex forms, respectively. Structural visualization was performed in CCP4MG {McNicholas, 2011}.

2.2.13. 5KF production from resting cell

2.2.13.1. Preparation of resting cell

The resting cells were prepared with the cells of *G. frateurii* CHM43 after cultivation for 36 h on mannitol medium (the composition is described in 2.2.2.). The cells were collected and washed two times with 5 mM acetate buffer, pH 5.0. The cell suspension of 240 mg wet wt./mL was used.

2.2.13.2. Determination of mannitol, fructose, 5KF in the reaction mixture

The reaction mixture (1 mL) containing 0.4 mL of cells (96 mg wet cells), 50 mg of mannitol, and 0.5 mL of 0.2 M acetate buffer, pH 5.0, was incubated. The reaction was shaken at 150 rpm at 25°C and the reaction was terminated periodically as indicated by the addition of trichloroacetic acid to 2%. After the reaction mixture was spun down by a table top centrifuge, an aliquot of the supernatant was used. Mannitol was measured by NADP-dependent mannitol dehydrogenase from *G. oxydans* NBRC 12528 {Adachi, 1999#3}. Fructose was measured by two ways {Terada,1961}: with FDH using potassium ferricyanide as electron acceptor and the membrane-bound FDH from *G. japonicus* NBRC 3260 {Ameyama, 1981}; {Terada,1961}, reduction of fructose to mannitol by reading decrease of optical density of NADPH at 340 nm with NAD-dependent mannitol dehydrogenase from *G. oxydans* NBRC 12528 {Adachi, 1999}. 5KF was measured by NADPH-dependent 5KF reductase (KFR) which can be prepared from one of the following strains: *G. japonicus* NBRC 3260, *G. frateurii* CHM43, or *G. oxydans* NBRC 3257 {Ameyama, 1981}.

2.2.13.3. Thin-layer cellulose plate of analytical

An aliquot of the culture medium was spotted on a thin-layer cellulose plate (TLC cellulose of analytical, Merck KGaA, Darmstadt, Germany) and developed with a solvent of t-butanol: formic acid: water = 4: 1: 1.5. TLC plate was sprayed by a mixture of triphenyltetrazolum chloride (TTC) and KOH. Sugar acids having intramolecular ketone are stained as a deep pink spot with TTC. F and 5KF mean the standard D-fructose and 5-keto-D-fructose, respectively.

2.3. RESULTS

2.3.1. The CHM43 strain highly produces 5KF

Crude membrane fraction of *G. frateurii* CHM43 showed a strong FDH activity (0.8–1.0 unit/mg protein) comparable to that of *G. japonicus* NBRC 3260 (0.7–1.0 unit/mg) {Ameyama, 1981}. When *G. frateurii* CHM43 was grown in mannitol medium, mannitol initially added was consumed, then fructose accumulation started within 3 days. Thereafter, 5KF accumulation came to the maximum level while fructose disappeared rapidly (Fig. 2.2.a). The pH of the culture medium gradually decreased to 4.0. The bacterial growth showed a biphasic (Fig. 2.2.a). The first phase was brought by mannitol oxidation and the second by fructose oxidation. In Fig. 2.2.b, an aliquot of the culture supernatant along the cultivation was spotted on a thin-layer cellulose plate (TLC) sheet. After it was developed and dried well, the TLC sheet was sprayed by an alkaline-triphenyl tetrazolium chloride (TTC) solution. Fructose and 5KF reacted with TTC but not mannitol. Since one ketone moiety is found in the molecule of fructose and two in 5KF, TTC reacted stronger with 5KF than fructose. When fructose formation during cultivation was assayed enzymatically, fructose accumulated as high as 82% to mannitol initially added, though fructose looked small from TLC chromatography. 5KF accumulated in the culture medium was finally measured to be 65% to the amount of mannitol initially added as shown in Fig. 2.2.a .

2.3.2. 5KF production from mannitol with almost 100 % yield by *G. frateurii* CHM43 resting cells

5KF production from mannitol was examined by resting cells of *G. frateurii* CHM 43 (Table 2.1), where 5KF was rapidly produced via fructose. No mannitol and fructose was detected by the enzymatic method described above at the end of the reaction, when the incubation was carried out in acetate buffer, pH 5.0, at 25°C for 12 h. Thus, the resting cells of *G. frateurii* CHM 43 were shown to be a potent catalyst for 5KF production from mannitol with almost 100% yield within a short period. Fructose behaved as a metabolic inter- mediate with a short lifetime.

2.3.3. Identification of *GLF_2050* as the gene for 5KF reductase

We discovered *GLF_2050* as the gene for 5KF reductase (KFR) in the course of a study on NADPH-dependent dihydroxyacetone reductase (NADPH-DHAR) of *Gluconobacter thailandicus* (formerly *Gluconobacter suboxydans*) {Adachi, 2008}. We found that NADPH-DHAR reduces 5KF at much higher rate (more than 20-times) than dihydroxyacetone. Thus, we

cloned the *GLF_2050* gene from the draft genome of *G. frateurii* CHM43 {Matsumoto, 2018}, which is a homolog of the gene encoding NADPH-DHAR of *G. thailandicus*, to construct recombinant *Escherichia coli* and *Gluconobacter* strains that overexpress *GLF_2050*. The soluble fractions of the recombinant strains showed higher KFR activity than the control strains that harbour the empty plasmid vectors (Fig. 2.S1). In addition, we constructed the derivative strain from *G. frateurii* CHM43 that lost the *GLF_2050* gene. The KFR activity in the soluble fraction of the Δ*GLF_2050* strain was lower than that of the wild-type strain; 0.36 ± 0.02 and 1.2 ± 0.08 U (mg protein)$^{-1}$ in the Δ*GLF_2050* and wild type, respectively. These results indicate that the *GLF_2050* gene is the gene for KFR, even though other gene(s) for KFR present in the CHM43 genome. Schweiger et al. reported that *Gluconobacter oxydans* strain 621H possesses two stereospecific NADPH-dependent ketone reductases, *GOX0644* (locus tag number for *G. oxydans* 621H strain and a homologous gene product was found in the CHM43 genome: *GLF_2244*) and *GOX1615* (*GLF_2040*) {Schweiger, 2010}. Chen et al. also reported that six NADPH-dependent ketone reductases including *GOX0525* (*GLF_2568*), *GOX1598* (*GLF_0138*), *GOX1462* (*GLF_2417*), and *GOX0290* (*GLF_0357*). The homologous proteins from the genes in the CHM43 genome might contribute the remaining activity in the Δ*kfr* derivative {Chen, 2014}.

2.3.4. The Δ*kfr* strain less consumes 5KF than the wild-type strain

We examined the physiological role of KFR in the mannitol metabolism of *G. frateurii* CHM43 through construction of the Δ*kfr* strain. The complemented Δ*kfr* strain was also constructed by introducing a plasmid carrying the *kfr* gene. The wild-type, Δ*kfr*, and the complementary (Δ*kfr*/kfr+) strains were cultivated on mannitol medium for 11 days to test the ability to consume 5KF. The periplasmic oxidation system oxidizes mannitol to fructose and the produced fructose to 5KF (Figs. 2.1 and 2.3). All *Gluconobacter* strains completely consumed mannitol at 2 d and produced fructose was oxidized to 5KF by 6 d. After 6 d, a difference in the amount of 5KF was observed between the Δ*kfr* and wild-type or complementary strains, although no effect on the growth was apparently observed (Fig. 2.S2). Even no fructose was left after 6 d, 5KF was slightly increased in the culture media of Δ*kfr* day by day (Fig. 2.3). We expect that this is due to the media being concentrated by evaporation during cultivation. The data for Fig. 2 were modified based on an assumption that 1.5% of water was evaporated day by day (Fig. 2.S3). If we consider the evaporation, the Δ*kfr* strain seems to maintain 5KF levels, while the wild-type and complementary strains consume 5KF (Fig. 2.S3). Thus, it is plausibly concluded that the Δ*kfr* strain less consumes 5KF than the wild-type strain. The conclusion could be supported by pH change on the culture media: when compared to wild type, decrease in the culture media of Δ*kfr* was slightly suppressed (Fig. 2.S2), suggesting low production of organic acid. Because acetic acid is the final metabolite of *G. frateurii* CHM43 like as the other *Gluconobacter* spp. {Matsumoto, 2018}, the Δ*kfr* presumably less produced acetic acid due to limited consumption

of 5KF. Taken together, we concluded that *GLF_2050* is the gene for the physiologically relevant KFR.

2.3.5. Characterization of KFR

KFR was purified from the recombinant *G. frateurii* CHM43 harbouring pNMT72 (*kfr*$^{+}$) to characterize its biochemical properties including structure (Fig. 2.S4). We attempted overexpression of KFR in *E. coli*, but the activity was much lower than that expressed in the CHM43 strain (Fig. 2.S1). Although we did not carefully characterize these issues, codon preference and protein folding in the *Gluconobacter* cell would be suitable for KFR. As summarized in Table 2.2, KFR of *G. frateurii* CHM43 showed similar characteristics to that of *Gluconobacter cerinus* NBRC3267 (formerly IFO3267) reported previously {Avigad, 1966}. The KFR activity was much higher in the reduction of 5KF with NADPH than the reverse reaction, D-fructose oxidation with $NADP^{+}$. The optimum pH and the Michaelis constant of 5KF reductase were similar to those of other *Gluconobacter* spp. in the previous reports {Ameyama, 1981}{Avigad, 1966}{Yamada, 1967}. I determined the molecular mass of KFR in solution to be 71 kDa by gel filtration column chromatography, suggesting a dimer of approx. 30-kDa protomers.

2.3.6. Structural overview of *Gluconobacter* 5KF reductase

We determined the crystal structures of the native (ligand-free) and NADPH-bound KFRs. The whole structure of native KFR and KFR·NADPH complex was modelled using CCP4 and COOT {Winn, 2011}{Emsley, 2010}. The overall structure of the KFR·NADPH complex shown in Fig. 2.4.A showed a dimer where the protomer contains cofactor-binding and substrate-binding domains (Fig. 2.4.B). Thus, it is suggested that the two active sites are involved in catalysis. Interprotomer interactions in the structure were analysed using PISA service {Krissinel, 2007} at the European Bioinformatics Institute. There are two KFR molecules in the asymmetric unit. The buried surface between molecule A and B is about 1213 $Å^2$. Analysis of protein interfaces suggests that the homodimer of molecules A and B with the free energy change of the intermolecule contact (ΔG^{int}) value of -15.7 kcal/mol is stable in solution. The substrate-binding domains of the two protomers were shown to face to each other in the dimer. Also, one molecule of NADPH binds to the cofactor-binding domain of each subunit. In the KFR·NADPH complex the residues interacting with NADPH through the hydrogen bond or salt bridge were Ala132, Gly134, Ala135, Asn155, Arg156, and Asp157 (Fig. 2.S5). Other residues were close proximity to the cofactor including Gly133, Lys160, Ser199, Val255, Gly248, and Leu252, which are shown to be important for cofactor recognition.

The difference in the distance between the Cα carbons of the main chains of the superposed amino acid residues the protomer of the native KFR onto the KFR·NADPH complex was calculated using SUPERPOSE {Krissinel, 2004} of CCP4i. The average distance between

Cα carbons was 0.42 Å and its r.m.s.d. was 0.46 Å, which shows that the two conformations are very similar (data not shown). Therefore, it was revealed that 5KFR had little conformational change associated with NADPH binding. In addition, the largest distance of 1.68 Å was found between the Cα carbons of the Ser182 residue, considered that this is caused by the movement of the side chain of the Arg156 residue associated with the binding of the adenine ring of NADPH.

2.3.7. Prediction of substrate-binding site in 5KF reductase

We attempted to understand the substrate binding in KFR by comparison of the structure of apo-form KFR with that of substrate-bound form of homologous protein. To identify the closest structural relatives to KFR, the PDBefold was used, and the top hit was for *Escherichia coli* SDH, with a Z-score of 17.4 based on 264 aligned C-alpha atoms with an r.m.s.d of 1.5 Å (PDB entry 1VI2). The top ten were SDHs from various species, followed by quinate dehydrogenase. Because of the highest homology in the SDH-shikimate complex, we referred to the structure of the ternary complex of SDH with both shikimate and NADPH from *Thermus thermophillus* to examine the substrate binding in KFR. The substrate-binding site in *Thermus* SDH is composed of 9 amino acid residues: Ser14, Ser16, Asn58, Thr60, Lys64, Asn85, Asp100, Tyr207, and Gln235 (Fig. 2.5). According to the comparison between two enzymes, a putative substrate-binding site in KFR was predicted, where the Ser14, Ser16, Thr60, and Tyr207 residues were replaced to Asn, Thr, Ser, and Pro, respectively. Since Ser14, Ser16, and Tyr207 of *Thermus* SDH interact with the carboxyl group of shikimate, these differences in amino acid residues may account for substrate specificity of KFR, i.e. reducing the accessibility of shikimate to the enzyme. Particularly, Asn21 appears to sterically hinder the binding to the carboxyl group of shikimate. In order to examine this hypothesis, we constructed the KFR derivatives having single amino acid replacement and the double replacements. Furthermore, we found that Lys72 and Asp108 in the substrate-binding site are conserved as the catalytic dyad in the SDH family {Lindner, 2005}{Peek, 2011}, which mediates a hydride ion transfer from the substrate to $NAD(P)^+$, producing protonated ε-amino group in the Lys residue. We examined the effect of the amino acid replacements in the catalytic dyad to evaluate the mechanism under the KFR catalysis.

2.3.8. KFR belongs to a small subgroup in the shikimate dehydrogenase family

We examined phylogenetic analysis for KFR. According to the results mentioned above, the structure of KFR is very similar to that of shikimate dehydrogenase (SDH). We retrieved homologous proteins similar to KFR, AroE-like protein of *Pseudomonas putida* (Pp_Ael1) {Singh, 2008}{Peek, 2011}, aminoshikimate dehydrogenase of *P. putida* (Pp_RifI2){Peek, 2013}, SDH of *Thermus thermophilus* (Tt_AroE), SDH-like protein of *Haemophilus influenzae* (Hi_SdhL) {Singh, 2005}, SDH of *Corynebacterium glutamicum* (Cg_AroE){Kubota, 2013}, and quinate dehydrogenase of *C. glutamicum* (Cg_QDH){Höppner, 2013} by BLASTP on our RefSeq dataset independently. All of 1,930 hit proteins were used for the phylogenetic analysis

(Fig. 2.6). We tentatively classified the phylogenetic tree into the twelve clades, where functionally validated proteins belong to the nine clades, while three clades do not have any characterized proteins (Fig. 2.6 and Table 2.S1). The clades 1, 2, 7, 8, 10, and 12 contain the members of SDH family with considerable shikimate oxidation rates {Michel, 2003}{Adachi, 2006 }{Liu, 2014}{Bagautdinov, 2007}{Kubota, 2013} {Schoepe, 2008}, whereas the clades 4 and 9 contain YdiB of *E. coli* and SdhL of *H. influenzae* with the low k_{cat} values for shikimate oxidation of 0.1 and 0.2 s^{-1}, respectively {Michel, 2003}{Singh, 2005}. The clade 11 contains the member with moderate activity {Peek, 2013}. KFR belongs to the clade 4, which is reasonable since it oxidized shikimate slowly with the k_{cat} value of 0.028 s^{-1}. However, no quinate oxidation at a rate lower than 0.01 s^{-1} was observed with KFR in the similar conditions to the shikimate oxidation, although YdiB of *E. coli* the representative of the clade 4 oxidizes quinate at a rate of 0.05 s^{-1} {Michel, 2003}.

We examined conservation of the nine amino acid residues on the putative substrate-binding site in the homologous proteins retrieved, i.e. Asn21, Thr23, Asn66, Ser68, Lys72, Asn93, Asp108, Pro227, and Gln255 in KFR. Even though Asn21, Thr23, Ser68, and Pro227 were different from the corresponding amino acid residues in other shikimate dehydrogenase family, the position of four amino acids, Lys72, Asn93, Asp108, and Gln255, were aligned with the conserved residues in the amino acid sequence alignment (Fig. 2.S6), allowing us to speculate the nine amino acid residues consist of the substrate-binding site in the retrieved 1,930 homologous proteins. Clade-level analyses on the conservation revealed that different amino acid conservation patterns were found in the several clades including clades 4, 9, 10, 11, and 12 (Fig. 2.S7). Since the conservation pattern of the clade 4 were different from those of all retrieved proteins and also from the pattern of KFR (data not shown), we retrieved the proteins having the similar amino acid pattern to that of KFR from the original 1,930 homologous proteins, which contains only one amino acid difference in the nine amino acid residues in the substrate-binding site. We found the 30 homologous proteins that shows similar conservation pattern in the substrate-binding site (Table 2.S1). When these 30 proteins are shown in red in the phylogenetic tree in Fig. 2.6.A, they clustered in a small sub-clade named as 4a. Conservation of the amino acid residues in the substrate-binding site of the clade 4a was high but the amino acid residues, Asn21, Thr23, and Pro227, were different from that of the other clade 4 members, i.e. the clade 4b (Fig. 2.6.B). Of these, the amino acid residues corresponding to Thr23 is Ser in SDH, but such the difference is also found in the other members of SDH family, such as Cgl0424 quinate dehydrogenase of *Corynebacterium glutamicum* in the clade 12, which oxidize shikimate with the k_{cat} value of 85.2 s^{-1} {Schoepe, 2008}. Therefore, we focused on the two positions, Asn21 and Pro227 to evaluate the impact of the amino acid substitutions on the substrate binding and the kinetic properties of KFR.

2.3.9. Properties of the KFR derivatives

I constructed an expression system for hexahistidine-tagged KFR in *Escherichia coli* for biochemical characterization of the KFR derivatives containing either single amino acid replacements of Asn21 to Ser (referred to as N21S) or Pro227 to Tyr (P227Y) and the double replacement with N21S and P227Y (SY). To evaluate the impact of the mutations on substrate binding, the kinetic properties of the KFR derivatives were determined by using 5KF as the substrate and NADPH as the cofactor. All of the KFR derivatives including wild type showed similar elution profiles in Ni^{2+}-chelated column chromatography (Fig. 2.S8), suggesting that the KFR derivatives were stably expressed in *E. coli* as the wild-type KFR.

The N21S derivative showed a 300-fold decrease in the specific 5KF reductase activity compared to the wild-type enzyme. It also exhibited a significant change in the K_M value for 5KF of 300-fold increase (Table 2.3). Similarly, the P227Y derivative showed a fivefold decrease in the specific 5KF reductase activity. The K_M value of P227Y for 5KF was increased eightfold. The SY derivative showed much lower activity, so that it was difficult to determine the kinetic parameters. As for oxidation direction, fructose dehydrogenase activities of the KFR derivatives were determined (Fig. 2.7). KFR catalyzes the reaction predominantly in the reduction direction using NADPH but affinities to the substrates are similar to each other (Table 2.2; {Avigad, 1966}). The rates of fructose oxidation in the KFR derivatives were different; P227Y showed relatively high activity but N21S showed much lower activity, and no activity was detected in SY. These amino acid replacements presumably resulted in loss of affinity to fructose as well as loss of affinity to 5KF.

Although we attempted to detect 3-dehydroshikimate reductase activities in the KFR derivatives with a limitation of substrate concentration of 4 mM due to the scarcity of the reagent available, the activity was not observed in any KFR derivatives. Then, we examined $NADP^+$-dependent shikimate dehydrogenase activities in the KFR derivatives (Fig. 2.7). There are no apparent differences in shikimate dehydrogenase activity of the P227Y and SY derivatives compared to wild-type KFR. On the other hand, the N21S derivative showed an approx. sevenfold higher activity than wild type even fructose dehydrogenase activity was much decreased by the amino acid replacement (Fig. 2.7). We examined the affinity to shikimate in the N21S derivative, but the K_M value seemed similar to that of wild-type KFR (Fig. 2.S9). Therefore, we considered the elevated catalytic efficiency of the N21S derivative was derived from the elevated specific activity to shikimate.

In order to explore the catalytic mechanism under KFR, either the Lys72 or Asp108 residue was replaced to Asn. Replacing to Asn may minimize the changes in side chain van der Waals volumes but can eliminate their functions in general acid-base catalysis {Lindner, 2005}{Peek, 2011}. We determined the kinetic parameters for the KFR derivatives on 5KF as a

substrate with NADPH as a cofactor (Table 2.3). The K72N and D108N derivatives exhibited approx. 2,300- and 13,000-fold decreased reaction rates of the wild-type enzyme. Nonetheless both showed only minor changes in the K_M values for 5KF, which were slightly increased from that of wild-type enzyme (Table 2.3). Therefore, these results clearly indicate the role of the Lys and Asp residues in the catalytic mechanism of KFR.

2.4. DISCUSSION

SDH is one of crucial enzymes in the shikimate pathway in plants and microbes, which connects to biosynthesis of aromatic amino acids and other aromatic compounds. The SDH family is a large protein family containing at least five discrete enzymes, AroE as typical SDH, YdiB (QDH), aminoshikimate dehydrogenase RifI, SDH-like protein SdhL, and AroE-like1 Ael1 {Peek, 2015}. We examined the structure, phylogeny, and enzymatic properties of KFR in this study. Although it has unique properties in the substrate specificity, the overall structure of the molecule and the amino acids residues responsible for NADPH binding were highly conserved. We also proposed the unique but important amino acid residues for the substrate recognition. Taken together, we suggest that KFR of *Gluconobacter* sp. is a member of a subclass in the SDH family.

We revealed that the *GLF_2050* gene encodes KFR, which is responsible for most of the cellular KFR activity and physiologically relevant to 5KF metabolism in vivo. KFR would reduce 5KF to generate fructose to supply it to the pentose phosphate pathway when *G. frateurii* CHM43 grows on mannitol. KFR activity of Δ*kfr* (Δ*GLF_2050*) strain still remains approx. 29% of wild-type CHM43, suggesting the Δ*kfr* strain has at least one gene responsible for the remaining KFR activity. The complete genome of *G. oxydans* 621H exhibits to have more approximately 70 uncharacterized oxidoreductases {Prust, 2005}, and the draft genome of the CHM43 strain also has a number of uncharacterized oxidoreductases that depend on nicotinamide cofactors {Matsumoto, 2018}. As mentioned in the Results section, one or more uncharacterized oxidoreductases may involve in the remained KFR activity in the Δ*kfr* strain. Even though, the Δ*kfr* strain apparently did not consume 5KF in our cultivation experiment, while the wild-type strain gradually consumed it, when mannitol and fructose were decreased to undetectable levels. These results suggest that the *GLF_2050* gene encodes KFR relevant to the 5KF metabolism.

We attempted to propose a possible route for development of KFR in the evolution. The overall structure of KFR was similar to that of SDH (Fig. 2.4C). Although we failed to obtain structure for substrate-bound form of KFR, we suggested the nine amino acid residues for substrate binding based on the structural similarity to substrate-bound form of SDH (Fig. 2.5) {Gan, 2007}{Bagautdinov, 2007}. The nine amino acid residues on the substrate binding of SDH are different from the predicted ones of KFR, which is consistent with the different substrate specificities of the two enzymes. Therefore, we examined conservation of these amino acid

residues in the SDH family by extracting the nine amino acid residues from the SDH family proteins (Figs. 2.S6 and S7). The homologs having similar patterns in the nine amino acid residues are clustered in the clade 4a. The clade 4b, which includes *E. coli* quinate/shikimate dehydrogenase YdiB, conserved the amino acid patterns similar to SDH, even though it is systematically close to the clade 4a (Fig. 2.6). Thus, we suggest that KFR is derived from a primordial molecule for the clade 4, but developed a unique amino acid pattern on the substrate binding to accommodate 5KF.

Based on this assumption, we attempted to enhance reactivity of KFR to shikimate or dehydroshikimate by site-directed mutagenesis at the substrate-binding site. Indeed, KFR can oxidize shikimate at extremely low rate (Fig. 2.7), while partially purified SDH of *G. oxydans* (Go_AroE: GOX1959) with shikimate oxidation activity of 24 U·(mg protein)$^{-1}$ showed no 5KF reduction activity less than 0.0018 U·(mg protein)$^{-1}$. The P227Y derivative also showed importance of Pro227 for 5KF binding, even though increase in the K_M value was moderate. The N21S derivative showed the extremely increased K_M value for 5KF, but apparently less effect on that for shikimate, suggesting a crucial function of Asn21 in 5KF recognition. Because the N21S derivative also enhanced the shikimate oxidation activity sevenfold, the N21S substitution somehow enhances the catalytic efficiency of oxidizing shikimate but not the affinity. More detailed biochemical and structural analyses are needed to understand how this amino acid substitution increases the reaction rate.

To understand the catalytic mechanism of 5KF reduction, we examined catalytic efficiency of the KFR derivatives that have the amino acid replacements in the catalytic dyad Lys72 and Asp108 {Lindner, 2005}{Gan, 2007}{Peek, 2011}. Both amino acid replacements resulted in large decreases in the V_{max} value but small impacts on the K_M value to 5KF, suggesting the amino acid replacements affect the rate of catalysis but not the substrate binding. From these results, we suggest the catalytic mechanism under 5KF reduction by KFR that Lys72 is protonated by the action of Asp108 to protonate C3 carbonyl oxygen. NADPH transfers hydride ion to the protonated 5KF to yield fructose and $NADP^+$, as suggested in SDHs of *T. thermophilus* and *Aquifex aeolicus* {Bagautdinov, 2007}{Gan, 2007}.

Structure of the substrate for KFR is a subject of debate. It was reported that gem-diol hydrate is the major form of 5KF in solution, which had been isolated from *Gluconobacter* cultures {Blanchard, 1982}{Siemen, 2018}. Blanchard et al. {Blanchard, 1982} detected a chain form of 5KF in solution at 70°C, suggesting this as a minor form of 5KF. It is plausibly considered that 5-keto-D-fructopyranose is a possible intermediate in the equilibrium between the gem-diol hydrate and the chain form (Fig. 2.S10). Because dihydroxyacetone was reduced by KFR (see the Results section), the chain form is presumably the substrate for KFR. We constructed modeled structures of the substrate-bound KFR with the three possible forms of 5-keto-D-fructose, i.e. the

pyranose, chain, and gem-diol hydrate forms (Fig. 2.S11). The pyranose and chain forms of 5KF seem to be accommodated in the substrate-binding site in KFR. However, Leu252 would be close to the hydroxyl group specific in the gem-diol hydrate form within 3.0 Å, which may sterically hinder the substrate binding. Thus, the structure modeling for the substrate-bound KFR supports that the substrate for KFR is the pyranose and chain forms than the gem-diol hydrate form, even if 5KF prefers the gem-diol hydrate from in solution.

2.5. CONCLUSION

A limited species of acetic acid bacteria, such as *G. frateurii* CHM43, produce 5-ketofructose at a high yield, a low calorie sweetener. Here, we propose mannitol is one of the most promising substrates to produce 5KF via fructose. In addition, we also show NADPH-dependent 5-ketofructose reductase (KFR) is involved in 5-ketofructose degradation and characterization of this enzyme as for the structure, phylogeny, and function. The structure of KFR was similar to that of shikimate dehydrogenase, which is functionally crucial in the shikimate pathway in bacteria and plants. Phylogenetic analysis suggested that KFR is positioned in a small sub-group of shikimate dehydrogenase family. Catalytically important amino acid residues were also conserved, which were validated by construction of the KFR derivatives with the amino acid substitution. Thus, we propose KFR as a new member of shikimate dehydrogenase family.

2.6. ACKNOWLEDGEMENTS

We would like to thank Dr. Osao Adachi, Applied Microbiology laboratory, Yamaguchi university, for 5KF production from resting cell method.

We would like to thank Dr. Masaru Goto and his student Yuki Hodoya, from Department of Biomolecular laboratory, Toho university, for KFR crystal structure and computational images.

We would like to thank Dr. Minenosuke Matsutani, NODAI genome research center, Tokyo university for phylogenetic analysis for KFR.

I would like to thank Hisashi Koike, member of our laboratory, for kindly gifted shikimate dehydrogenase partially purified from his recombinant strain of his master thesis.

TABLES AND FIGURES IN CHAPTER TWO

Table 2.S1. List of shikimate dehydrogenase used in phylogenetic and conservation analysis

Access website: http://ds0n.cc.yamaguchi-u.ac.jp/~oubi/sube.html

Table 2.1. 5-keto-D-fructose production from mannitol with resting cells of *G. frateurii* CHM43

Incubation (h)	Mannitol[a] (g/L)	Fructose[a] (g/L)	5KF[a] (g/L)
0	50.0	0	0
3	27.4	38.8	11.2
6	tr.[b]	10.5	26.7
12	tr.[b]	tr.[b]	50.0

[a] Mannitol, fructose, 5KF were measured under the same methods as described in Materials and Methods section.

[b] tr., trace amount less than 0.01 mM

Table 2.2. Properties of KFRs of *Gluconobacter* spp.

	This study	{Avigad, 1966}
Optimum pH		
5KF reduction	pH 7.5	pH 7.4
D-Fructose oxidation	pH 10	n.i.[‡]
Coenzyme specificity	NADPH	NADPH
Specific activity [U·(mg protein)$^{-1}$]		
5KF reduction	440 ± 30	627
D-Fructose oxidation	1.7 ± 0.02	0.44[§]
L-Sorbose oxidation	n.d.[#]	0.31[§]
Product of 5KF reduction	D-fructose	D-fructose
Kinetic constants		
K_M for 5KF (mM)	4.2 ± 0.4	4.5
V_{max} for 5KF [U·(mg protein)$^{-1}$]	920 ± 20	n.i.
K_M for D-fructose (mM)	8.5 ± 0.6	70
V_{max} for D-fructose [U·(mg protein)$^{-1}$]	12 ± 0.2	n.i.
Molecular mass[¶]	71 kDa	n.i.

[¶] Gel filtration.

[#] n.d., not detected.

[‡] n.i., no information.

[§] Enzyme assay at pH 7.4.

Table 2.3. The kinetic parameters for His-tagged KFR and its derivatives.

	Sp. act.[a] [U·(mg protein)$^{-1}$]	V_{max} [U·(mg protein)$^{-1}$]	Turnover number (s^{-1})[c]	K_M (mM)	k_{cat}/K_M (s^{-1} mM^{-1})[d]
Wild type	340 ± 1	410 ± 6	680	2.1 ± 0.1	320
N21S	1.4 ± 0.1	140 ± 30	2.8	620 ± 160	0.58
P227Y	70 ± 5	220 ± 5	140	17 ± 1	28
SY	0.12 ± 0.01	n.t.[b]	0.25	n.t.[b]	n.t.[b]
K72N	0.18 ± 0.01	0.20 ± 0.005	0.36	3.4 ± 0.3	0.11
D108N	0.031 ± 0.004	0.071 ± 0.002	0.063	6.7 ± 0.7	0.0066

[a] Sp. act., specific activity; [b] n.t., not tested; [c] Turnover number was calculated from the specific activity by assuming that the KFR dimer possesses two catalytic sites from the crystal structure; [d] Catalytic efficiency (k_{cat}/K_M) was calculated from linear regression of the Lineweaver-Burk plot.

Table 2.4. *Gluconobacter* strains and plasmids used in this study.

Strains and plasmids	Relevant characteristics	Source or reference
Gluconobacter sp.		
ATCC621H	*Gluconobacter oxydans* wild type	ATCC
CHM43	Wild type	{Moonmangmee, 2000}
NMT912	CHM43 Δ*kfr*	This study
Plasmid		
pKOS6b	Suicide vector, *mob* codAB, Km^R	{Kostner, 2013}
pCM62	Broad-host-range vector, *mob*, Tc^R	{Marx, 2001}
pTTQ18	Expression vector, $lacI^Q$, P_{tac}, Ap^R	{Stark, 1987}
pJY19	pTTQ18, opposite orientation of multiple cloning site	{Yorimitsu, 2003}
pBBR1MCS-4	Broad-host-range vector, *mob*, Ap^R	{Kovach, 1995}
pSHO8	pBBR1MCS-4, promoter for the *adhAB* gene of *G. oxydans* ATCC621H	{Kawai, 2013}
pET3a	Expression vector, P_{T7}, Ap^R	Novagen
pNMT91	pKOS6b, Δ*kfr*	This study
pNMT72	pSHO8, *kfr* (*GLF_2050*)	This study
pNMT4	pJY19, *kfr* (*GLF_2050*)	This study
p9KX6264	pCM62, *kfr* (*GLF_2050*)	This study
pbqNK1	pTTQ18, *his-kfr*	This study
pJ808	pET3a, aroE (*GOX1959*) of *G. oxydans* ATCC621H	H. Koike thesis (2017)

aroE, the gene for shikimate dehydrogenase.

Table 2.5. Oligonucleotides used in this study.

Name	Sequence (5' → 3') [a]	Objective [b]
ex-GLF_2050-5-Hin(+)	aagcttcagagacagtctcggaataag	*kfr*$^+$
ex-GLF_2050-3-Xba(-)	tctagatggtatgaaaacccctgc	*kfr*$^+$
ΔGLF_2050-5-Kpn(+)	ggtacccattacgcgactgaag	Δ*kfr*
ΔGLF_2050-5-RI(-)	gaattccaccatcgccacggtag	Δ*kfr*
ΔGLF_2050-3-RI(+)	gaattcggaacagaaaataagtaagc	Δ*kfr*
ΔGLF_2050-3-Xba(-)	tctagaaggcagaattactttcctg	Δ*kfr*
RI-His6-3C-kfr(+)	gaattcgcatcaccatcaccatcacctggaagttctgttccaggggc ccagcggacaaggctt	N-His6
5KFR-N21S(+)	cacccccctgcgccgacTCtcctaccgtggcgatg	N21S
5KFR-N21S(-)	catcgccacggtaggaGAgtcggcgcaggggggtg	N21S
5KFR-P227Y(+)	gttgcggatgtcattTAcaacccgcctcagac	P227Y
5KFR-P227Y(-)	gtctgaggcgggttgTAaatgacatccgcaac	P227Y
5KFR-K72N(+)	ctccctgccccacaaCgtcgccgttctcgatc	K72N
5KFR-K72N(-)	gatcgagaacggcgacGttgtggggcagggag	K72N
5KFR-D108N(+)	gattggtcataacactAaTggcaagggctttc	D108N
5KFR-D108N(-)	gaaagcccttgccAtTagtgttatgaccaatc	D108N
GOX1959-5-Eco(+)	gaattccatatgattgacggtcacacgaaac	*aroE*
GOX1959-3-SphBgl(-)	agatctgcatgcggcgaccgtacttttcc	*aroE*

[a] Recognition sites for the restriction endonucleases (KpnI, EcoRI, XbaI, HindIII, NdeI, SphI, and BglII) are underlined. Uppercase letters show substituted bases.

[b] Δ*kfr*, construction of the Δ*kfr* strain; *kfr*$^+$, construction of the expression plasmid; N-His6, construction of the gene for N-terminally hexahistiidine tagged KFR.

Table 2.6. Data collection and processing

Crystal	ligand free	NADPH complex
Diffraction source	KEK, PF, BL1A	KEK, PF-AR, NW12A
Wavelength (Å)	1.1000	1.0000
Temperature (K)	100	95.0
Detector	Eiger X4M	ADSC Quantum270r
Crystal-detector distance (mm)	74.63	244.00
Rotation range per image (°)	0.5	0.5
Total rotation range (°)	240	150
Exposure time per image (s)	1.0	2.0
Space group	$P2_1$	$P2_1$
a, b, c (Å)	41.53, 63.47, 93.92	40.50, 61.53, 96.86
α, β, γ (°)	90.00, 93.42, 90.00	90.00, 96.82, 90.00
Mosaicity (°)	0.20	0.60
Resolution range (Å)	41.45 - 1.50	40.21 - 1.95
	(1.58 - 1.50)	(2.06 – 1.95)
Total No. of reflections	351914	105580
No. of unique reflections	77600	33451
Completeness (%)	99.5 (99.8)	96.7 (93.1)
R_{merge}	9.4 (51.0)	6.0 (15.1)
Redundancy	4.5 (4.7)	3.2 (3.0)
$\langle I/\sigma(I)\rangle$	9.4 (3.6)	13.1 (6.3)
$R_{r.i.m.}$	0.107 (0.577)	0.072 (0.184)
Overall B factor from Wilson plot (Å^2)	13.941	20.890

Values for the outer shell are given in parentheses.

Table 2.7. Structure solution and refinement

Crystal	ligand free	NADPH complex
Resolution range (Å)	41.453 - 1.500	40.213 - 1.950
Completeness (%)	99.367	96.440
σ cutoff	0	0
No. of reflections, working set	73708	31710
No. of reflections, test set	3862	1723
Final R_{work}	0.2319	0.2085
Final R_{free}[a]	0.2544	0.2637
No. of non-H atoms		
Protein	3992	4005
Ligand (NADPH)	-	96
Water	231	399
R.m.s. deviations		
Bonds (Å)	0.0092	0.0092
Angles (°)	1.3870	1.4284
Average B factors (Å2)		
Protein	17.66	23.40
Ligand (NADPH)	-	33.97
Water	24.45	33.31
Ramachandran plot		
Most favoured (%)	98.9	97.8
Allowed (%)	1.1	2.0

Values for the outer shell are given in parentheses.

[a] R_{free} was monitored with 5% of the reflection data excluded from the refinement.

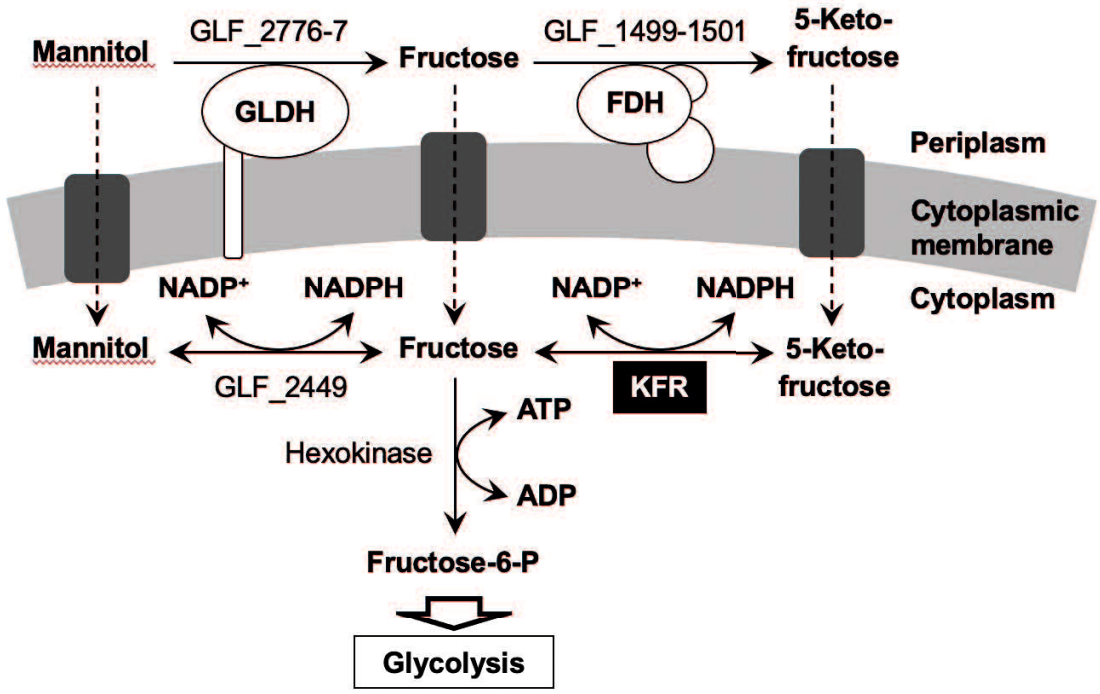

Figure 2.1. Putative metabolic pathway on mannitol in *G. frateurii* CHM43.

GLDH, pyrroloquinoline quinone-dependent glycerol dehydrogenase; FDH, fructose dehydrogenase; KFR, 5-ketofructose reductase (*GLF_2050*); *GLF_2449*, $NADP^+$-dependent mannitol dehydrogenase {Adachi, 1999}{Zahid, 2016}.

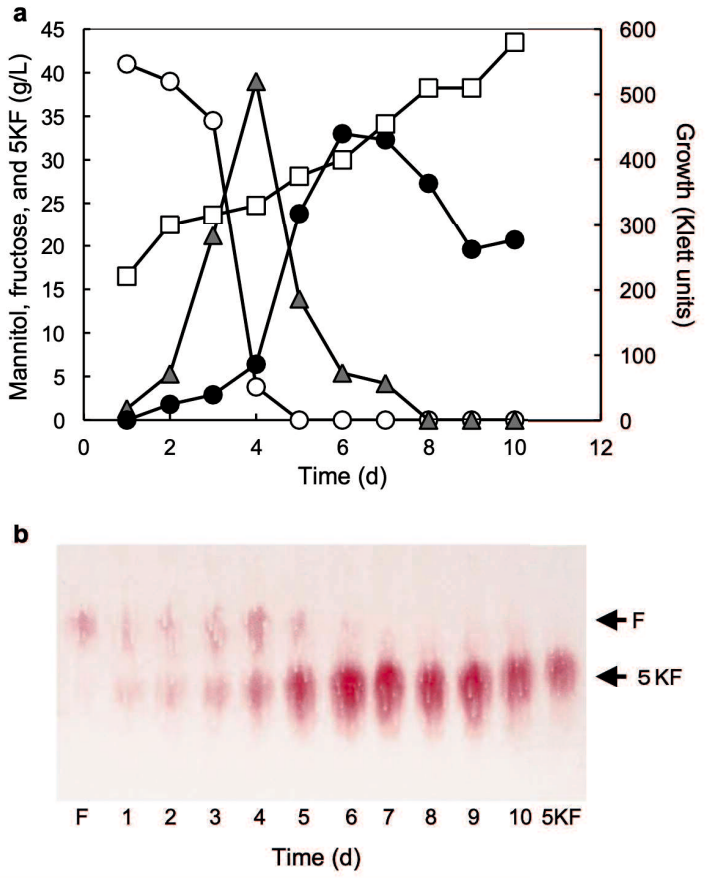

Figure 2.2. Production of 5-keto-D-fructose during cultivation of *G. frateurii* CHM43.
(a) The organism was cultured on a mannitol medium 150 mL was put in an Erlenmeyer flask of 500 mL volume with a sided arm. The cultivation was done at 30°C under shaking at 200 rpm. The bacterial growth (□) was recorded by a Klett Summerson colorimeter through the side arm without taking the cotton stopper off. Incubation was carried out for the period as indicated. The amounts of mannitol (○), fructose (▲), and 5KF (●) in the culture medium were measured as described in the text. (b) An aliquot of the culture medium was spotted on a thin-layer cellulose plate (TLC cellulose of analytical, Merck KGaA, Darmstadt, Germany) and developed with a solvent of t-butanol: formic acid: water = 4: 1: 1.5. TLC plate was sprayed by a mixture of triphenyltetrazolum chloride (TTC) and KOH. Sugar acids having intramolecular ketone are stained as a deep pink spot with TTC. F and 5KF mean the standard fructose and 5-keto-D-fructose, respectively.

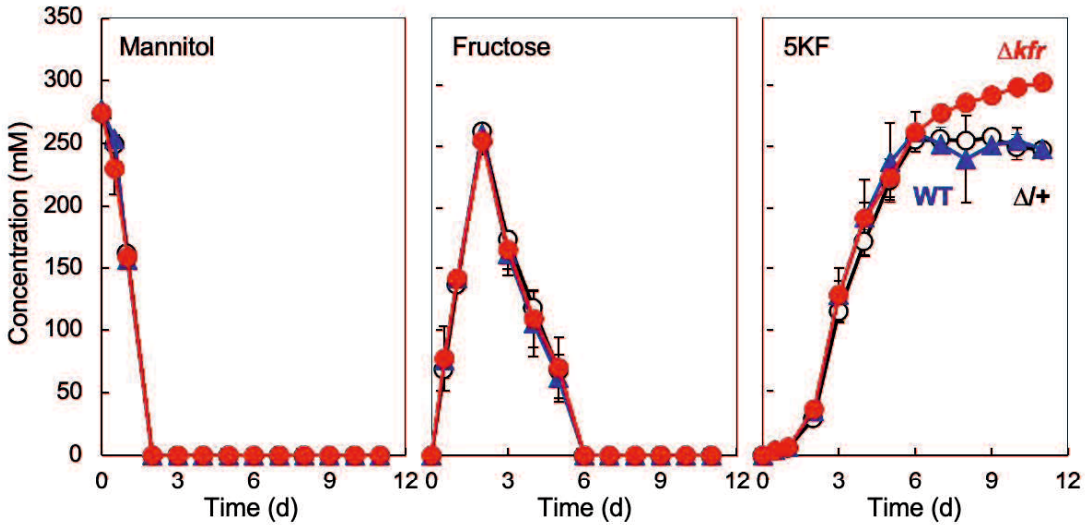

Figure 2.3. Mannitol, fructose and 5KF in the culture medium.

The wild-type (blue triangle), Δ*kfr* (red circle), and complementary strains (Δ/+; white circle) were cultivated in 100-mL mannitol medium in 500-mL Erlenmyere flask at 30°C with shaking. Samples were taken and centrifuged at 10,000 rpm at 4°C for 10 min to remove the cells. Then samples were filtered with 0.4-μm pore size filter and analyzed by HPLC to determine mannitol, fructose, and 5KF.

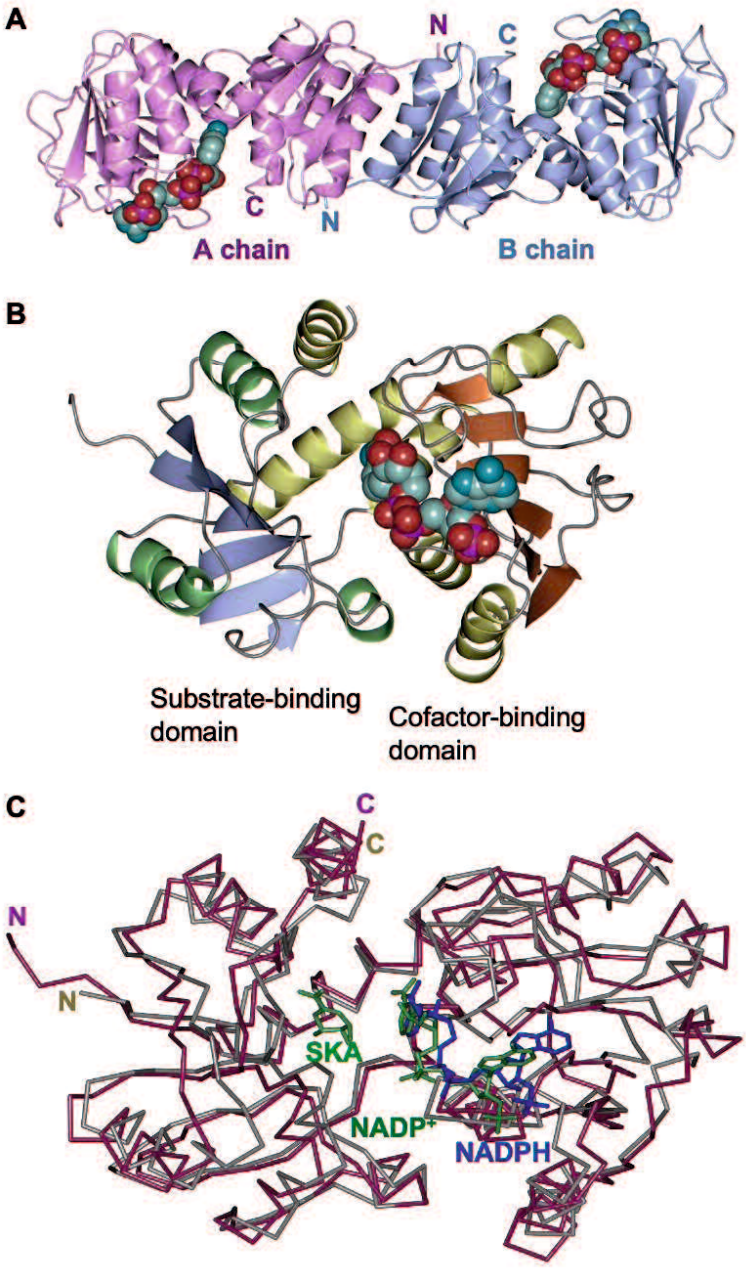

Figure 2.4. Crystal structure of KFR

A. Overall structure of NADPH-bound KFR dimer: chains A (pink color) and B (blue color) in ribbon model with NADPH in space-filling model. N: N terminus; C: C terminus. **B.** Subunit structure of KFR-NADPH complex. **C.** Superimposed image of NADPH-KFR complex of *G. frateurii* CHM43 (dark purple) and tripartite complex of shikimate, NADPH, and SDH of *Thermus thermophilus* HB8 {Bagautdinov, 2007} (grey). NADPH and shikimate are in blue and green, respectively.

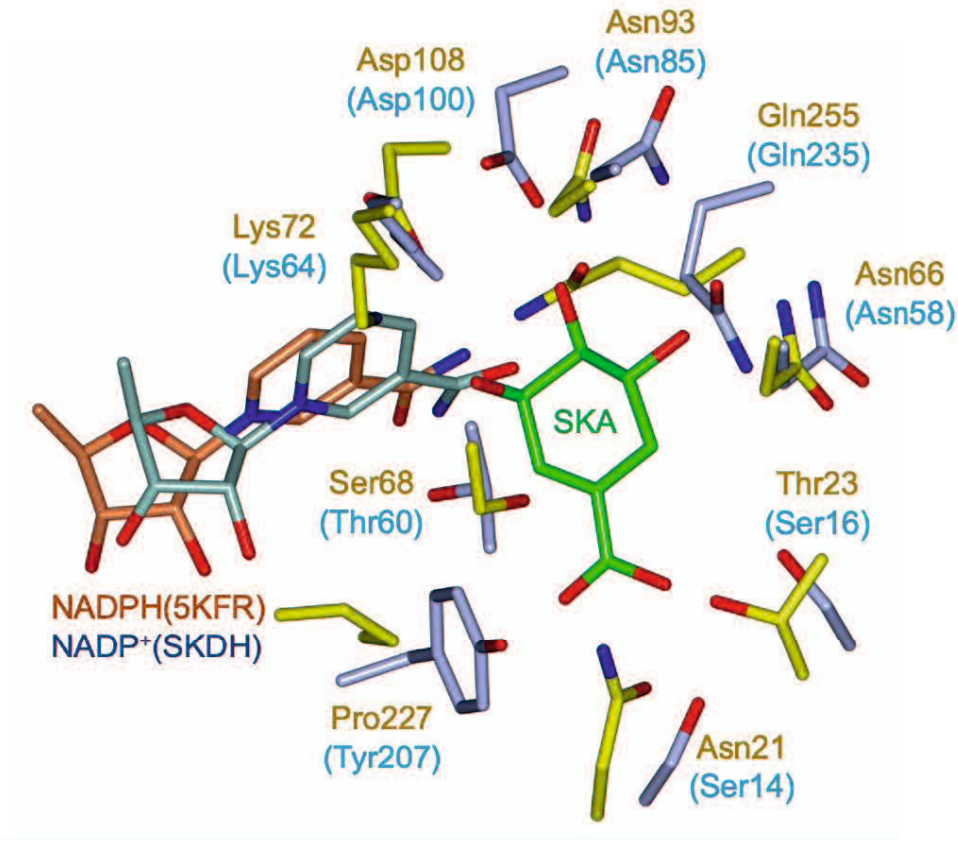

Figure 2.5. Superimposed image of the substrate binding site of tripartite NADPH-shikimate-SDH complex and the corresponding site of NADPH-KFR complex.
The substrate binding site of SDH of *T. thermophilus* HB8 {Bagautdinov, 2007} complexed with shikimate (green) and NADPH (blue) includes 9 residues showing in light blue. The corresponding site in KFR of *G. frateurii* CHM43 shown in yellow complexed with NADPH (light red) was similar to that of *T. thermophilus* SDH but included 4 different amino acid residues.

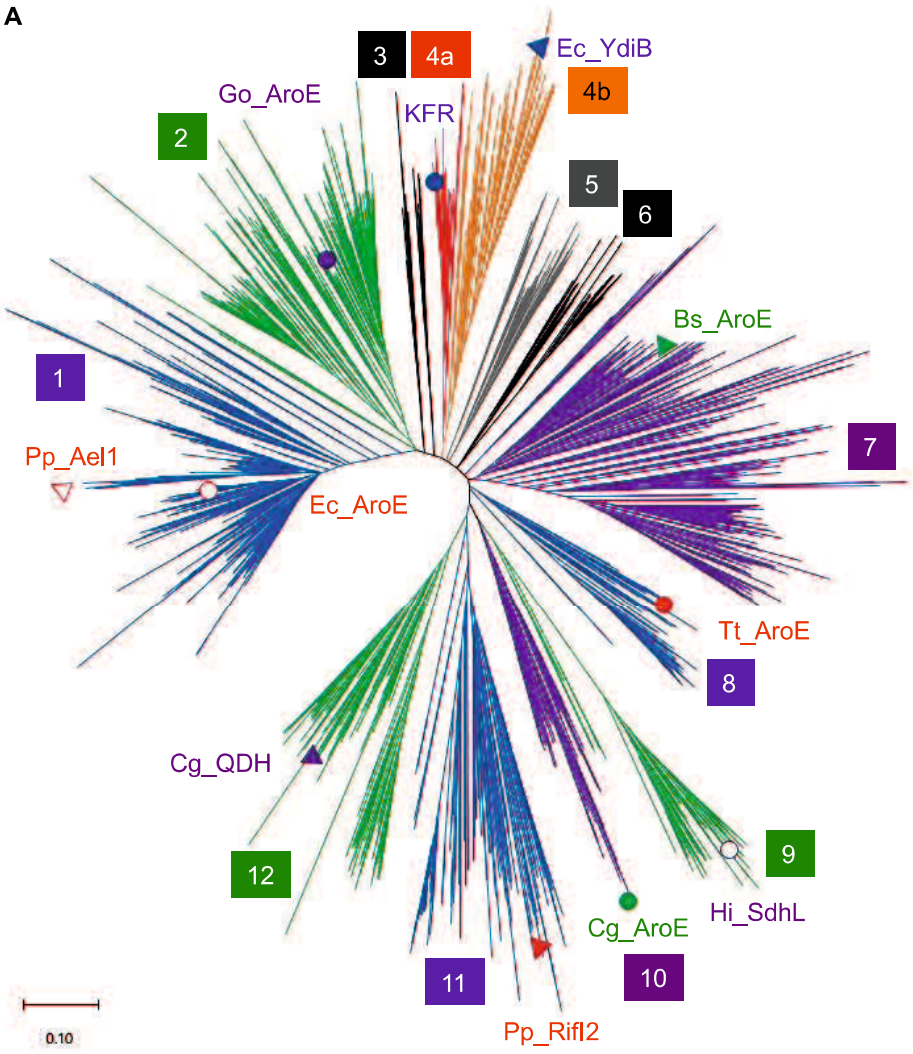
A
3
4a
Ec_YdiB
4b
Go_AroE
2
KFR
5
6
Bs_AroE
1
7
Pp_AeI1
Ec_AroE
Tt_AroE
8
Cg_QDH
9
12
Hi_SdhL
Cg_AroE
11
10
Pp_RifI2
0.10

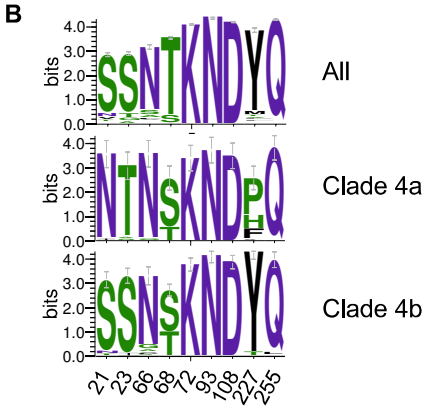
B
bits
All
Clade 4a
Clade 4b
21 23 66 68 72 93 108 227 255

Figure 2.6. Phylogenetic analysis and amino acid residues in substrate-binding site of KFR.

A. Unrooted neighbor-joining phylogenetic tree of SDH family proteins. The phylogenetic tree of 1,929 SDH homologs was constructed using the MEGAX 10.1.8 package {Tamura, 2007}{Stecher, 2020}. The scale bar represents 0.1 substitutions per site. The elven experimentally validated functional sequences are designated as follows, KFR (filled blue circle), Ec_AroE (open red circle), Ec_YdiB (filled blue triangle), Pp_Ael1 (open red triangle), Pp_RifI2 (closed red triangle), Bs_AroE (filled green triangle), Tt_AroE (closed red circle), Hi_SdhL (open purple circle), Cg_AroE (filled green circle), Cg_QDH (filled purple triangle), and Go_AroE (filled purple circle). The tree was tentatively divided into 12 clades; the clade 4 was further divided in sub-clades 4a and 4b. **B.** Conservations of amino acid residues in the substrate binding sites of 1,929 proteins and in the sub-clades 4a and 4b were illustrated by WebLogo using stacks of symbols, one stack for each position in the sequence. The size of symbols within the stack indicates the relative frequency of each base at that position {Crooks, 2004}. KFR: GLF_2050, KFR of *G. frateurii* CHM43; Ec_AroE: b3281, SDH of *E. coli* {Michel, 2003}; Ec_YdiB: b1692, quinate/shikimate dehydrogenase of *E. coli* {Michel, 2003}{Benach, 2003}; Pp_Ael1: PP3002, AroE-like protein of *Pseudomonas putida* {Singh, 2008}{Peek, 2011}; Pp_RifI2: PP_2608, aminoshikimate dehydrogenase of *Pseudomonas putida* {Peek, 2013};Bs_AroE: BSU25660, SDH of *Bacillus subtilis* {Liu, 2014}; Tt_AroE: TTHA1050, SDH of *Thermus thermophilus* ; Hi_SdhL: HI0607, SDH-like protein of *Haemophilus influenzae* {Singh, 2005}; Cg_AroE: cgR_1677, SDH of *Corynebacterium glutamicum* {Kubota, 2013}; Cg_QDH: Cgl0424, quinate dehydrogenase of *C. glutamicum* {Schoepe, 2008}; Go_AroE: GOX_1959, SDH of *Gluconobacter oxyd*ans {Adachi, 2006}.

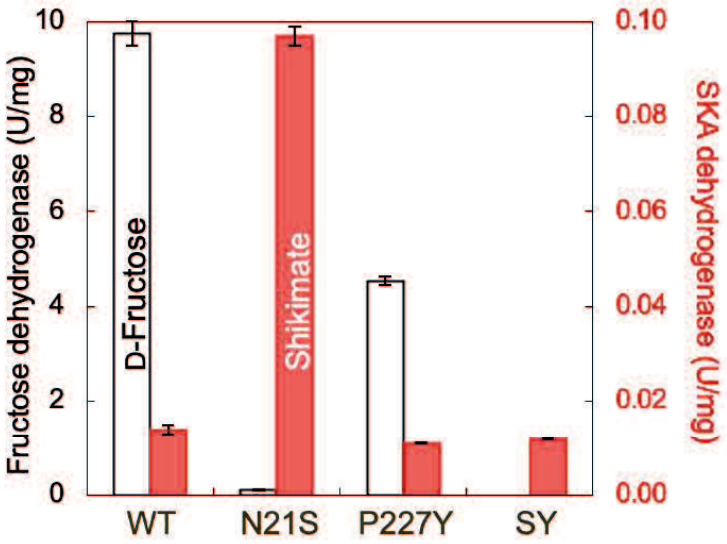

Figure 2.7. Replacement of 21st Asn to Ser in KFR improves shikimate dehydrogenase activity.

Fructose (white bar) and shikimate (red bar) dehydrogenase activities of the KFR derivatives were examined in the presence of $NADP^+$.

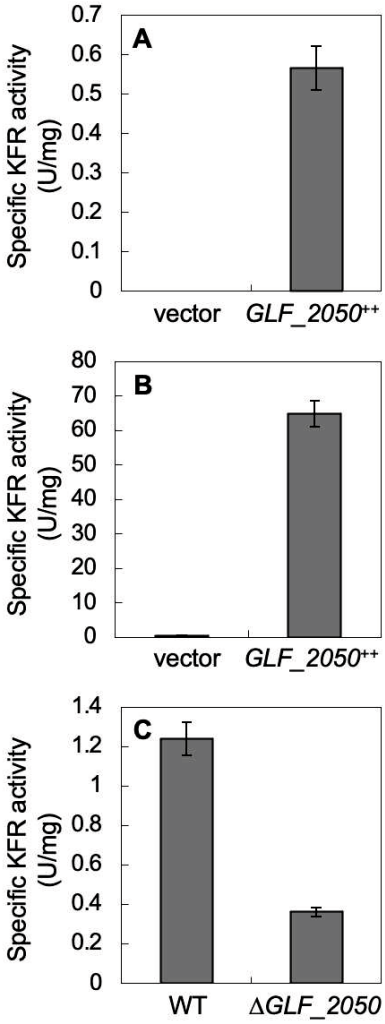

Figure 2.S1. The *GLF_2050* gene is the gene for 5-ketofructose reductase (KFR).
A. Specific KFR activity in the soluble fractions of *Escherichia coli* harboring the plasmid carrying the *GLF_2050* gene (*GLF_2050*$^{++}$) and its empty vector plasmid (vector). **B.** Specific KFR activity in the soluble fractions of *G. frateurii* CHM43 strain CHM43 harboring the plasmid carrying the *GLF_2050* gene (*GLF_2050*$^{++}$) and its empty vector plasmid (vector). **C.** Specific KFR activity in the soluble fractions of wild-type *G. frateurii* CHM43 (WT) and its derivative lost the *GLF_2050* gene (Δ*GLF_2050*). The mean value and standard deviation are shown from triplicate enzyme assay.

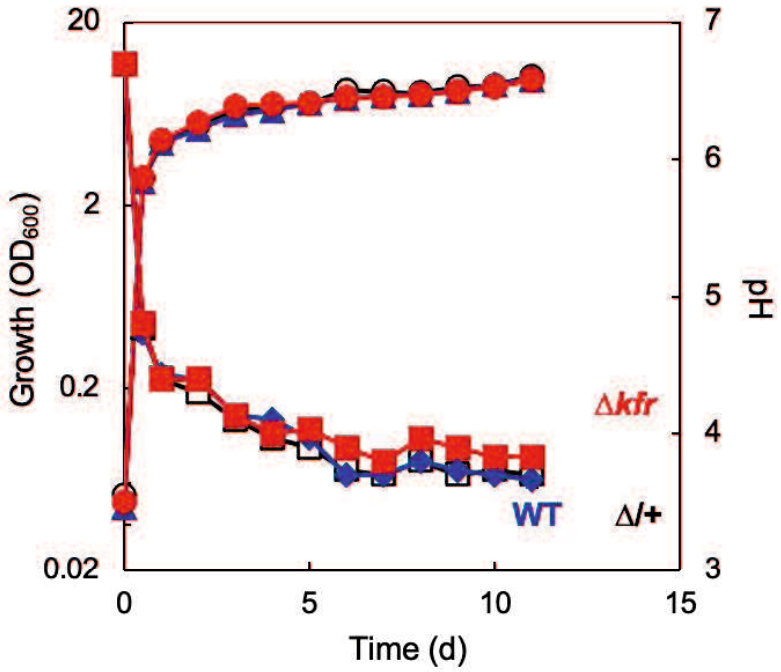

Figure 2.S2. Growth and pH change on mannitol medium.

The wild-type strain harboring pCM62 (WT, blue), the Δ*kfr* strain harboring pCM62 (Δ*kfr*, red), and the Δ*kfr* strain harboring p9KX6264 (Δ/+, white) were cultivated in 100-mL mannitol medium in 500-mL Erlenmyere flask at 30°C with shaking. The OD_{600} values for growth are shown with blue triangle (WT), red circle (Δ*kfr*), and white circle (Δ/+). The pH values are shown with blue diamond (WT), red square (Δ*kfr*), and white square (Δ/+).

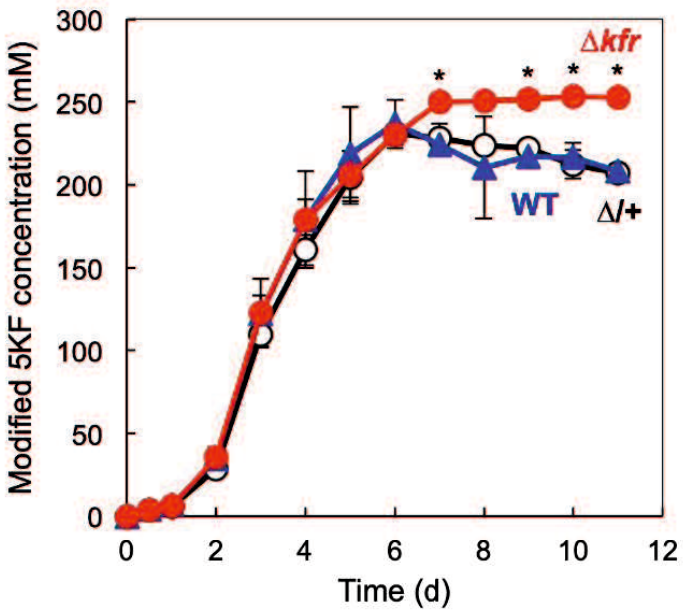

Figure 2.S3. Modified 5-keto-D-fructose levels in the growth medium

The 5KF levels in Fig. 1.3 were modified by consideration of evaporation of 1.5% water day by day. The mean values of triplicate cultivation were plotted and the error bars represent the standard deviation. The wild-type strain harboring pCM62 (WT, blue), the Δ*kfr* strain harboring pCM62 (Δ*kfr*, red), and the Δ*kfr* strain harboring p9KX6264 (Δ/+, white) were cultivated in 100 mL mannitol medium in 500- mL Erlenmeyer flasks at 30°C with shaking. The OD_{600} values for growth are shown with blue triangles (WT), red circles (Δ*kfr*), and white circles (Δ/+). *, $P < 0.05$ versus wild type (Student's *t* test).

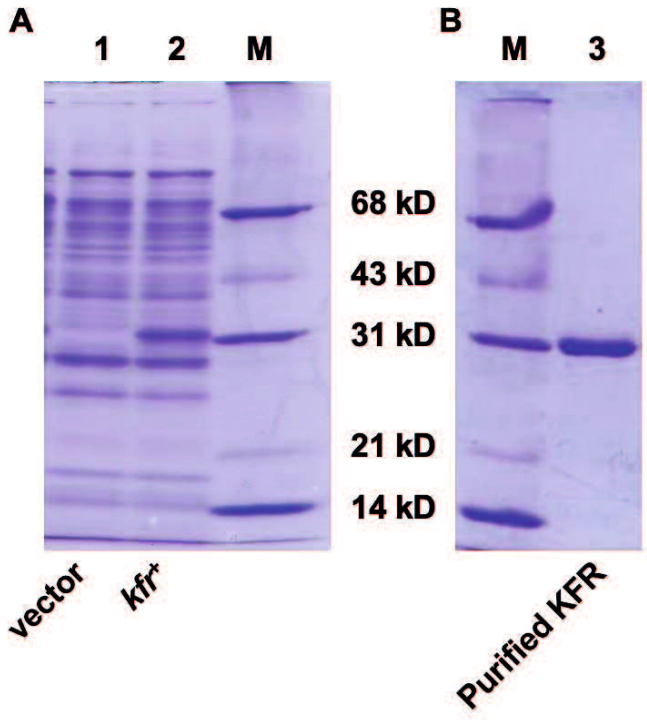

Figure 2.S4. SDS-PAGE of purified native KFR expressed in *Gluconobacter* cells.
A. The soluble fractions of *G. frateurii* CHM43 harboring the empty vector pSHO8 (lane 1) and harboring pNMT72 (*kfr*$^{+}$) (lane 2) was loaded on SDS-PAGE (10 µg protein) and stained with Coomassie Brilliant Blue R-250. **B.** Purified KFR from the recombinant *Gluconobacter* strain (6 µg protein) was loaded (lane 3). M, Molecular standards.

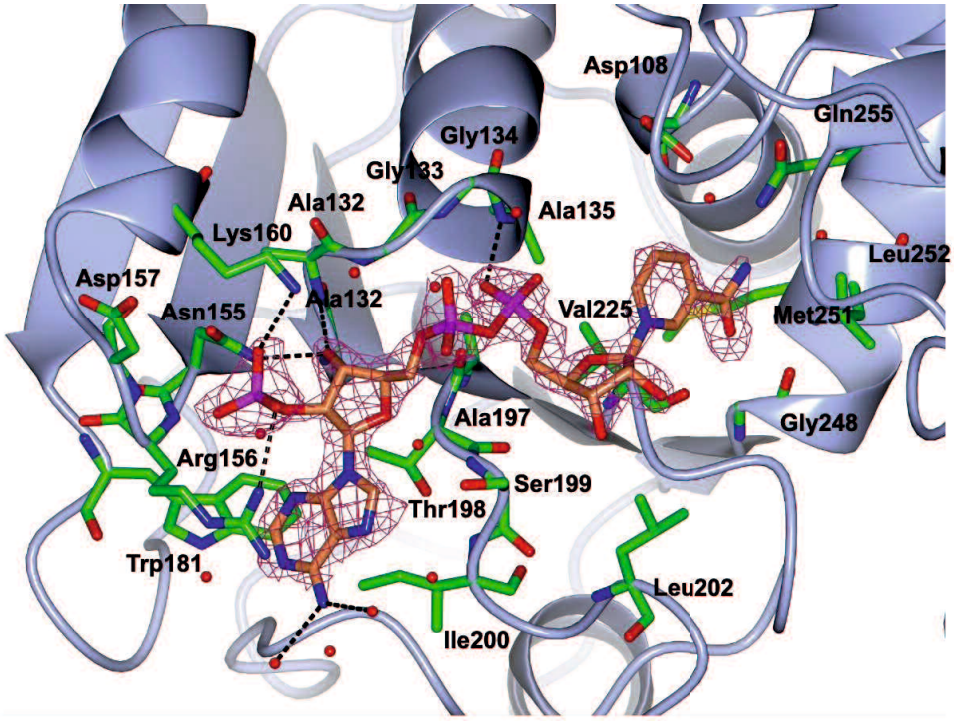

Figure 2.S5. Amino acid residues for cofactor recognition in the binary KFR-NADPH complex.

The ribbon model for the main chain of KFR is shown in pale blue. Electron density that corresponds to NADPH is shown with purple mesh. NADPH is shown in orange stick model. Amino acid residues close to NADPH are shown in green. The hydrogen bond and salt bridge are shown with dotted line.

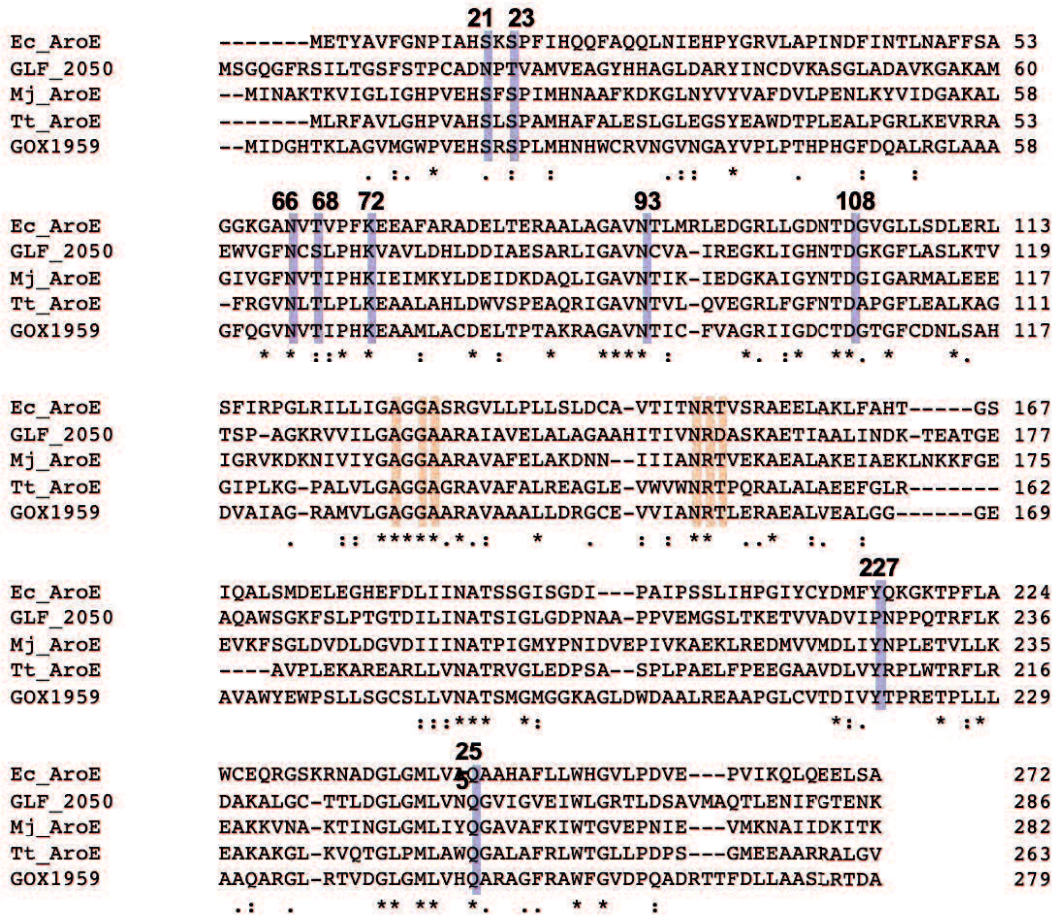

Figure 2.S6. Amino-acid sequence alignment of the KFR homologs.

The KFR (GLF_2050) and SDH proteins of *Gluconobacter oxydans* (GOX1959), *Thermus thermophilus* (Tt_AroE), *Escherichia coli* (Ec_AroE), and *Methanococcus jannaschii* (Mj_AroE) were compared on MUSCLE. Residues for the cofactor recognition identified in this study are highlighted in orange, while residues for the substrate recognition in *Thermus* SDH are highlighted in blue. The numbers in bold faces are the amino acid residues replaced in this study. *, fully conserved residue with identical amino acid; :, fully conserved residue with amino acid of "strong" similarity; ., fully conserved residue with amino acid of "weaker" similarity.

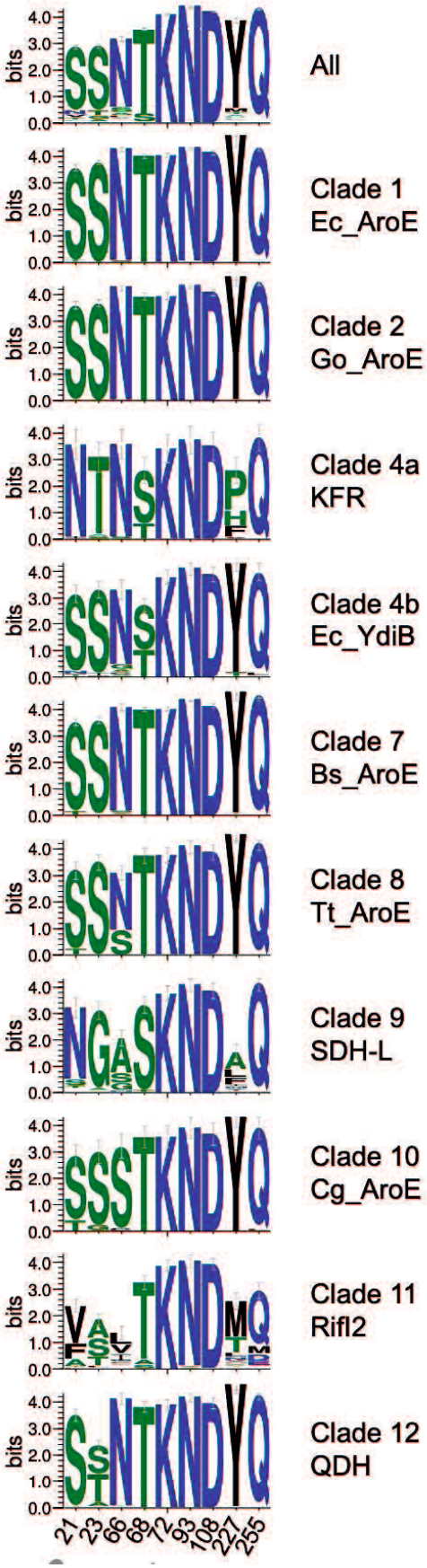

Figure 2.S7. Amino acid conservation in the substrate binging site of the SDH family.
Amino acids aligned to the those for substrate binding from each clade of phylogenetic tree were illustrated by WebLogo using stacks of symbols, one stack for each position in the sequence. The size of symbols within the stack indicates the relative frequency of each base at that position {Crooks, 2004}.

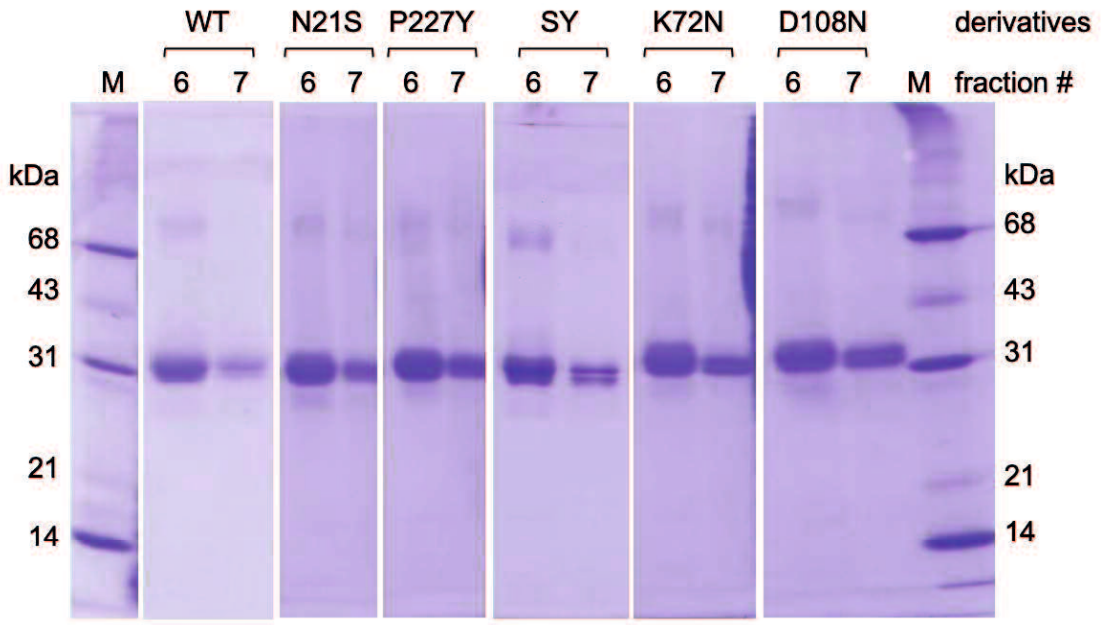

Figure 2.S8. SDS-PAGE analysis for hexahistidine-tagged wild-type KFR and its derivatives.

The N-terminally His-tagged wild-type KFR (WT) and its derivatives were expressed in *E. coli*. The proteins were bound to Ni^{2+}-loaded magnetic beads (Toyobo, Osaka, Japan) and eluted with imidazole. The eluted materials were loaded to SDS-PAGE, which showed similar elution profile. M, molecular standard composed of bovine serum albumin (68 kDa), ovalbumin (43 kDa), carbonic anhydrase (31 kDa), trypsin inhibitor (21 kDa), and lysozyme (14 kDa).

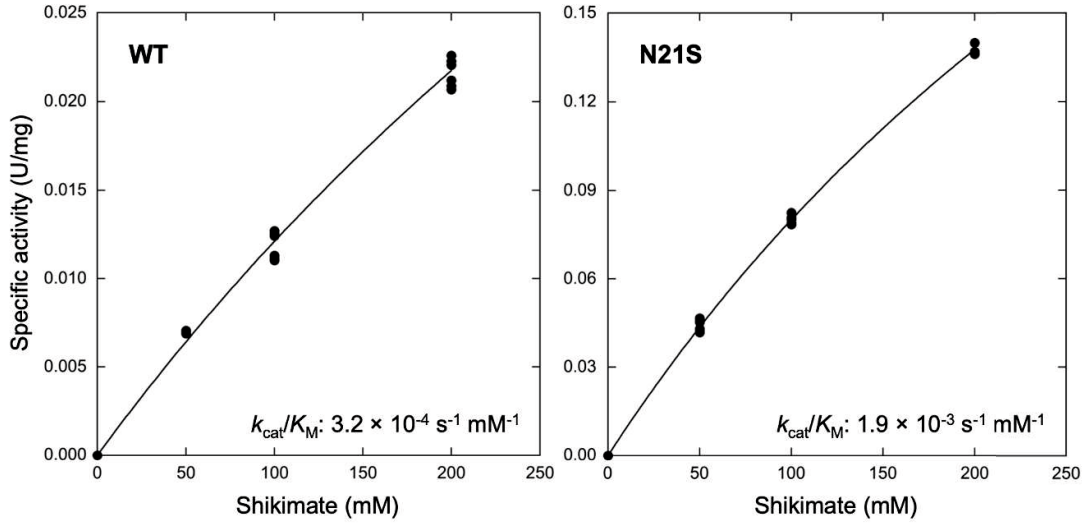

Figure 2.S9. The oxidation of shikimate by wild-type (left) and N21S (right) KFRs with $NADP^+$ were measured as a function of shikimate concentration.

The charts were produced using KaleidaGraph (ver. 4.5, Synergy Software). The catalytic efficiencies (*k*cat/*K*M) were determined from liner regression of the the Lineweaver-Burk plots.

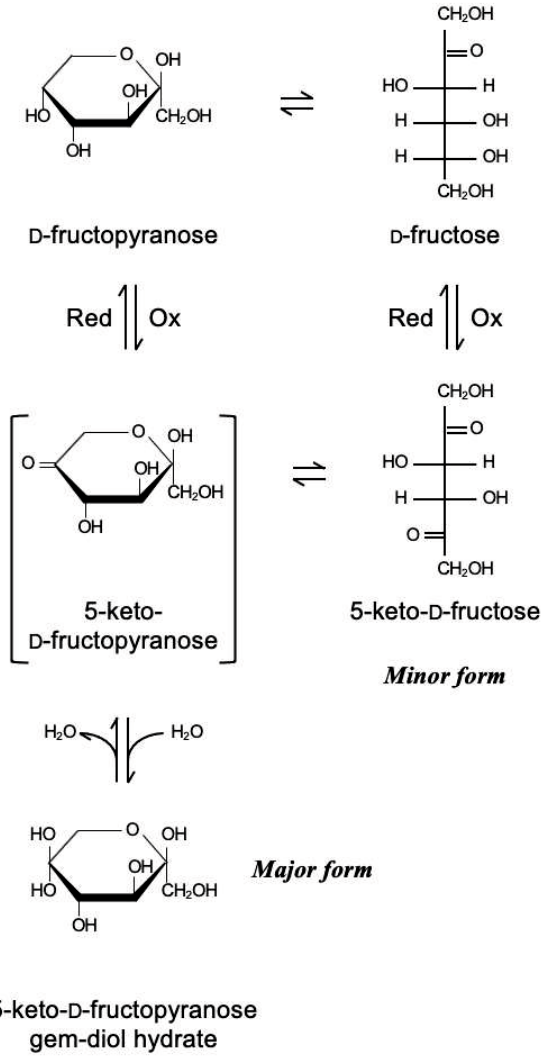

Figure 2.S10. Structure and possible equilibrium of 5-keto-D-fructose in solution.

5-Keto-D-fructopuronose gem-diol hydrate is a major form of 5-keto-D-fructose (5KF) in solution. The chain form of 5KF has been also suggested as a minor form {Blanchard, 1982}. 5-Keto-D-fructopyranose bracketed was suggested as a possible intermediate form of 5KF and the substrate for KFR.

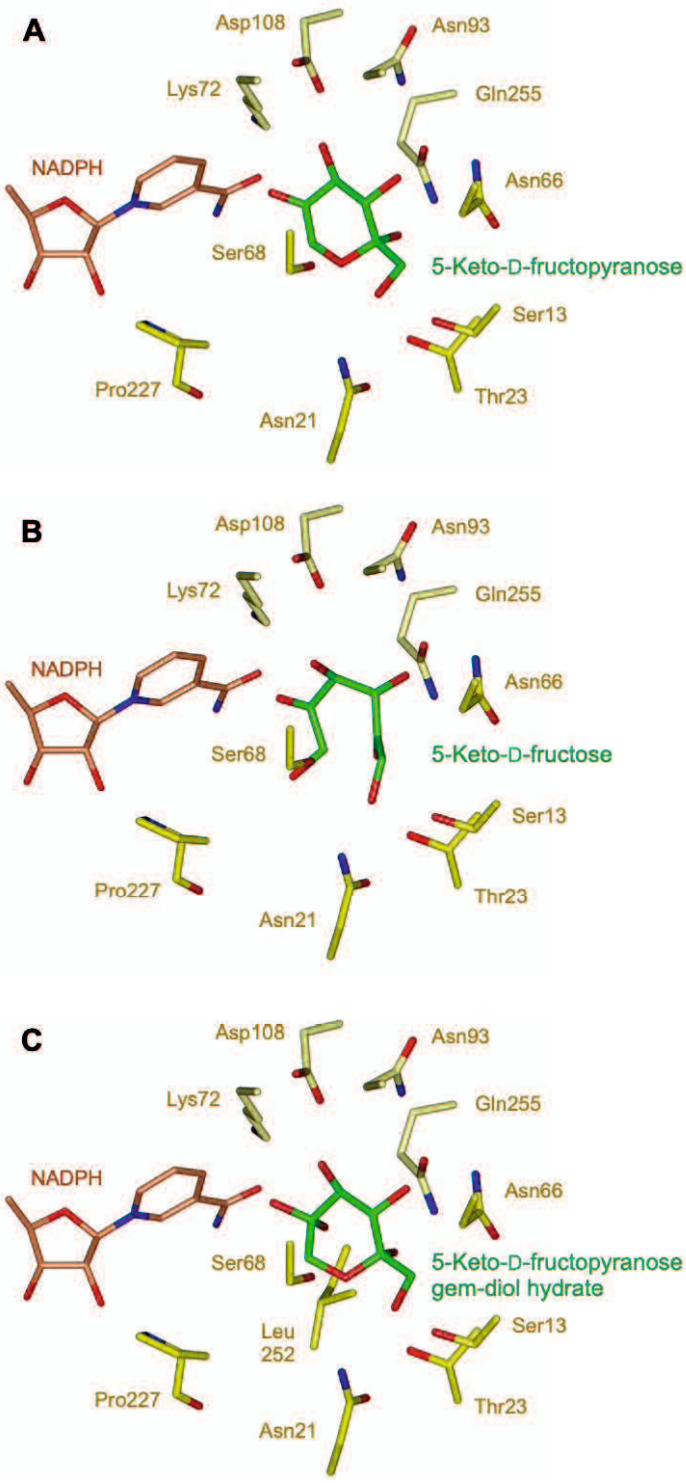

Figure 2.S11. Modeled structures of the substrate-bound KFR with the three possible forms of 5-keto-D-fructose.

The modeled structures were constructed with PRODRG {Schüttelkopf et al. 2004}. **A.** KFR·NADPH·5-keto-D-fructopyranose complex. **B.** KFR·NADPH·5-keto-D-fructose (chain form) complex. **C.** KFR·NADPH·5-keto-D-fructopyranose gem-diol hydrate complex.

Schüttelkopf AW, van Aalten DM. 2004. PRODRG: a tool for high-throughput crystallography of protein-ligand complexes. Acta Crystallogr D Biol Crystallogr 60:1355-63.

CHAPTER THREE

Characterization of a cryptic, pyrroloquinoline quinone-dependent dehydrogenase of *G. frateurii* CHM43

ABSTRACT

I characterized the pyrroloquinoline quinone (PQQ)-dependent dehydrogenase 9 (PQQ-DH9) of *Gluconobacter frateurii* CHM43, which is a homolog of PQQ-dependent glycerol dehydrogenase (GLDH). I used a plasmid construct to express PQQ-DH9. The expression host was a derivative strain of CHM43, which lacked the genes for GLDH and the membrane-bound alcohol dehydrogenase and consequently had minimal ability to oxidize primary and secondary alcohols. The membranes of the transformant exhibited considerable D-arabitol dehydrogenase activity, whereas the reference strain did not, even if it had PQQ-DH9-encoding genes in the chromosome and harbored the empty vector. This suggests that PQQ-DH9 is not expressed in the genome. The activities of the membranes containing PQQ-DH9 and GLDH suggested that similar to GLDH, PQQ-DH9 oxidized a wide variety of secondary alcohols but had higher Michaelis constants than GLDH with regard to linear substrates such as glycerol. Cyclic substrates such as *cis*-1,2-cyclohexanediol were readily oxidized by PQQ-DH9.

3.1. INTRODUCTION

Acetic acid bacteria are widely used for industrial purposes because they can oxidize sugars, alcohols, polyols, carbohydrates, and related compounds. Such oxidation reactions are incomplete processes that oxidize substrate only one or several times and are conducted by several primary dehydrogenases located on the periplasmic surface of the cytoplasmic membrane {Matsushita et al., 1994}. For instance, *Gluconobacter* spp. oxidize D-sorbitol by the membrane-bound glycerol dehydrogenase to L-sorbose, which is accumulated in the culture at the nearly stoichiometric levels and is used for the precursor of the industrial vitamin C production {Pappenberger and Hohmann, 2014}. These dehydrogenases are distinguished by their cofactors: pyrroloquinoline quinone (PQQ; pink in Fig. 3.S1), flavin adenine dinucleotide (FAD; yellow in Fig. 3.S1), and molybdopterin (green in Fig 3.S1). Based on the genomic data, PQQ-dependent proteins (quinoproteins) can be categorized into six groups according to the compositions of their subunits and their primary sequences in acetic acid bacteria {Matsutani and Yakushi, 2018}; however, a significant number of orphan quinoproteins remain uncharacterized.

According to the draft genome {Matsumoto et al., 2018}, GenBank accession no. BADZ02000001 to BADZ02000044, we previously reported that the orphan PQQ-dependent dehydrogenase 9 (PQQ-DH9) in *G. frateurii* CHM43 is a homolog of membrane-bound glycerol dehydrogenase (GLDH; also referred to as polyol dehydrogenase or sorbitol dehydrogenase) {Adachi et al., 2001; Miyazaki et al., 2002}. However, the functions of PQQ-DH9 remain unknown {Yakushi et al., 2018a}. PQQ-DH9 consists of two gene products—GLF_2583 and GLF_2584—which are similar to the transmembrane subunit SldB and the catalytic subunit SldA of GLDH, respectively. The GLF_2583 and GLF_2584 proteins have amino acid identities of 97% and 82% to their counterparts SldB (GLF_2777) and SldA (GLF_2776) of the CHM43 strain, respectively.

GLDH has wide substrate specificity; it oxidizes "secondary alcohols" in the D-erythro configuration at the penultimate carbon, according to the Bertrand–Hudson rule {Hann et al., 1938; Kulhánek, 1989; Matsushita et al., 2003}. Glycerol and D-sorbitol are oxidized by GLDH to yield dihydroxyacetone, which is used as a chemical suntanning agent, and L-sorbose, which is used as a precursor of vitamin C, respectively {Gupta et al., 2001; Pappenberger and Hohmann, 2014}. The oxidation of 1-(2-hydroxyethyl) amino-1-deoxy-D-sorbitol by GLDH produces 6-(2-hydroxyethyl) amino-6-deoxy-L-sorbose, which is a precursor of the antidiabetic drug miglitol {Yang et al., 2008}. Recently, sugars such as D-fructose and L-ribose have been added to the list of GLDH substrates {Ano et al., 2017; Yakushi et al., 2018b}. Herein, we attempted to characterize the enzymatic properties of PQQ-DH9 by comparing them to those of GLDH. We conducted a membrane-associated enzyme activity assay on a recombinant *Gluconobacter* strain created using a combination of gene deletion and plasmid-based overproduction.

3.2. MATERIALS AND METHODS

3.2.1. Chemicals

Yeast extract and Hipolypepton were obtained from Oriental Yeast (Tokyo, Japan) and Nihon Pharmaceutical (Tokyo, Japan), respectively. Restriction endonucleases were obtained from Toyobo (Osaka, Japan). 2,3-Butanediol was obtained from Wako Pure Chemical (Osaka, Japan). All other materials were of analytical grade and were purchased from commercial sources. For the enzyme assays, 2-hexanol, cyclohexanol, and 1-cyclohexylethanol were dissolved in ethanol.

3.2.2. Bacterial strains and culture condition

Gluconobacter frateurii CHM43 (NBRC101659; http://www.nite.go.jp/en/nbrc/index.html) {Moonmangmee et al., 2000}, its Δ*adhAB* derivative SEI46, and its Δ*adhAB* Δ*sldBA* derivative TORI4 were used in this study {Yakushi et al., 2018b}. All the *Gluconobacter* strains were cultivated in a sorbitol medium consisting of 50 g of D-sorbitol, 3 g of yeast extract, and 3 g of Hipolypepton per liter. For metabolite analyses, culture media were collected and centrifuged at 10,000 × *g* for 5 min at 4°C to remove the cells. The supernatants were passed through a filter with 0.4-μm pores (Merck Millipore, Burlington, MA, USA) prior to analysis by high-performance liquid chromatography (HPLC). *Escherichia coli* strain DH5α was used to construct the plasmid {Hanahan, 1983}, which was cultivated in Luria Bertani medium at 30°C. Tetracycline was used at final concentrations of 10 μg mL^{-1} for *E. coli* and *Gluconobacter*.

3.2.3. Plasmid construction

PCR analysis was performed using the following components: the genomic DNA of *G. frateurii* CHM43, which had been purified as described in the literature {Marmur, 1961}; a pair of oligonucleotides [ex-GLF_2583-Xba(+) (5′-tctagaacctcaccttctacag-3′; the *Xba*I recognition site is underlined) and ex-GLF_2584-Kpn(-) (5′-ggtacctgcccgcatcaagaaatg-3′; the *Kpn*I recognition site is underlined]; and Herculase DNA Polymerase (Stratagene). Approximately 2.7-kb PCR products were digested with *Xba*I and *Kpn*I prior to insertion into the corresponding sites of pCM62 {Marx and Lidstrom, 2001}. The resulting p62sGLDH2-11 plasmid was used to transform the TORI4 (Δ*adhAB* Δ*sldBA*) strain via electroporation, as described previously {Yakushi et al., 2018b}.

3.2.4. Membrane preparation

The TORI4 (Δ*adhAB* Δ*sldBA*) and SEI46 (Δ*adhAB*) strains harboring the pCM62 plasmid and the TORI4 strain harboring the p62SGLDH2-11 plasmid were cultivated in 100 mL of sorbitol medium containing 10 μg mL^{-1} tetracycline; the culture was shaken at 30°C until the late exponential phase of growth was reached. The cells were harvested at 4°C by centrifugation at 10,000 × *g* for 10 min, then washed twice with 10 mM MES-KOH (pH 6.0) containing 2 mM $CaCl_2$. The cell paste was resuspended in four volumes of the same buffer (4 mL per 1 g wet

weight of the cells). The cell suspensions were passed through a French pressure cell press (1,100 kg cm^{-2}) twice. After centrifugation for 10 min at 10,000 × *g* and 4°C to remove cell debris, the supernatants were centrifuged for a further 1 h at 100,000 × *g* and 4°C. The precipitates were resuspended in the same buffer and used as the membrane fraction.

3.2.5. Enzyme assays

Enzyme activity was measured spectrophotometrically at 522 nm by phenazine methosulfate (PMS) reductase activity coupled with 2,6-dichlorophenol indophenols (DCPIP) at 25°C. The reaction mixture contained the enzyme solution, 50 mM Na^+-acetate (pH 5.0), 0.2 mM PMS, 0.11 mM DCPIP, and 100 mM substrate (in the case of 2-hexanol, cyclohexanol and 1-cyclohexylethanol were used at 25 mM and were dissolved in ethanol prior to the enzyme assay). One unit of enzyme activity was defined as the amount of enzyme required to catalyze the conversion of 1 μmol of substrate per min. A millimolar extinction coefficient of 8.6 (cm^{-1} mM^{-1}) was used for DCPIP (Armstrong, 1964).

3.2.6. EDTA treatment and holoenzyme formation

The pH of EDTA stock solution was adjusted to 6.0 with NaOH. A membrane suspension comprising 10 mg protein mL^{-1} in 10 mM MES-KOH (pH 6.0) was incubated with 2, 5, 10, and 20 mM EDTA on ice overnight.

The EDTA-treated membranes were sedimented by ultracentrifugation (100,000 × *g*, 1 h, and 4°C) and resuspended in 10 mM MES-KOH (pH 6.0) containing 2 mM $CaCl_2$. This step was repeated once, and the holoenzyme was formed by incubating the resulting membrane suspension at 25°C for 30 min with 5 μM PQQ and 2 mM $CaCl_2$.

3.2.7. Biotransformation

Five milliliters of the reaction mixture consisting of 1.0 mg protein mL^{-1} of the membranes and 100 mM substrates in 50 mM Na^+-acetate (pH 5.0) was incubated in a disposable 50-mL plastic tube with an eight-hole cap (hole diameters of 2 mm), which was shaken at 150 rpm and 30°C for 24 h. An aliquot (500 μL) of the reaction mixture was taken periodically, and the membranes were removed after ultracentrifugation for 1 h at 100,000 × *g* and 4°C. Subsequently, the supernatant was passed through a filter with 0.4-μm pores.

3.2.8. Analytical procedures

The filtered samples were analyzed using a HPLC system (Shimadzu) equipped with a refractive index (RI) detector and a photodiode array (PDA). Distilled and deionized water was used as the mobile phase of a Pb^{2+}-loaded cation-exchange column (SUGAR SP0810; 8.0 mm I.D. × 300 mm L; Shodex; Showa Denko KK, Kawasaki, Japan) for chromatography at 80°C at a flow rate of 0.5 mL/min. Chromatographic peak detection and quantification was done using retention time and peak height. Protein concentrations were determined using the modified Lowry method, with bovine serum albumin as the standard (Dulley and Grieve, 1975).

3.3. RESULTS AND DISCUSSIONS

3.3.1. PQQ-DH9 complements L-sorbose production in the GLDH-deficient strain

To characterize PQQ-DH9, we attempted to express the *GLF_2583* and *GLF_2584* genes using the broad-host-range plasmid vector pCM62 in the Δ*adhAB* Δ*sldBA* derivative of CHM43, because membrane-bound alcohol dehydrogenase (ADH) and GLDH are the predominant enzymes of the primary and secondary alcohol dehydrogenases, respectively {Matsushita et al., 2003; Yakushi and Matsushita, 2010}. Therefore, we constructed a Δ*adhAB* Δ*sldBA* strain—which harboring p62sGLDH2-11, a pCM62 derivative carrying the gene for PQQ-DH9 (hereafter, referred to as the *pqq9*$^{+}$ strain)—and a strain harboring the empty vector pCM62 (hereafter, referred to as the reference strain). For comparison, we constructed a Δ*adhAB* strain harboring the control vector pCM62, which included the *sldBA* gene for GLDH (hereafter referred to as the *sldBA*$^{+}$ strain).

I examined the function of PQQ-DH9 *in vivo* by cultivating the *Gluconobacter* strains in D-sorbitol, i.e. L-sorbose production and the accompanying D-sorbitol consumption were evaluated (Fig. 3.1). Wild-type CHM43 harboring pCM62 was included for comparison. Although the growth of the GLDH-deficient strain was similar to that of the wild-type strain, L-sorbose production by the GLDH-deficient strain (Δ*sldBA* Δ*adhAB*) was abolished (Fig. 3.1 and 3.S2). The *pqq9*$^{+}$ strain produced L-sorbose at a lower rate than the wild-type. The sorbose production rates were 7.0, 6.7, 2.7, and 0.056 mM h^{-1} for the wild-type, *sldBA*$^{+}$, *pqq9*$^{+}$, and reference strains, respectively. D-Sorbitol consumption by the reference strain without L-sorbose accumulation is presumably due to assimilation of D-sorbitol {Soemphol et al., 2012}. The results indicate that PQQ-DH9 can function as a primary dehydrogenase in the sorbitol oxidation system of *Gluconobacter*.

3.3.2. Expression of PQQ-DH9

As mentioned above, the reference strain (Δ*adhAB* Δ*sldBA* harboring pCM62), which had PQQ-DH9-encoding genes, produced a marginal amount of L-sorbose. This suggested that the genes were rarely expressed in the chromosome under the cultivation conditions used in the present experiment. The membranes of the reference strain oxidized D-arabitol at a rate below the detection limit, while those of the *pqq9*$^{+}$ strain had a D-arabitol dehydrogenase activity of 0.20 U (mg of protein)$^{-1}$ (Fig. 3.2). These results suggest that PQQ-DH9 is a cryptic enzyme. It is currently under investigation what culture conditions induce the expression of PQQ-DH9, which is one of the most important issues to be answered. In contrast, the membranes of the *sldBA*$^{+}$ strain exhibited higher dehydrogenase activity (0.41 U mg of protein)$^{-1}$ owing to the presence of GLDH (Fig. 3.2). The optimum pH for PQQ-DH9 dehydrogenase activity was 5.0–6.0, i.e., similar to that for GLDH dehydrogenase activity. These results indicated that PQQ-DH9 was

functionally expressed by the constructed plasmid in the *Gluconobacter* strain and supported the suggestion mentioned above that it is expressed in small amounts by the genome.

3.3.3. Substrate specificity of PQQ-DH9

We determined the substrate specificities of the dehydrogenases in membranes at pH 5.0 to evaluate the substrate specificity of PQQ-DH9. The reference strain demonstrated considerable activity on a wide variety of substrates, particularly on sugars, owing to the presence of membrane-bound glucose dehydrogenase (Table 3.1). Therefore, we evaluated the dehydrogenase activities of PQQ-DH9 and GLDH by subtracting the specific activity of the reference strain from the specific activity of the *pqq9*$^+$ strain or that of the *sldBA*$^+$ strain, and in each case we referred to the result as the Δ activity (Table 3.1). Similar to the membranes of the *sldBA*$^+$ strain, those of the *pqq9*$^+$ strain oxidized a wide variety of substrates. The *pqq9*$^+$ strain had a higher Δ activity with regard to *cis*-1,2-cyclohexanediol than the *sldBA*$^+$ strain. In addition, L-ribose was oxidized well by both membranes. However, glycerol, ribitol, D-mannitol, D-sorbitol, isopropanol, and 1,2-butanediol were not oxidized well by the *pqq9*$^+$ membranes; i.e., the *pqq9*$^+$ membranes had much lower activities with regard to those substrates than the *sldBA*$^+$ membranes.

PQQ-DH9 preferentially oxidized *cis*-1,2-cyclohexanediol over the *trans* isomer (Table 3.1). The Δ activity values of the *pqq9*$^+$ membranes were 520 and 10 mU mg^{-1} for the *cis* and *trans* forms, respectively. However, the *sldBA*$^+$ strain oxidized the *cis* and *trans* forms at 240 and 230 mU mg^{-1}, respectively, which was consistent with the previous observation by Moonmangmee et al. {Moonmangmee et al., 2001}.

3.3.4. Michaelis constants for the substrates

The K_M values of dehydrogenases in the membrane fractions of the *pqq9*$^+$ and *sldBA*$^+$ strains were determined with regard to glycerol, L-ribose, D-arabitol, 2,3-butanediol, and the *cis*- and *trans*- isoforms of 1,2-cyclohexanediol (Table 3.2). The K_M values of the *pqq9*$^+$ membranes with regard to glycerol, D-arabitol, and 2,3-butanediol were higher than those of the *sldBA*$^+$ membranes. However, the K_M values of the two membranes with regard to L-ribose and *cis*-1,2-cyclohexanediol were comparable. If, as we have suggested {Yakushi et al., 2018b}, GLDH oxidizes the pyranose form of L-ribose to produce L-ribonolactone, it is plausible that the affinity of PQQ-DH9 for cyclic substrates is comparable to that of GLDH, but its affinity for linear substrates is lower than that of GLDH.

The K_M value of the *pqq9*$^+$ membranes with regard to 1,2-cyclohexanediol was higher for the *trans*- isoform than for the *cis*- isoform, whereas the K_M value of the *sldBA*$^+$ membranes with regard to 1,2-cyclohexanediol was lower for the *trans*- isoform than for the *cis*- isoform (Table 3.2). The mechanism by which the two enzymes discriminate between the *cis*- and *trans*-isoforms is intriguing and requires further biochemical analyses including structural determinations.

3.3.5. Effects of EDTA on dehydrogenase activity

We examined the sensitivity of the dehydrogenases to EDTA. Because PQQ is attached to the enzyme via Ca^{2+} {Ghosh et al., 1995}, EDTA reversibly inactivates the PQQ-dependent enzyme by chelating Ca^{2+}. Treatment with various concentrations of EDTA of up to 20 mM on ice inactivated D-arabitol dehydrogenase in both the *pqq9*$^+$ and *sldBA*$^+$ membranes (Fig. 3.3). At 20 mM EDTA, the *sldBA*$^+$ membranes retained 60% of the activity of the control membranes in the absence of EDTA, whereas the *pqq9*$^+$ membranes lost 80% of their activity. The results suggest that PQQ-DH9 is less stable than GLDH following treatment with EDTA. We confirmed the recovery of activity by adding 5 μM PQQ and 2 mM Ca^{2+} after removing the EDTA (data not shown). Therefore, the detachment of PQQ and Ca^{2+} from the enzymes accounted for the reduced activities resulting from EDTA treatment, indicating that PQQ-DH9 works in a PQQ-dependent manner. This suggests that PQQ and Ca^{2+} are detached more readily from PQQ-DH9 than from GLDH.

3.3.6. Biotransformation of D-arabitol, 2,3-butanediol, *cis*-1,2-cyclohexanediol, and L-ribose

I examined the oxidation products of D-arabitol, 2,3-butanediol, *cis*-1,2-cyclohexanediol, and L-ribose obtained using the membrane fractions of *sldBA*$^+$ and *pqq9*$^+$, as described in the Materials and Methods section. The reaction products from the two membranes were eluted at retention times were close to each other: 20.5, 30.3, 43.2, and 20.6 min for the oxidation products of D-arabitol, 2,3-butanediol, *cis*-1,2-cyclohexanediol, and L-ribose, respectively (Fig. 3.S4). Therefore, we concluded that the products resulting from the activity of PQQ-DH9 were the same as those resulting from the activity of GLDH.

I found two peaks in the HPLC chromatogram of 2,3-butanediol at retention times of 31.9 and 32.9 min in the product of the 0-h reactions (Fig. 3.S4C), both of which were consumed as a function of the duration of the oxidation reaction with the two membranes. I refer to the isoforms eluted at 31.9 and 32.9 min as substrates A and B, respectively. Commercially available 2,3-butanediol is a mixture of three isoforms: 2*S*,3*S*-, 2*R*,3*R*-, and the *meso*-form, and substrate B would be one of these isoforms. Substrate B was consumed at a lower rate than substrate A (Fig. 3.S5) and oxidized more slowly by the *pqq9*$^+$ membranes than by the *sldBA*$^+$ membranes (Fig. 3.S5B). Because the peak intensity of the oxidation product (30.3 min retention time) produced by the *sldBA*$^+$ membranes was higher than that produced by the *pqq9*$^+$ membranes (Fig. 3.S5C), the difference in the peak intensities corresponded to the difference in the consumption of substrate B (Fig. 3.S5B). Therefore, I suggest that PQQ-DH9 and GLDH oxidize 2,3-butanediol in a stereoisomer-specific manner. The oxidation product of 2,3-butanediol would be acetoin, which is a valuable biochemical used in the dairy, cosmetic, and pharmaceutical industries, as well as in chemical synthesis. *G. oxydans* strain DSM2003 produces (3*S*)-acetoin and (3*R*)-

acetoin from (2*S*,3*S*)- and (2*R*,3*R*)-2,3-butanediol, respectively, and it converts *meso*-2,3-butanediol stereo selectively to (3*S*)-acetoin {Wang et al., 2013}. Since (3*S*)-acetoin and (3*R*)-acetoin run on HPLC as a single peak {Wang et al., 2013}, the oxidation product (30.3 min retention time) might contain the 3*S*- and 3*R*-isomers of acetoin.

3.4. CONCLUSIONS

Several attempts have been made to characterize the orphan PQQ-dependent dehydrogenases of *Gluconobacter oxydans* from the metagenome {Mientus et al., 2017; Peters et al., 2017; Peters et al., 2013}. I characterized the GLF_2583-2584 proteins as PQQ-DH9, which was similar to GLDH but had different substrate specificities: PQQ-DH9 oxidized linear substrates—such as glycerol, ribitol, and D-mannitol—at lower rates and with lower affinities than GLDH, whereas it oxidized circular substrates—such as *cis*-1,2-cyclohexanediol and the pyranose form of L-ribose—with affinities and rates comparable to those of GLDH. Since the reaction products of the *pqq9*$^{+}$ membranes showed similar retention times to those of the *sldBA*$^{+}$ membranes on HPLC, it is plausibly speculated that 2-keto-cyclohexanol is produced from *cis*-1,2-cyclohexanediol, and L-ribose is converted to L-ribono-1,5-lactone and subsequently to L-ribonic acid, based on analogy with GLDH catalysis {Yakushi et al., 2018b}. I suggested that PQQ-DH9 is a cryptic enzyme, since the activity of the chromosomal expression level was not detected in our experiment. Culture conditions for the expression of PQQ-DH9 are the important issues to understand the physiological role of this enzyme.

3.5. ACKNOWLEDGEMENTS

We would like to thank Dr. Naoya Kataoka and his student, Kotone Naoki, our laboratory member, for primary idea and information to start with PQQ-DH9.

TABLES AND FIGURES IN CHAPTER THREE

Table 3.1. *Gluconobacter* strains and plasmids used in this study.

Strains and plasmids	Relevant characteristics	Source or reference
Gluconobacter sp.		
CHM43	Wild type	{Moonmangmee, 2000}
SEI46	CHM43 Δ*adhBA*	{Yakushi, 2018b}
TORI4	CHM43 ΔadhBA ΔsldBA	{Yakushi, 2018b}
Plasmid		
pCM62	Broad-host-range vector, *mob*, Tc^R	{Marx, 2001}
p62SGLDH2-11	pCM62, GLF_2583-2584	This study

Table 3.2. Substrate specificities of pyrroloquinoline quinone-dependent dehydrogenase 9 and glycerol dehydrogenase

	Reference	*pqq9*$^+$		*sldBA*$^+$
	Specific activity (mU mg^{-1})[a]	Specific activity (mU mg^{-1})[a]	Δ activity (mU mg^{-1})[b]	Δ activity (mU mg^{-1})[c]
Glycerol	4.0 ± 5	18 ± 10	14	490
meso-Erythritol	0 (*n* = 2)	190 (*n* = 2)	190	330
D,L-Threitol	0 (*n* = 2)	3.1 (*n* = 2)	3.1	25
Xylitol	0 (*n* = 2)	0 (*n* = 2)	0	3.3
Ribitol	0 (*n* = 2)	28 (*n* = 2)	28	260
D-Arabitol	0	170 ± 20	170	400
L-Arabitol	0	0	0	4.6
Galactitol	0 (*n* = 2)	0 (*n* = 2)	0	8.5
D-Mannitol	0	27 ± 10	27	210
D-Sorbitol	2.8 ± 3	55 ± 10	52	410
Inositol	31 ± 19	0 ± 0	< 0	< 0
Isopropanol	8.0 ± 8	35 ± 10	27	240
2-Butanol	26 (*n* = 2)	140 (*n* = 2)	114	380
2-Hexanol	7.0 (*n* = 2)	30 (*n* = 2)	23	78
1,2-Butanediol	2.1 (*n* = 2)	80 (*n* = 2)	78	460
1,3-Butanediol	11 (*n* = 2)	65 (*n* = 2)	54	140
2,3-Butanediol	26 ± 8	400 ± 50	370	770
2,4-Pentanediol	25 ± 7	85 ± 4	60	240
1,2-Cyclopentandiol	119 (*n* = 2)	350 (*n* = 2)	230	630
cis-1,2-Cyclohexanediol	35 ± 13	550 ± 90	520	240
trans-1,2-Cyclohexanediol	0 ± 0	10 ± 0.4	10	230
1-Cyclohexylethanol	6.3 (*n* = 2)	22 (*n* = 2)	16	43
Cyclohexanol	5.1 (*n* = 2)	84 (*n* = 2)	79	270
Glyceraldehyde	63 (*n* = 1)	140 (*n* = 1)	77	120
D-Xylose	220 ± 90	120 ± 50	< 0	23
D-Ribose	14 ± 3	90 ± 30	76	120
L-Ribose	25 ± 2	200 ± 7	180	210
D-Arabinose	9.8 (*n* = 2)	5.2 (*n* = 2)	< 0	18
L-Arabinose	157 (*n* = 2)	120 (*n* = 2)	< 0	16
D-Lyxose	5.5 ± 3	100 ± 10	95	89
D-Galactose	240 ± 100	130 ± 10	< 0	45
D-Gluconate	140 ± 40	130 ± 10	< 0	82

[a]Specific activity was calculated from three independent enzyme assays, shown in mean value ± standard deviation. Otherwise, results of the numbers (*n*) of enzyme assays indicated in parentheses were used for the calculation of mean value.

[b]Δ activity in the *pqq9*$^+$ membrane was calculated by subtracting the mean specific activity of the reference strain from the corresponding mean specific activity of the *pqq9*$^+$ strain.

[c]Δ activity in the *sldBA*$^+$ membrane was calculated by subtracting the specific activity of the reference strain (*n* = 1) from the corresponding specific activity of the *sldBA*$^+$ strain (*n* = 1).

Table 3.3. K_M values (mM) of membrane-associated dehydrogenases with regard to various substrates[a]

	pqq9$^+$	*sldBA*$^+$
Glycerol	450 ± 40	8.4 ± 0.7
L-Ribose	41 ± 2	61 ± 3
D-Arabitol	88 ± 4	5.5 ± 0.3
2,3-Butanediol	9.4 ± 0.4	1.8 ± 0.2
cis-1,2-Cyclohexanediol	2.8 ± 0.3	4.6 ± 0.6
trans-1,2-Cyclohexanediol	19 ± 3	0.49 ± 0.07

[a]The K_M values were determined by a phenazine methosulfate/2,6-dichlorophenol indophenol assay using membranes from the *pqq9*$^+$ and *sldBA*$^+$ strains grown on sorbitol medium with various concentrations of the substrate in 50 mM Na^+-acetate (pH 5.0) at 25°C, followed by data analysis using KaleidaGraph (ver. 4.5, Synergy Software). See Fig. 3.S3.

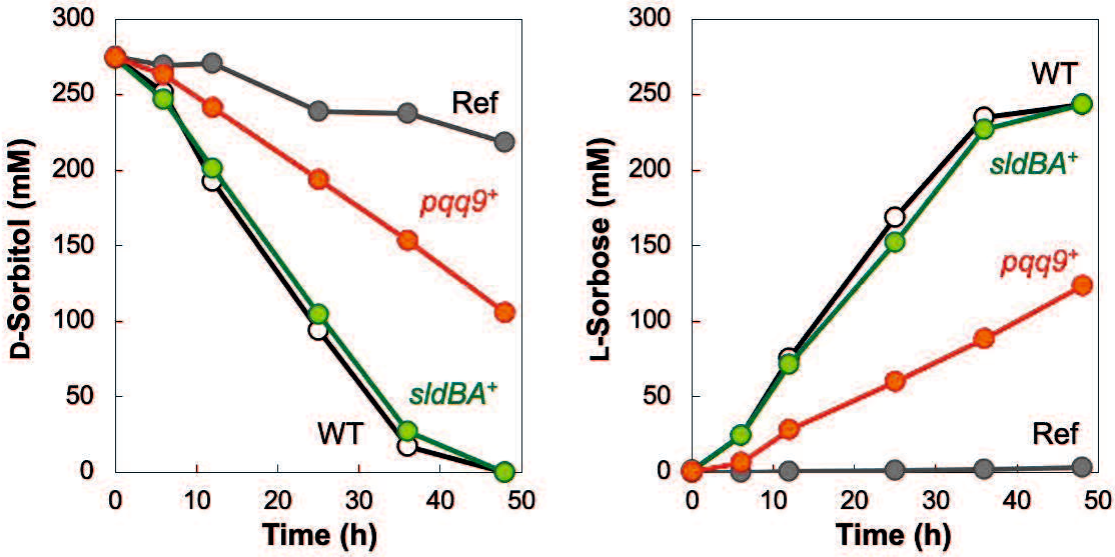

Figure 3.1. PQQ-DH9 complements deficiency in L-sorbose production by the Δ*adhAB* Δ*sldBA* strain.

Gluconobacter strains were cultivated on sorbitol medium. The wild-type strain harboring pCM62 (WT, white circles), the Δ*adhAB* Δ*sldBA* strain harboring pCM62 (Ref, gray circles), the Δ*adhAB* strain harboring pCM62 (*sldBA*$^{+}$, lime green circles), the Δ*adhAB* Δ*sldBA* strain harboring pCM62 (Ref for the reference strain), and the Δ*adhAB* Δ*sldBA* strain harboring p62sGLDH2-11 (*pqq9*$^{+}$, orange circles). D-Sorbitol and L-sorbose levels in the medium were determined by high-performance liquid chromatography.

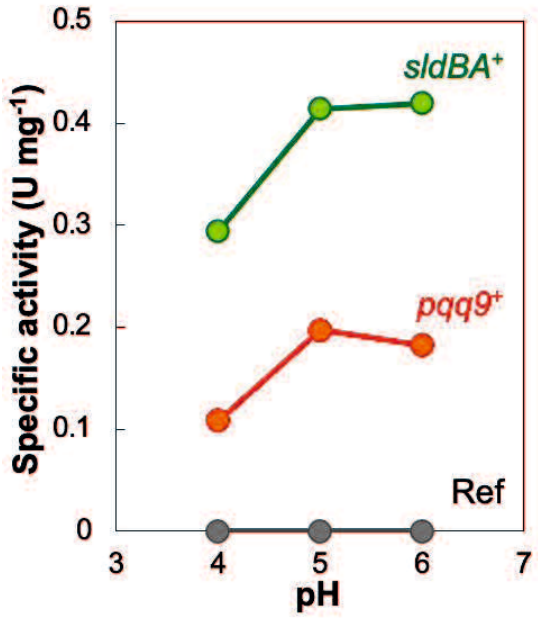

Figure 3.2. D-arabitol dehydrogenase assay indicates the functional expression of PQQ-DH9.

D-arabitol dehydrogenase activity in the membranes of the Δ*adhAB* strain harboring pCM62 (*sldBA*$^{+}$, lime green circles), the Δ*adhAB* Δ*sldBA* strain harboring pCM62 (Ref for the reference strain, gray circles), and the Δ*adhAB* Δ*sldBA* strain harboring p62sGLDH2-11 (*pqq9*$^{+}$, orange circles) grown on sorbitol medium were determined by PMS/DCPIP assay with 100 mM D-arabitol in 50 mM Na^{+}-acetate (pH 4.0, 5.0, and 6.0) at 25°C. The membranes of the reference strain (Ref) had activities below the detection limit (0.001 U mg^{-1}).

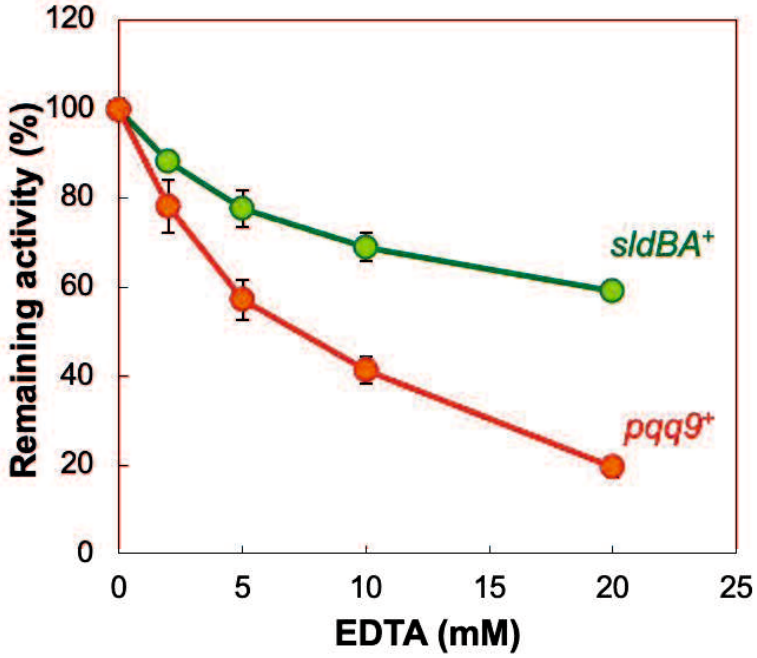

Figure 3.3. Effects of EDTA treatment on dehydrogenase activity.

The membranes of the Δ*adhAB* strain harboring pCM62 (*sldBA*$^{+}$, lime green circles) and the Δ*adhAB* Δ*sldBA* strain harboring p62sGLDH2-11 (*pqq9*$^{+}$, orange circles) were treated with 2, 5, 10, and 20 mM EDTA on ice overnight. Then, D-arabitol dehydrogenase activity in the EDTA-treated membrane was determined by PMS/DCPIP assay in 50 mM Na^{+}-acetate (pH 5.0) at 25°C. The remaining activity relative to that of the control membrane was expressed as a percentage.

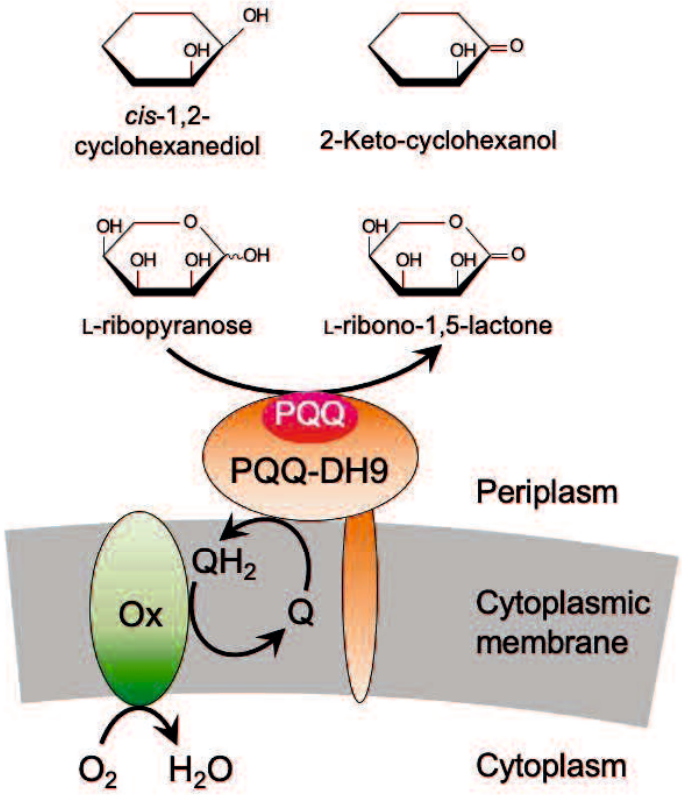

Figure 3.4. Graphical abstract

Pyrroloquinoline quinone-dependent dehydrogenase 9 (PQQ-DH9) of *G. frateurii* CHM43 oxidizes cyclic secondary alcohols. Ox, ubiquinol oxidase; Q, ubiquinone.

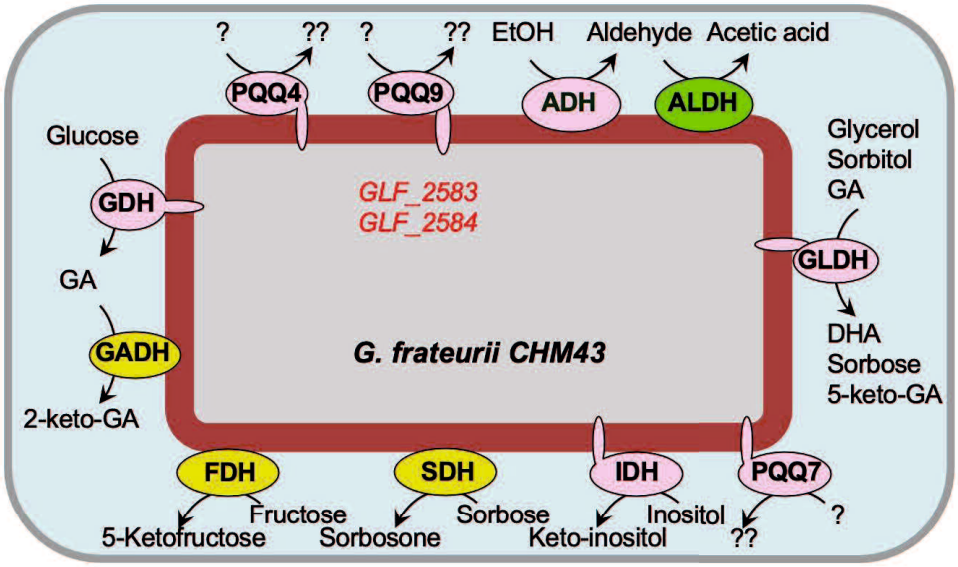

Figure 3.S1. Membrane-bound dehydrogenases in *G. frateurii* CHM43

IDH: Innositol dehydrogenase, PQQ7, ADH: alcohol dehydrogenase, ALDH: aldehyde dehydrogenase, GLDH: glycerol dehydrogenase, PQQ9, PQQ4, SDH: sorbose dehydrogenase, FDH: fructose dehydrogenase, GADH: gluconate 3-phosphate dehydrogenase, GDH: glucose dehydrogenase.

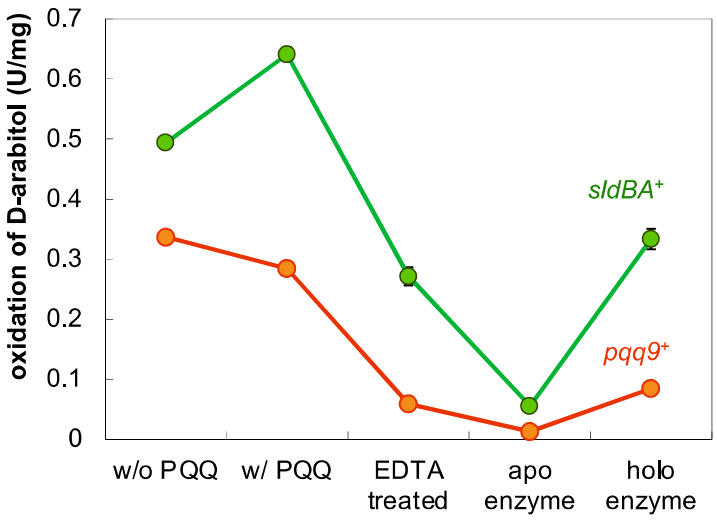

Figure 3.S2. Effects of EDTA treatment on dehydrogenase activity and recovery enzyme

The membrane suspension of 10 mg of protein/mL in 10 mM MES-KOH (pH 6.0) was incubated with 20 mM in an ice bath for overnight. EDTA was removed from the membrane suspension by ultracentrifugation at 90,000 x g for 60 min. The precipitate was resuspended with 10 mM MES-KOH, pH 6.0, to wash EDTA out of the membrane fraction and then followed by ultracentrifugation again under the same conditions. The resulting precipitate was resuspended with the same buffer. This membrane suspension obtained was used as apo-enzyme. Conversion of the apo-enzyme to holo-enzyme, PQQ and Ca^{2+} were added to 5 µM and 2 mM, respectively, and incubated for 30 min at 25°C.

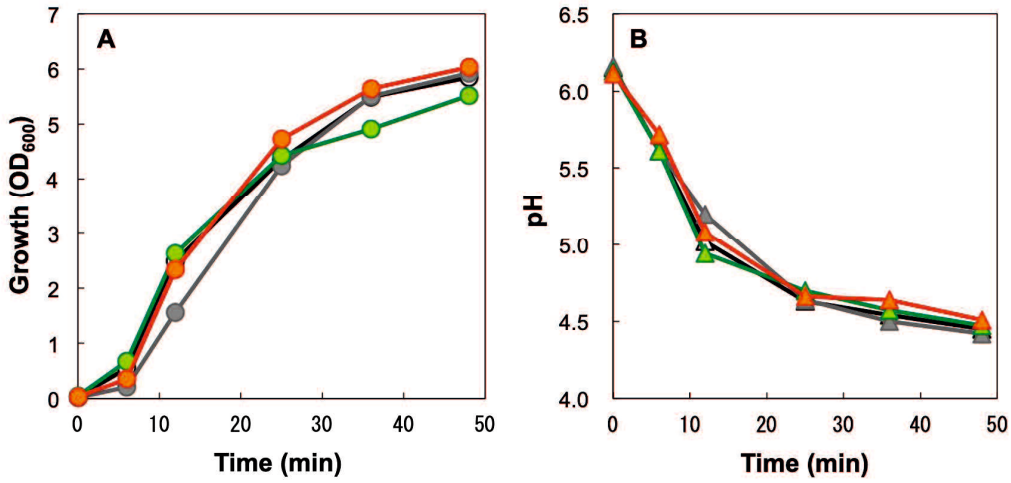

Figure 3.S3. Growth of the recombinant *Gluconobacter* strains on sorbitol medium. The *Gluconobacter* strains were cultivated on sorbitol medium: the wild-type strain harboring pCM62 (WT, white circles), the Δ*adhAB* Δ*sldBA* strain harboring pCM62 (Ref, gray circles), the Δ*adhAB* strain harboring pCM62 (*sldBA*$^{+}$, lime green circles), and the Δ*adhAB* Δ*sldBA* strain harboring p62sGLDH2-11 (*pqq9*$^{+}$, orange circles). The OD_{600} (A) and pH (B) values of the medium were determined.

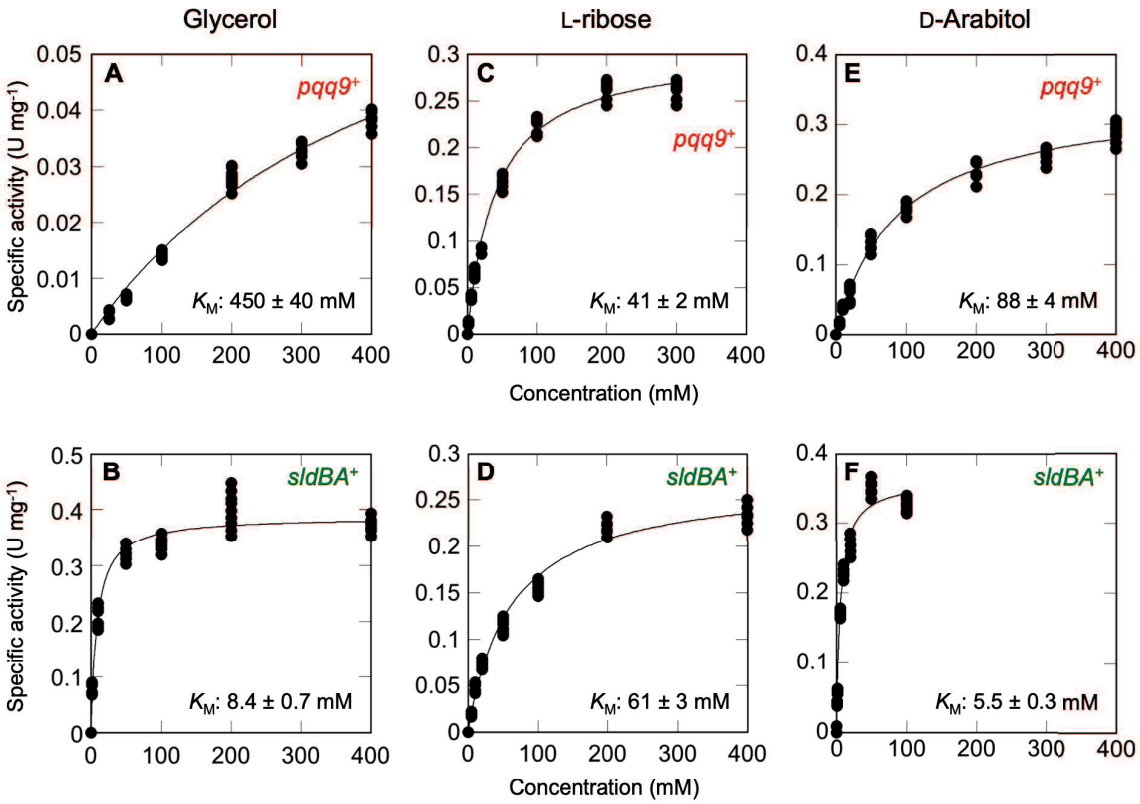

Figure 3.S4. The *K*M values of the *pqq9*$^+$ and *sldBA*$^+$ membranes for the several substrates.

Dehydrogenase activities of the *pqq9*$^+$ (A, C, E, G, I, and K) and *sldBA*$^+$ (B, D, F, H, J, and L) membranes were measured with different concentrations of various substrates: glycerol (A and B), L-ribose (C and D), D-arabitol (E and F), 2,3- butanediol (G and H), *cis*-1,2-cyclohexanediol (I and J), and *trans*-1,2- cyclohexanediol (K and L). Triplicate enzyme assays were done at the each substrate concentration. The *K*M value was calculated on KaleidaGraph ver. 4.5 (Synergy Software, Reading, PA, USA).

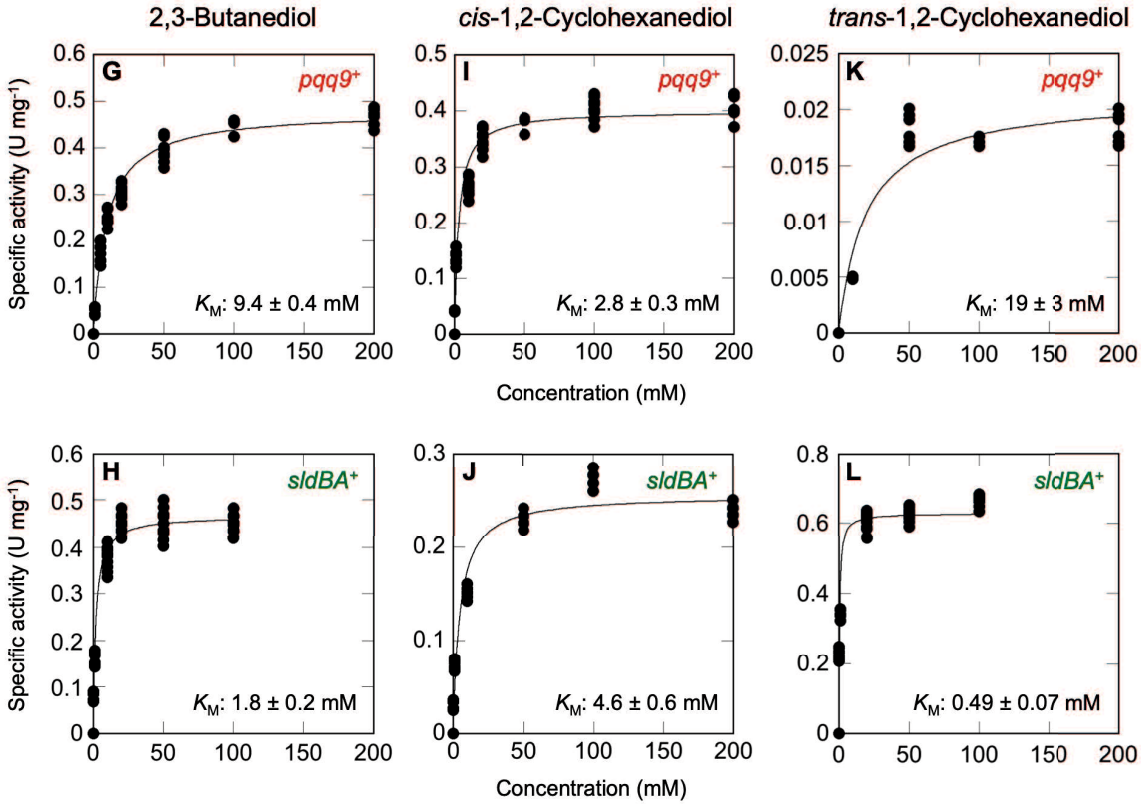

Figure 3.S4. The *K*M values of the *pqq9*$^+$ and *sldBA*$^+$ membranes for the several substrates.

Dehydrogenase activities of the *pqq9*$^+$ (A, C, E, G, I, and K) and *sldBA*$^+$ (B, D, F, H, J, and L) membranes were measured with different concentrations of various substrates: glycerol (A and B), L-ribose (C and D), D-arabitol (E and F), 2,3- butanediol (G and H), *cis*-1,2-cyclohexanediol (I and J), and *trans*-1,2- cyclohexanediol (K and L). Triplicate enzyme assays were done at the each substrate concentration. The *K*M value was calculated on KaleidaGraph ver. 4.5 (Synergy Software, Reading, PA, USA).

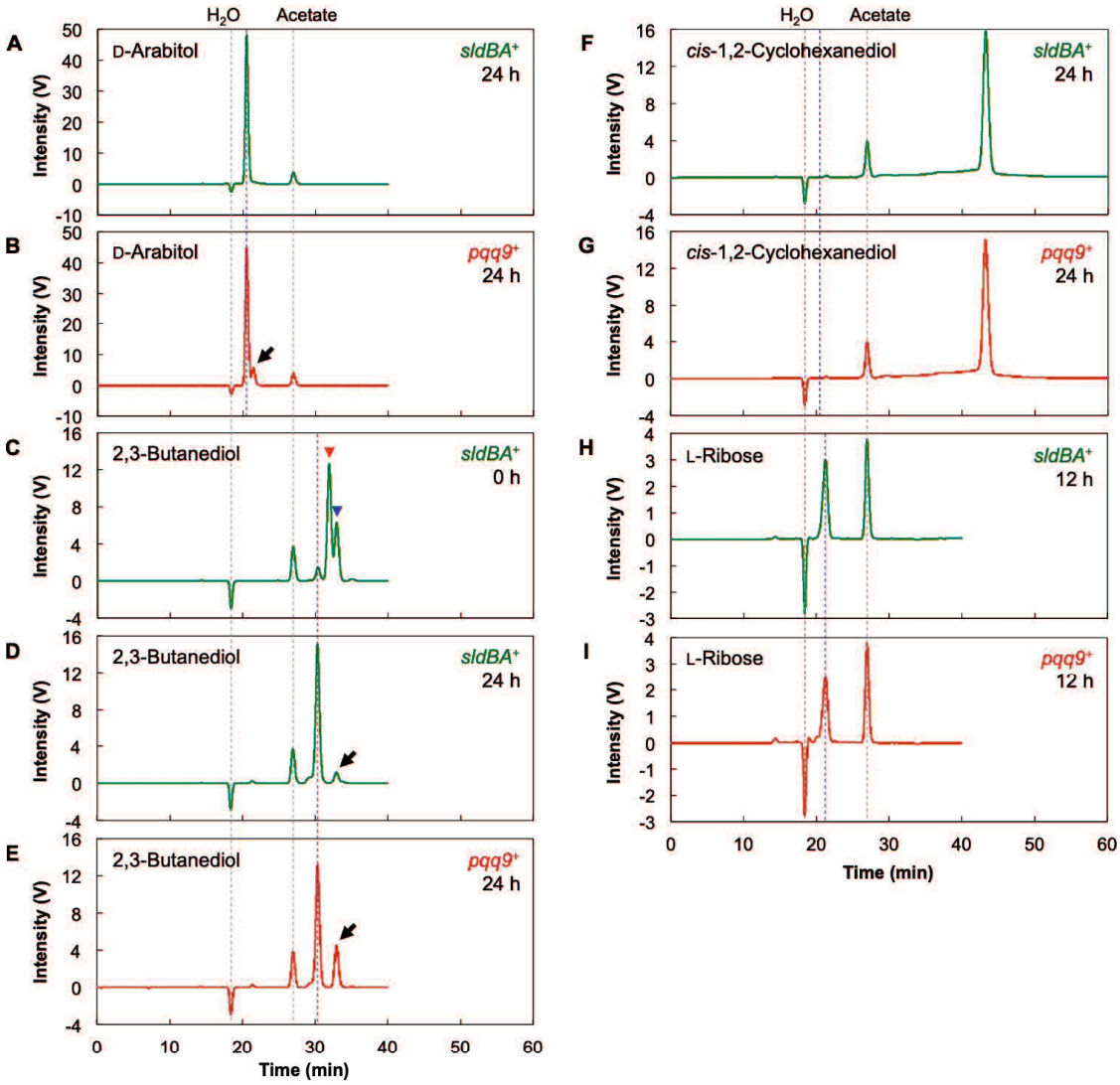

Figure 3.S5. High-performance liquid chromatography (HPLC) chromatograms of the reaction products resulting from the action of the membranes on several substrates.
The reaction products were run on an organic acid column and were detected with a refractive index (RI) detector. A and B: Reaction products resulting from the oxidation of D-arabitol by the *sldBA*$^+$ (A) and *pqq9*$^+$ (B) membranes for 24 h. The blue dashed line indicates the peaks attributable to the reaction products. The black arrow indicates the peak attributable to the remaining substrate. C, D, and E: The reaction products resulting from the oxidation of 2,3-butanediol by the *sldBA*$^+$ (C and D) and *pqq9*$^+$ (E) membranes for 0 h (C) and 24 h (D and E). The purple dashed line indicates the peaks attributable to the reaction products. The red and blue arrow heads indicate the peaks attributable to the substrates A and B, respectively. The black arrows indicate the peaks attributable to the remaining substrate B after the 24-h reactions. F and G: The reaction products resulting from the oxidation of *cis*-1,2-cyclohexanediol by the *sldBA*$^+$ (F) and *pqq9*$^+$ (G) membranes for 24 h. The blue dashed line indicates the peaks attributable to the reaction products. H and I: The reaction products resulting from the oxidation of L-ribose by the *sldBA*$^+$ (H) and *pqq9*$^+$ (I) membranes for 12 h. The purple dashed line indicates the peaks attributable to the reaction products. The gray dashed lines indicate the trough attributable to water and the peak attributable to acetate, which was used as a buffer in the oxidation reactions.

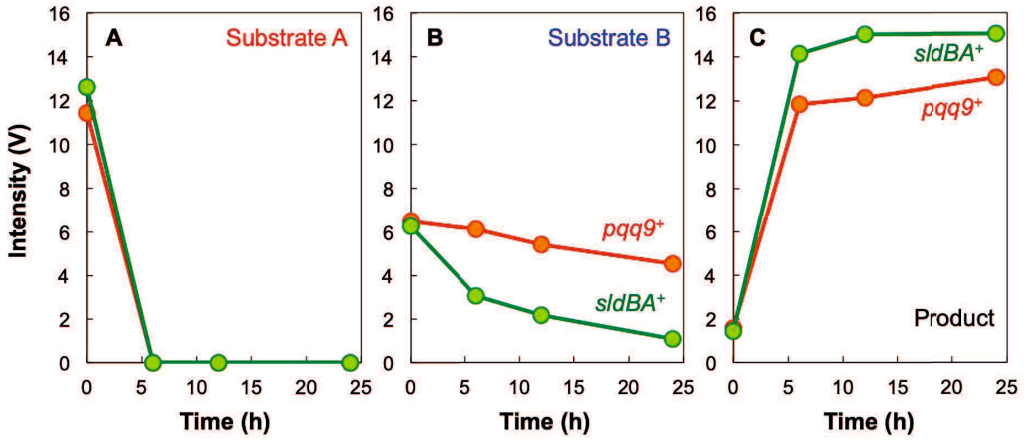

Figure 3.S6. Time course of the oxidation of 2,3-butanediol by the membranes.

2,3-Butanediol was treated with the *sldBA*$^{+}$ (lime green) and *pqq9*$^{+}$ (orange) membranes for 0, 6, 12, and 24 h. The reaction products were run on an organic acid column and detected with a refractive index (RI) detector. The peak intensities of substrate A (31.9 min retention time), substrate B (32.9 min retention time), and the product (30.3 min retention time) are shown in panels A, B, and C, respectively.

CHAPTER FOUR

Three different enzymes responsible for dihydroxyacetone phosphorylation in *Gluconobacter thailandicus* NBRC3255

ABSTRACT

Gluconobacter sp. oxidize glycerol to dihydroxyacetone (DHA) then utilized DHA produced in the cytoplasm. In this research, *G. thailandicus* NBRC3255 roughly consumed DHA produced in 1 % glycerol while *G. oxydans* 621H did poorly. Both strains have DHA kinase activity higher than DHA reductase activity. And DHA kinase activity of NBRC3255 strain was 18 times higher than that of 621H. According to draft genome sequence, NBRC3255 strain has two genes annotated with DHA kinase (*NBRC3255_2003* (*dhaK*) and *NBRC3255_3084* (*derK*)) whereas 621H strain has one gene (*GOX2222*). The NBRC3255Δ*dhaK* Δ*derK* strain showed DHA kinase activity similar to wild type so that we purified DHA kinase in the Δ*dhaK* Δ*derK* cells. N-terminal amino acid sequence of the purified DHA kinase was determined to match with that of glycerol kinase (*NBRC3255_0651*: *glpK*). The NBRC3255 Δ*glpK* strain remained 10% DHA kinase activity of wild type. Several combinations of deletions in *dhak*, *derK* and *glpK* were constructed. These mutant strains lacked of both *derK* and *glpk*, lost DHA kinase activity and did not grow in glycerol medium. However, the Δ*derK* Δ*glpK* strain consumed DHA in the later growth phase in YPGD medium. Triple mutants lost DHA kinase activity, did not grow in glycerol medium and accumulated DHA in YPGD medium. Therefore, DhaK, DerK and GlpK are involved in DHA metabolism in *G. thailandicus* NBRC 3255.

4.1. INTRODUCTION

Dihydroxyacetone is a valuable bioproduct in industry. It has been approved all over the world to be a chemical in self-tanning-products for several decades {Rosaria, 2018}. At this moment, there are many researches about produce DHA from oxidation of glycerol by *Gluconobacter* sp. {Xi Lin, 2016}{Yu Peng Liu, 2013}. However, the DHA metabolism is unknown.

In this study, *G. thailandicus* NBRC 3255 and *G. oxydans* 621H oxidize glycerol by GLDH to produce dihydroxyacetone (DHA), then DHA is degraded. However, the ability of degrading DHA is different between two strains. In 1 % glycerol medium, *G. thailandicus* NBRC 3255 absolutely degraded DHA after 100 hours while few DHA was degraded and accumulated later in case of *G. oxydans* 621H (Fig. 4.1). We suggest some difference in DHA metabolism between NBRC 3255 strain and 621H strain.

NBRC 3255 strain has two pathways for DHA metabolism: DHA reductase and DHA kinase (Fig. 4.2). The specific activity of DHA kinase (590 mU mg^{-1}) was much higher than the specific activity of DHA reductase (with NADH: 20 mU mg^{-1} and with NADPH: < 1 mU mg^{-1}) (Table 4.2). The DHA kinase activity of NBRC 3255 was also much higher than that of 621H strain (33 mU mg^{-1}). *G. thailandicus* NBRC 3255 has two putative genes for DHA kinase, *NBRC3255_2003* and *NBRC3255_3084* {Matsutani et al., 2013} while 621H strain has only one gene (*GOX2222*). There are two families of DHA kinases. One is ATP-dependent DHA kinase with two subunits (DhaK and DhaL) {Daniel et al., 1995; Siebold et al., 2003}. The second is the phosphoenolpyruvate (PEP)-dependent DHA kinase with three subunits (DhaK, DhaL and DhaM) {Gutknecht et al., 2001; Zurbriggen et al., 2008; Bachler et al., 2005}. Since NBRC 3255 strain did not detect the activity of PEP-dependent DHA kinase, it has only ATP-dependent DHA kinase. When BLAST was performed with UniProt (Swiss-Prot) as a target, DHA kinase of *Citrobacter freundii* was the first hit for *NBRC3255_2003*, and D-erythrulose kinase of *Mycobacterium* was the first hit for *NBRC3255_3084*. Therefore, *NBRC3255_2003* was named DhaK, and *NBRC3255_3084* was named DerK. I would like to understand the DHA metabolism in *G. thailandicus* NBRC3255 and *G. oxydans* 621H

4.2. MATERIALS AND METHODS

4.2.1. Materials

Dihydroxyacetone was obtained from MP Biomedicals (Santa Ana, CA). Yeast extract and polypeptone were obtained from Oriental Yeast (Osaka, Japan) and Nihon Pharmaceutical (Tokyo, Japan), respectively. 5-Fluorocytosine was purchased from Fluorochem (Glossop, UK). Restriction endonucleases and modification enzymes for genetic engineering were purchasd from Toyobo (Osaka, Japan). All other materials were purchased from a commercial source of analytical grade.

4.2.2. Bacterial strains and cultivation

The *G. thailandicus* strains used in this study are listed in Table 4.1. *G. thailandicus* strain NBRC3255 was obtained from the NITE Biological Resource Center (NBRC, https://www.nite.go.jp/nbrc/). *G. thailandicus* cells were cultivated in ΔP (10 g yeast extract, 10 g polypeptone, 5 g glucose, and 20 g glycerol per liter), YPGD (5 g yeast extract, 5 g polypeptone, 5 g glycerol, and 5 g glucose per liter), YPG (5 g yeast extract, 5 g polypeptone, and 10 g glycerol per liter), or YPDHA (5 g yeast extract, 5 g polypeptone, and 5 g DHA per liter) medium. A stock solution of DHA at 40% (w/v) was freshly prepared and sterilized by filtration (0.22 μm). The cells were pre-cultivated in 2 mL of ΔP medium in a tube at 30°C with shaking at 200 rpm. For the main cultivation, 1 mL of the pre-culture was transferred into a 100-mL medium in a 500-mL Erlenmeyer flask, and the cells were cultivated at 30°C with shaking at 200 rpm. For *G. thailandicus*, kanamycin and ampicillin were used at final concentrations of 100 and 50 μg mL^{-1}, respectively.

Escheria coli strains DH5α {Hanahan, 1983} and HB101 {Boyer and Roulland-Dussoix, 1969} were used for plasmid construction and triparental mating, respectively. *E. coli* cells were cultivated in modified Luria-Bertani (LB) medium {Sambrook and Russel, 2001}, which consists of 5 g of yeast extract, 10 g of polypeptone, and 5 g of NaCl per liter, adjusted

pH to 7 with NaOH. For *E. coli*, kanamycin and ampicillin were used at final concentration of 50 μg mL^{-1}.

4.2.3. Construction of plasmids

The plasmids used in this study are listed in Table 4.1. Herculase DNA polymerase (Stratagene, Santa Clara, CA, USA) was used for PCR. The DNA primers used in this study are listed in Table S2. The nucleotide sequence of the PCR products was confirmed by Sanger sequencing after DNA cloning. Genomic DNA used as the parental DNA for PCR was isolated from *G. thailandicus* strain NBRC3255 as described by Marmur (Marmur, 1961), with some modifications {Kawai et al., 2013}. To construct plasmids for the deletion of *dhaK* (*NBRC3255-2003*), a ca. 2.8-kb DNA fragment containing the 5′ and 3′ flanking regions of *dhaK* was amplified with a pair of the primers, namely ΔGTH2012-5-Pst(+) and ΔGTH2012-3-Bam(-). The DNA fragment was digested with *Pst*I, *Bam*HI, and *Sph*I to obtain two DNA fragments ca. 0.8-kb 5′ region and ca. 0.8-kb 3′ region to be inserted into the *Pst*I and *Bam*HI sites of pK18mobGII, yielding pEK12. To construct plasmids for the deletion of *derK* (*NBRC3255-3084*), a ca. 2.3-kb DNA fragment containing the 5′ and 3′ flanking regions of *derK* was amplified with a pair of primers, namely ΔGTH3096-5-Sal(+) and ΔGTH3096-3-Bam(-). The DNA fragment was digested with *Sal*I, *Bam*HI, and *Nco*I to obtain two DNA fragments, a ca. 0.7-kb 5′ region and ca. 0.6-kb 3′ region, to be inserted into the *Sal*I and *Bam*HI sites of pK18mobGII, yielding pEK15. pEK15 was treated with *Sal*I and *Sma*I to obtain the ca. 1.3 kb DNA fragment containing the Δ*derK* allele, which was then inserted into the corresponding site of pKOS6b to yield pKH4.

glpK (*NBRC3255_0651*) was amplified with a pair of primers, ΔglpK-5-Hin(+) and ΔglpK-3-Xba(-), and inserted into the *Eco*RV site of pT7Blue (Novagen) to yield pKH7. The pKH7 plasmid was treated with *Hin*dIII and *Eco*RV to obtain a ca. 0.7-kb DNA fragment containing the 5′ flanking region of *glpK*. Then, the 3′ flanking region of *glpK* was obtained by PCR with a pair of primers, ΔglpK-5-RV(+) and ΔglpK-3-Xba(-), and the PCR product was treated with *Eco*RV and *Xba*I. The 5′ and 3′ regions of *glpK* were inserted into the *Hin*dIII and *Xba*I sites of pKOS6b to yield pKH10.

The pKH7 plasmid carrying *glpK* (*NBRC3255_0651*) was treated with *Sma*I and *Sal*I to obtain a ca. 2.7-kb DNA fragment containing *glpK*. It was then inserted into the corresponding site of pBBR1MCS-4 to yield pKH18. To construct the plasmid for expression of *derK* (*NBRC3255_3084*), a 2.1-kb DNA fragment was obtained with a pair of primers, namely GTH3096-5-Kpn(+) and GTH3096-3-Sal(-). The DNA fragment was treated with *Kpn*I and *Sal*I to be inserted into the corresponding site of pBBR1MCS-4 to yield pKH24. For the *dhaK* (*NBRC3255_2003*) expression, the plasmid pEK20 was constructed by a similar procedure with a pair of primers, GTH2012-5-Kpn(+) and GTH2012-3-Sal(-).

4.2.4. Construction of gene deletion mutants

G. thailandicus strain NBRC3255 was transformed with plasmids via a triparental mating method, as described previously {Kawai et al., 2013}. In the case of pK18mobGII derivatives, the first recombinants with kanamycin-resistant (Km^R) and β-glucuronidase-positive (GUS^+) phenotypes were screened to conduct second recombination procedures. Non-blue colonies were screened on ΔP agar in the presence of 20 μg mL^{-1} 5-bromo-4-chloro-3-indoyl-β-D-glucuronide (cyclohexylammonium salt). Thus, β-glucuronidase-negative (GUS^-) and kanamycin-sensitive (Km^S) second recombinants were isolated, and their target alleles were confirmed by PCR. In the case of pKOS6b derivatives, the first recombinants with Km^R and 5-fluorocytocine-sensitive (5-FC^S) phenotypes were screened to conduct second recombination procedures. FC-resistant (5-FC^R) colonies were screened on ΔP agar in the presence of 60 μg mL^{-1} 5-FC. Thus, 5-FC^R and Km^S second recombinants were isolated, and their target alleles were confirmed by PCR. Second recombinants with only the allele deletion were obtained and referred to as the deletion mutant strains.

4.2.5. Determination of glycerol and DHA

The glycerol and DHA concentrations in the media were analyzed using a high-performance liquid chromatography (HPLC) system equipped with a refractive index (RI) detector. Glycerol and DHA were quantified with a Pb^{2+} cation-exchange column [SP0810 (SUGAR), 8.0 mm I.D. × 300 mm L; Shodex, Showa Denko KK, Kawasaki, Japan] at 80°C

using H_2O as the mobile phase at a flow rate of 0.5 mL min^{-1}. The retention times for glycerol and DHA were 28.5 and 30.9 min, respectively.

4.2.6. Preparation of the soluble fraction

Gluconobacter cells were cultivated on YPG or YPGD medium until the late exponential phase. After cultivation, the cells were collected by centrifugation at 9,000 × *g* for 10 min at 4°C. The collected cells were suspended in 50 mM K^+-phosphate (pH 7.0) and disrupted using a French pressure cell press at 1,100 kg cm^{-2}. The cell debris was removed by centrifugation at 9,000 × *g* for 10 min at 4°C. The resulting supernatant was centrifuged at 100,000 × *g* for 1 h at 4°C to separate the membranes. The supernatant was used as the soluble fraction for measuring enzyme activity.

4.2.7. Enzyme assays

DHA kinase activity was measured using a coupled method by reducing dihydroxyacetone phosphate with glycerol-3-phosphate dehydrogenase (G3PDH) (Sigma-Aldrich, St. Louis, MO), as described previously {Siebold et al., 2003}. The assay mixture consisted of 100 mM Tris-HCl (pH 6.5 or 7.0, as specified), 25 mM DHA, 5 mM $MgCl_2$, 2.5 mM ATP, 0.16 mM NADH, 2.5 U mL^{-1} G3PDH, 1 mM KCN, 7 mM NaN_3, and the appropriate amount of enzyme. The activity was determined by the rate of decrease in the absorbance at 340 nm with a molecular coefficient of 6.22 mM^{-1} cm^{-1}. The glycerol kinase activity was measured in a similar way {Deutscher and Sauerwald, 1986}. The assay mixture consisted of 100 mM K_2CO_3-$NaHCO_3$ (pH 10), 2 mM glycerol, 4 mM $MgCl_2$, 1 mM ATP, 3 mM NAD^+, 2.5 U mL^{-1} G3PDH, and an appropriate amount of enzyme. The activity was measured by the rate of increase in absorbance at 340 nm by the oxidation of glycerol-3-phosphate with G3PDH.

NADH-dependent DHA reductase activity was measured by the rate of decrease in absorbance at 340 nm concomitant with the oxidation of NADH. The assay mixture consisted of 50 mM Tris-HCl (pH 7.5), 7 mM NaN_3, 1 mM KCN, 0.125 mM NADH, 10 mM DHA, and an appropriate amount of enzyme, as described previously {Adachi et al., 2008}. NADPH-dependent DHA reductase activity was measured by the rate of decrease in absorbance at 340 nm with a molecular coefficient of 6.22 mM^{-1} cm^{-1}. The assay mixture consisted of 50 mM Tris-HCl (pH 7.5), 0.125 mM NADPH, 10 mM DHA, and an appropriate amount of enzyme, as described previously {Adachi et al., 2008}. One unit of enzyme activity was defined as the amount of enzyme catalyzing the phosphorylation or reduction of 1 μmol of substrate per min under the assay conditions.

The protein content was determined by a modified Lowry method with bovine serum albumin as the standard protein {Dulley and Grieve, 1975}.

4.3. RESULTS AND DISCUSSIONS

4.3.1. DHA metabolism in *G. thailandicus* NBRC3255

4.3.1.1. Glycerol kinase is one of DHA kinase enzyme

The three NBRC3255 derivatives Δ*dhaK*, Δ*derK*, and Δ*dhaK* Δ*derK* were constructed as described in 4.2.3. All of the constructed strains showed DHAK activities and DHA consumption similar to that of the wild type (Table 4.2) (Fig. 4.3). The result suggested that there are another genes code for another DHA kinase. This DHA kinase remained in Δ*dhaK*Δ*derK* strain was purified (Kaori, master thesis 2017). N-terminal amino acid sequence of the purified DHA kinase was determined to match with that of Glycerol kinase (*NBRC3255_0651*, GlpK). The gene *NBRC3255_0651* was disrupted to construct the Δ*glpK* strain. The DHA kinase activity of the Δ*glpK* strain was decreased to less than 10% of that of the wild type (Table 4.2). The result showed that GlpK accounts for a major part of DHAK activity in *G. thailandicus* NBRC 3255.

4.3.1.2. The involvement of DhaK and DerK in DHA metabolism

On the Δ*glpK* strain background, other derivatives were constructed with disruption on *dhaK* and *derK* and triple mutant). The Δ*dhaK* Δ*glpK* strain showed considerable DHAK activity (Table 4.2). On the other hand, the Δ*derK* Δ*glpK* double mutant strain showed DHAK activity less than a detection limit of 0.5 mU mg^{-1} (Table 4.2) and was unable to grow in a glycerol or DHA as a sole carbon in the medium (Fig. 4.4). This result showed that DerK accounted for remaining DHAK activity of *G. thailandicus* NBRC3255.

Because the Δ*dhaK* Δ*derK* Δ*glpK* and Δ*derK* Δ*glpK* strains cannot grow on glycerol or DHA as sole carbon sources, the medium contained glucose and glycerol (YPGD medium) was used. The triple deletion strain showed worse growth than the double deletion strain, particularly in the late phase of growth (Fig. 4.5). The two deletion derivatives maintained much higher concentrations of DHA than the wild type. The triple disrupted Δ*dhaK*Δ*derK*Δ*glpK* strain accumulated DHA accumulated higher DHA than the double deletion strain (Fig. 4.5). These results suggest that DhaK plays a role in DHA metabolism in the late phase of growth, although no roles of *dhaK* in DHA metabolism were found when the deletion derivatives were cultivated in glycerol medium.

Each DHAK was forcibly expressed in the triple disrupted strain. When these strains were grown in glycerol medium, all the DHAK expressing strains could all grow, although empty vector could not (Fig. 4.6). Furthermore, it was these strains had DHA kinase activity (Fig. 4.6). Therefore, it was suggested that these three DHAKs are involved in glycerol metabolism and act as DHA kinase.

4.3.2. DHA Metabolism in *G. oxydans* 621H

DHA kinase activity of 621H strain is much smaller than NBRC3255 strain so that glycerol kinase activity of 621H strain is also smaller than 621H. Because glycerol kinase is also DHA kinase that found in NBRC3255 strain (Fig. 4.7). So that the overexpress strain of *glpK* (*GOX2090*) of 621H strain was constructed. This strain greatly increased both DHA kinase and glycerol kinase activity (Fig. 4.8).

4.4. CONCLUSIONS AND DISCUSSIONS

The triple gene disrupted strain in which all three of *dhaK*, *derK* and *glpK* were disrupted could not consume DHA and not detected growth on glycerol and DHA medium. In addition, since this strain was unable to detect DHA kinase activity, so that *dhak*, *derK* and *glpK* are independently involved in DHA metabolism.

The Δ*glpK* decreased the DHA kinase activity to approx. 10% compared with wild-type strain. Therefore, it is suggested that GlpK accounts for the majority of the DHA kinase activity in NBRC 3255. DerK was responsible for the remaining DHA kinase activity of Δ*glpK*. And the DhaK is also DHA kinase that expressed in later growth phase.

There is a different in activity of GlpK between 621H and NBRC 3255, GlpK strain is considered to have a lower expression level in 621H than in NBRC3255 strain. An explanation is obtained from the genetic analysis. The predicted *glpK* operon of 621H is shorter than that of NBRC 3255, probably due to the abrogation of the N-terminus of glycerol-3-phosphate regulon repressor upstream of *glpK* (Kaori, master thesis 2017).

4.5. ACKNOWLEDGEMENTS

I am grateful to Kaori Hirata, our laboratory member. I would like to thank her for kind cooperation.

TABLES AND FIGURES OF CHAPTER FOUR

Table 4.1. Bacterial strains and plasmids used in this study.

Strains or plasmids	Description	Source or reference
Gluconobacter thailandicus		
NBRC3255	Wild type	NBRC
KAO-1	NBRC3255 Δ*dhaK*	This study
KAO-2	NBRC3255 Δ*derK*	This study
KAO-3	NBRC3255 Δ*dhaK* Δ*derK*	This study
KAO-4	NBRC3255 Δ*glpK*	This study
KAO-5	NBRC3255 Δ*dhaK* Δ*glpK*	This study
KAO-6	NBRC3255 Δ*derK* Δ*glpK*	This study
KAO-7	NBRC3255 Δ*dhaK* Δ*derK* Δ*glpK*	This study
Plasmid		
pRK2013	Plasmid for conjugal plasmid transfer, Km^R	(Figurski and Helinski, 1979)
pT7Blue	Cloning vector, T7 promoter, Ap^R	Novagen
pK18mobGII	Suicide vector, *mob gusA*, Km^R	(Katzen et al., 1999)
pKOS6b	Suicide vector, *mob codBA*, Km^R	(Kostner et al., 2013)
pBBR1MCS-4	Broad-host-range plasmid, *mob*, *lacZ* promoter, Ap^R	(Kovach et al., 1995)
pEK12	pK18mobGII, a 1.6-kb fragment of the Δ*dhaK* allele	This study
pEK15	pK18mobGII, a 1.3-kb fragment of the Δ*derK* allele	This study
pKH4	pKOS6b, a 1.3-kb fragment of the Δ*derK* allele	This study
pKH7	pT7Blue, a 2.7-kb fragment of *glpK*	This study
pKH10	pKOS6b, a 1.4-kb fragment of the Δ*glpK* allele	This study
pKH18	pBBR1MCS-4, a 2.7-kb fragment of *glpK*	This study
pKH24	pBBR1MCS-4, a 2.1-kb fragment of *derK*	This study
pEK20	pBBR1MCS-4, a 1.8-kb fragment of *dhaK*	This study
Gluconobacter oxydans 621H	wild type	ATCC
Plasmid		
pKH14	pSHO8, 1.7-kb fragment of the $glpK^{621H}$	This study
pKH15	pBBR1MCS-4, 1.7-kb fragment of the $glpK^{621H}$	This study

dhaK, *NBRC3255_2003*; *derK*, *NBRC3255_3084*; *glpK*, *NBRC3255_0651*

Table 4.2. Enzyme activity in the soluble fraction of *G. thailandicus* NBRC 3255 and its derivatives.[a]

Bacterial strain	Enzyme	Activity (mU mg^{-1})
Wild type	DHA reductase (NADH)	20 ± 3
	DHA reductase (NADPH)	<1
	DHA kinase	450 ± 60
	Glycerol kinase	64 ± 3
Δ*glpK*	DHA kinase	30 ± 7
	Glycerol kinase	n.d.[b]
Δ*dhaK* Δ*derK*	DHA kinase	590 ± 10
Δ*dhaK* Δ*glpK*	DHA kinase	56 ± 6
Δ*derK* Δ*glpK*	DHA kinase	n. d.[b]
Δ*dhaK* Δ*derK* Δ*glpK*	DHA kinase	n. d.[b]

[a] The cells were cultivated in YPGD medium until the late exponential growth phase. The soluble fraction was prepared by cell disruption on a French press followed by ultracentrifugation for removal of cell membranes.

[b] n.d., not detected, less than a detection limit of 0.5 mU mg^{-1}.

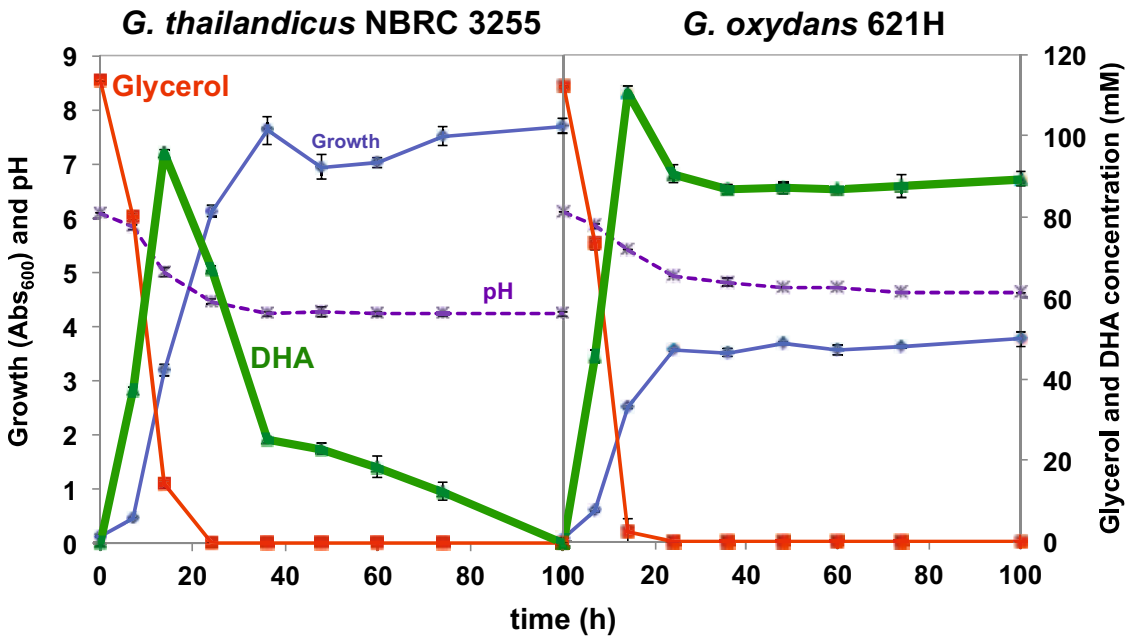

Figure 4.1. The DHA utilization ability of NBRC 3255 is higher than 621H.

NBRC 3255 and 621H were precultured on 2 ml of P′ medium at 30ºC for a day, and then transferred to 100 ml of 0.5% YPG medium (1% glycerol). OD_{600}, pH, glycerol and DHA concentrations were measured three times per day. NBRC 3255 and 621H converted glycerol to DHA, and DHA is accumulated in medium. NBRC3255 utilized DHA accumulated in the medium, but 621H did little DHA.

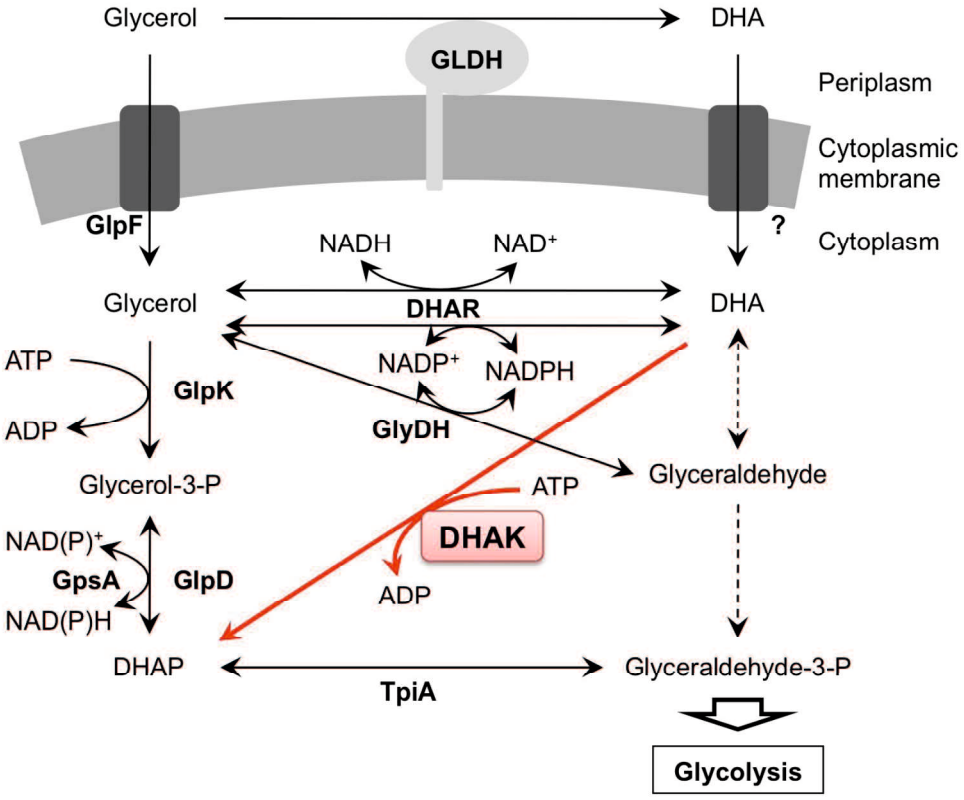

Figure 4.2. Potential metabolic pathway for glycerol and DHA in *Gluconobacter thailandicus* NBRC 3255.

The metabolic pathways for glycerol and DHA were constructed from Adachi et al. (2008) and from the genome information of *G. oxydans* ATCC621H and *G. thailandicus* NBRC3255. Dashed arrows indicate the pathways where the responsible enzymes are missing in the genome data. The gene products corresponding to the enzymes shown here are as follows. Glycerol uptake facilitator (GlpF), NBRC3255_0655; PQQ-dependent glycerol dehydrogenase (GLDH), NBRC3255_0026-27 or NBRC3255_0238-39; NADH-dependent DHA reductase (NADH-DHAR), NBRC3255_0712; NADPH-dependent DHA reductase (NADPH-DHAR), NBRC3255_1149; glycerol kinase (GlpK), NBRC3255_0654; $NAD(P)^+$-dependent glycerol-3-phosphate dehydrogenase (GpsA), NBRC3255_0877; acceptor-dependent glycerol-3-phosphate dehydrogenase (GlpD), NBRC3255_0656; $NADP^+$-dependent glycerol dehydrogenase (GlyDH), NBRC3255_1138; DHA kinase (DHAK), NBRC3255_2012 and NBRC3255_3096, Triosephosphate isomerase (Tpi), NBRC3255_0730, NBRC3255_0831, NBRC3255_0667, or NBRC3255_3012.

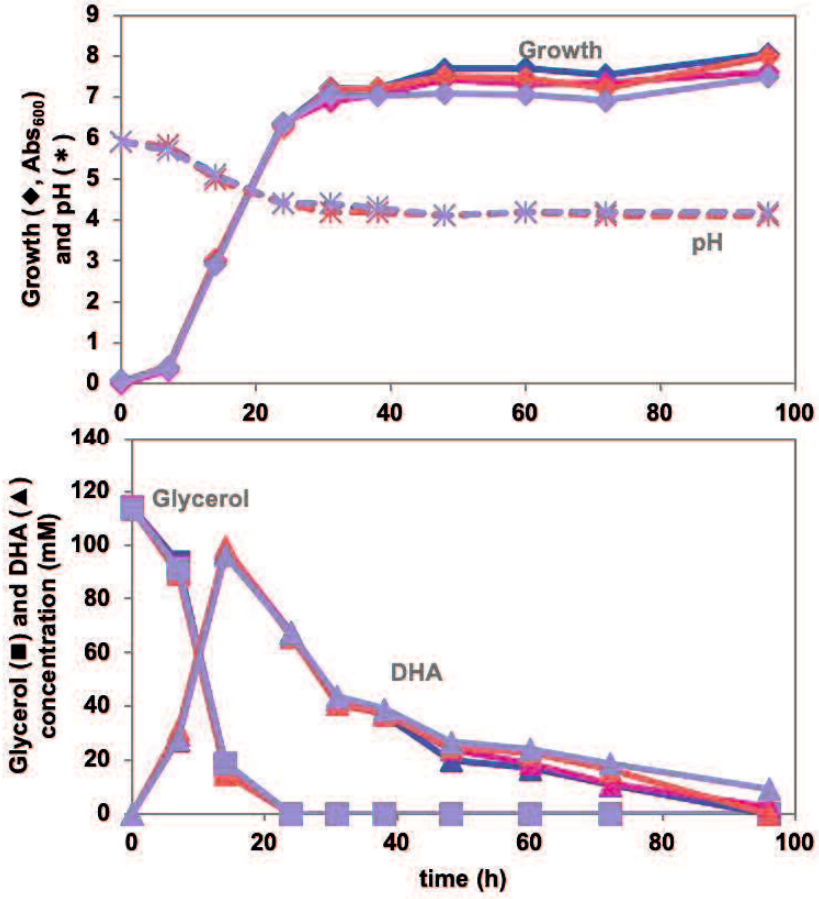

Figure 4.3. Growth and pH in medium and glycerol and DHA concentration in medium of wild type NBRC 3255 and the deletion mutants on 1% glycerol medium.

DHA kinase activity in the soluble fraction were measured at pH 6.5 and 25ºC**.** NBRC 3255, blue; Δ*dhaK*, salmon pink; Δ*derK*, pink; Δ*dhaK* Δ*derK*, purple.

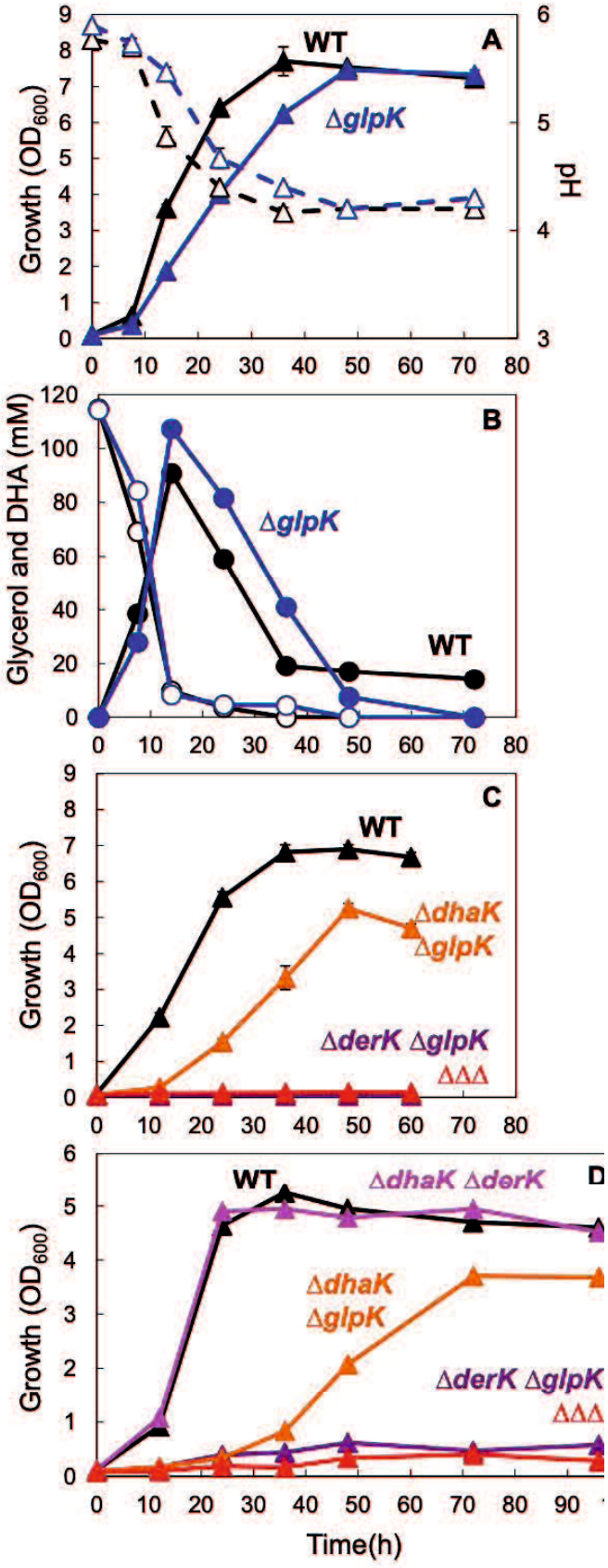

Figure 4.4. Growth, pH, and metabolite profile of the wild-type and deletion mutant strains on glycerol and DHA. Each strain was pre-cultivated on ΔP medium overnight. The pre-culture was inoculated into YPG (panels A, B, and C) and YPDHA (panel D) at a 1% ratio. The OD_{600} (solid lines in panels A, C, and D) and pH (dashed lines in panel A) values, and glycerol (open symbols in panel B) and DHA (closed symbols in panel B) concentrations in the medium were measured. The mean values and standard deviations were calculated from the triplicate cultivations in panels A, B, and C. Wild type, black; Δ*glpK*, blue; Δ*dhaK* Δ*glpK*, orange; Δ*derK* Δ*glpK*, purple; Δ*dhaK* Δ*derK*, magenta; Δ*dhaK* Δ*derK* Δ*glpK*, red.

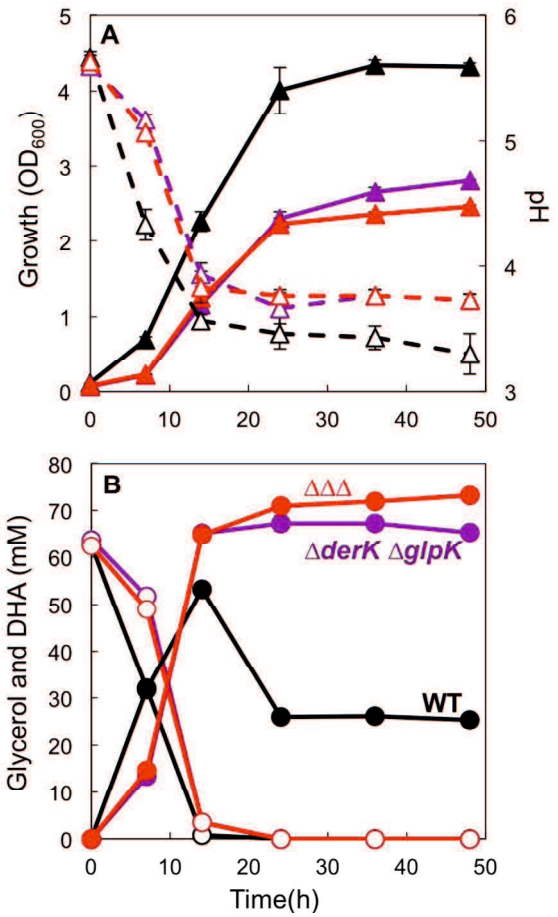

Figure 4.5. Growth, pH, and metabolite profile of the wild-type and multiple gene deletion strains on YPGD medium.

The wild-type, Δ*derK* Δ*glpK*, and Δ*dhaK* Δ*derK* Δ*glpK* cells were pre-cultivated overnight on ΔP medium. Then, 1 mL of preculture was inoculated into 100-mL YPGD medium. The OD_{600} (solid lines in panel A) and pH values (dashed lines in panel A) and glycerol (open symbols in panel B) and DHA (closed symbols in panel B) concentrations in the medium were measured. The mean values and standard deviations were calculated from triplicate cultivations. Wild type (WT), black; Δ*derK* Δ*glpK*, purple; Δ*dhaK* Δ*derK* Δ*glpK* (ΔΔΔ), red.

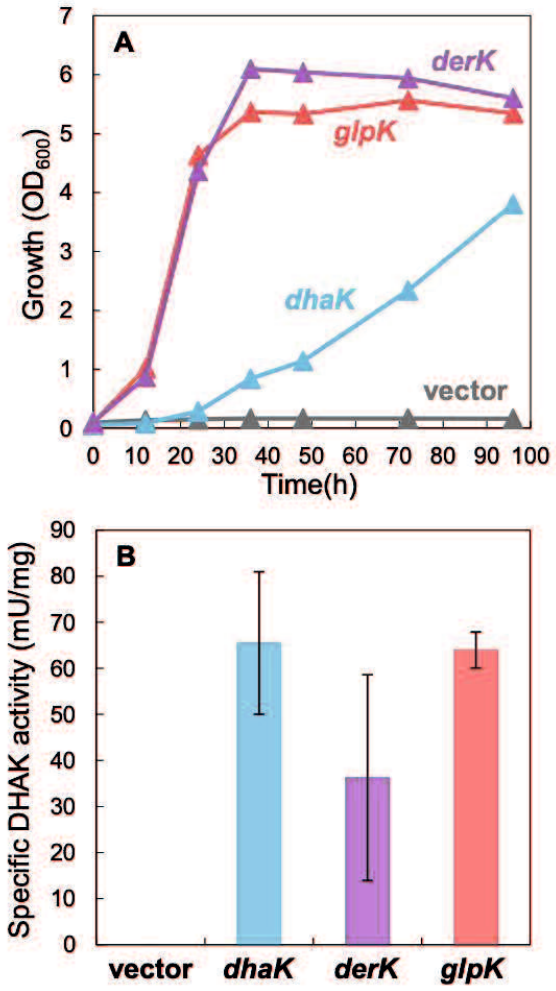

Figure 4.6. The triple deletion mutant strain harboring the plasmid carrying *dhaK*, *derK*, or *glpK*.
(A) Growth of the recombinant strains on the YPG medium. Each strain was pre-cultivated on ΔP medium overnight. The preculture was inoculated in YPG medium at a 1% (v/v) ratio. (B) DHA kinase activity in the soluble fraction of each strain was measured at pH 7.0. Mean values and standard deviations were calculated from triplicate enzyme assays. ΔΔΔ/pBBR1MCS-4 (vector), gray; ΔΔΔ/pEK20 (*dhaK*), sky blue; ΔΔΔ/pKH24 (*derK*), lilac; ΔΔΔ/pKH18 (*glpK*), salmon pink.

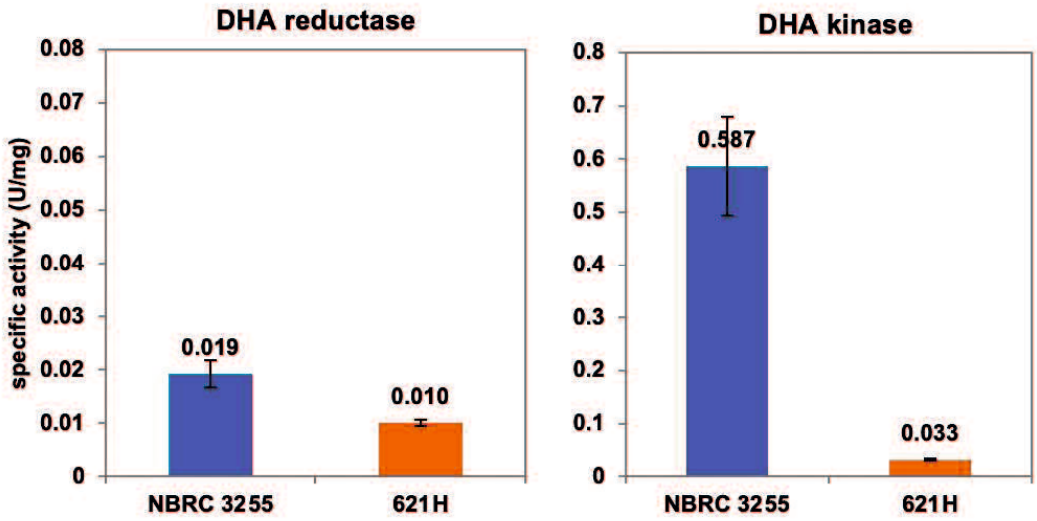

Figure 4.7. NADH-dependent DHA reductase and DHA kinase activities in the NBRC 3255 and 621H cells.

NADH-dependent DHA reductase and DHA kinase activities in the soluble fraction were measured at pH 7.5 and 7.0, respectively, and 25ºC.

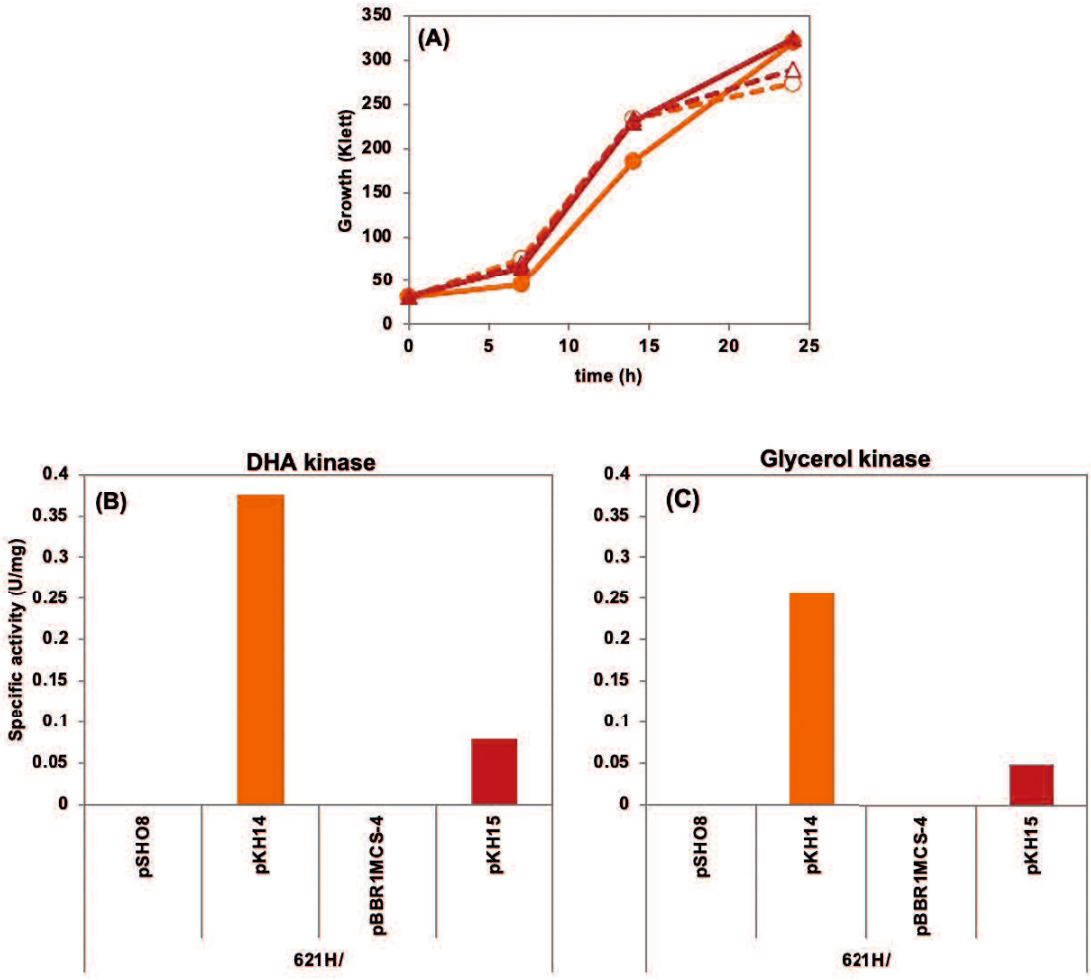

Figure 4.8. (a) Growth, (b) DHA kinase activity and (c) glycerol kinase activity of *glpK*^{621H} overexpressing strain.

○, 621H/pSHO8; ●, 621H/pKH14; △, 621H/pBBR1MCS4; ▲, 621H/pKH15.

REFERENCES

1. Adachi O., Ano Y., Shinagawa E., Matsushita K. (2008). Purification and properties of two different dihydroxyacetone reductases in *Gluconobacter suboxydans* grown on glycerol. Biosci Biotechnol Biochem. 72(8):2124-32.
2. Adachi O., Fujii Y., Ghaly MF., et al., (2001). Membrane-bound quinoprotein D-arabitol dehydrogenase of *Gluconobacter suboxydans* IFO 3257: a versatile enzyme for the oxidative fermentation of various ketoses. Biosci Biotechnol Biochem. 2001;65:2755-2762.
3. Adachi O, Toyama H, Matsushita K. (1999). Crystalline NADP-dependent D-mannitol dehydrogenase from *Gluconobacter suboxydans*. Biosci Biotechnol Biochem 63:402-407.
4. Adachi O, Ano Y, Toyama H, Matsushita K. (2006)a. Enzymatic preparation of metabolic intermediates, 3-dehydroquinate and 3-dehydroshikimate, in the shikimate pathway. Biosci Biotechnol Biochem 70:3081-3. Epub 2006 Dec 7.
5. Adachi O, Ano Y, Toyama H, Matsushita K. (2006)b. Purification and properties of NADP-dependent shikimate dehydrogenase from *Gluconobacter oxydans* IFO 3244 and its application to enzymatic shikimate production. Biosci Biotechnol Biochem 70:2786-9.
6. Ameyama M, Matsushita K, Shinagawa E, Adachi O. (1981)a. 5-Keto-D-fructose reductase of *Gluconobacter industrius*: Purification, crystallization and properties. Agric Biol Chem 45:863-869.
7. Ameyama M, Shinagawa E, Matsushita K, Adachi O. (1981)b. D-Fructose dehydrogenase of *Gluconobacter industrius*: purification, characterization, and application to enzymatic microdetermination of D-fructose. J Bacteriol 145:814-23.
8. Aida K, Yamada Y. (1964). A new enzyme, 5-ketofructose reductase. Agric Biol Chem 28:74-75.
9. Avigad G, Englard S, Pifko S. (1966). 5-Keto-D-fructose. IV. A specific reduced nicotinamide adenine dinucleotide phosphate-linked reductase from Gluconobacter cerinus. J Biol Chem 241:373-8.
10. Altschul SF, Madden TL, Schaffer AA, Zhang J, Zhang Z, Miller W, Lipman DJ. 1997. Gapped BLAST and PSI-BLAST: a new generation of protein database search programs. Nucleic Acids Res 25:3389-402.
11. Armstrong JM. The molar extinction coefficient of 2,6-dichlorophenol indophenol. Biochim Biophys Acta. 1964;86:194-197.
12. Ano Y, Hours RA, Akakabe Y, et al. Membrane-bound glycerol dehydrogenase catalyzes oxidation of D-pentonates to 4-keto-D-pentonates, D-fructose to 5-keto-D-fructose, and D-psicose to 5-keto-D-psicose. Biosci Biotechnol Biochem. (2017) ;81:411-418.
13. Barbe JC, De Revel G, Joyeux A, Bertrand A, Lonvaud-Funel A. 2001. Role of botrytized grape micro-organisms in SO_2 binding phenomena. J Appl Microbiol 90:34-42.
14. Bagautdinov B, Kunishima N. (2007). Crystal structures of shikimate dehydrogenase AroE from Thermus thermophilus HB8 and its cofactor and substrate complexes: insights into the enzymatic mechanism. J Mol Biol 373:424-38.
15. Battling S, Wohlers K, Igwe C, et al. Novel plasmid-free *Gluconobacter oxydans* strains for pro- duction of the natural sweetener 5-ketofructose. Microb Cell Factor. 2020;19:article number 54. .
16. Blanchard JS, Brewer CF, Englard S, Avigad G. (1982). Solution structure of 5-keto-D-fructose: relevance to the specificity of hexose kinases. Biochemistry 21:75-81.
17. Blasi M, Barbe JC, Dubourdieu D, et al. New method for reducing the binding power of sweet white wines. J Agr Food Chem. 2008;56:8470–8474.
18. Boyer, H.W., Roulland-Dussoix, D. (1969) A complementation analysis of the restriction and modification of DNA in *Escherichia coli. J Mol Biol.* 41, 459-472.
19. Benach J, Lee I, Edstrom W, Kuzin AP, Chiang Y, Acton TB, Montelione GT, Hunt JF. (2003). The 2.3-A crystal structure of the shikimate 5-dehydrogenase orthologue YdiB from *Escherichia coli* suggests a novel catalytic environment for an NAD-dependent dehydrogenase. J Biol Chem 278:19176-82.
20. Charoenyingcharoen, P., Matsutani, M., Yakushi, T., Theeragool, G., Yukphan, P., Matsushita, K. (2015) A functionally critical single nucleotide polymorphism in the gene encoding the membrane-bound alcohol dehydrogenase found in ethanol oxidation-deficient *Gluconobacter thailandicus*. Gene 567, 201-207
21. Crooks GE, Hon G, Chandonia JM, Brenner SE. 2004. WebLogo: a sequence logo generator. Genome Res 14:1188-90.

22. Chen R, Liu X, Lin J, Wei D. 2014. A genomic search approach to identify carbonyl reductases in *Gluconobacter oxydans* for enantioselective reduction of ketones. Biosci Biotechnol Biochem 78:1350-6.
23. Dulley JR, Grieve PA. A simple technique for eliminating interference by detergents in the Lowry method of protein determination. Anal Biochem. 1975;64:136-141.
24. Deutscher, J., Sauerwald, H. (1986) Stimulation of dihydroxyacetone and glycerol kinase activity in *Streptococcus faecalis* by phosphoenolpyruvate-dependent phosphorylation catalyzed by enzyme I and HPr of the phosphotransferase system. J Bacteriol 166, 829-836
25. Emsley P, Lohkamp B, Scott WG, Cowtan K. 2010. Features and development of Coot. Acta Crystallogr D Biol Crystallogr 66:486-501.
26. Evans PR. 2011. An introduction to data reduction: space-group determination, scaling and intensity statistics. Acta Crystallogr D Biol Crystallogr 67:282-92.
27. Edgar RC. 2004. MUSCLE: multiple sequence alignment with high accuracy and high throughput. Nucleic Acids Res 32:1792-7.
28. Edgar RC. 2004. MUSCLE: a multiple sequence alignment method with reduced time and space complexity. BMC Bioinformatics 5:113.
29. Figurski, D.H., Helinski, D.R. (1979) Replication of an origin-containing derivative of plasmid RK2 dependent on a plasmid function provided in trans. Proc Natl Acad Sci U S A. 76, 1648-1652.
30. Gan J, Wu Y, Prabakaran P, Gu Y, Li Y, Andrykovitch M, Liu H, Gong Y, Yan H, Ji X. 2007. Structural and biochemical analyses of shikimate dehydrogenase AroE from *Aquifex aeolicus*: implications for the catalytic mechanism. Biochemistry 46:9513-22.
31. Ghosh M, Anthony C, Harlos K, et al. The refined structure of the quinoprotein methanol dehydrogenase from *Methylobacterium extorquens* at 1.94 A. Structure. 1995;3:177-187.
32. Gupta A, Singh VK, Qazi GN, et al. *Gluconobacter oxydans*: its biotechnological applications. J Mol Microbiol Biotechnol. 2001;3:445-456.
33. Hattori, H., Yakushi, T., Matsutani, M. *et al.* High-temperature sorbose fermentation with thermotolerant *Gluconobacter frateurii* CHM43 and its mutant strain adapted to higher temperature. Appl Microbiol Biotechnol 95**,** 1531–1540 (2012).
34. Hanahan D. Studies on transformation of *Escherichia coli* with plasmids. J Mol Biol. 1983;166:557-580.
35. Hann RM, Tilden EB, Hudson CS. The oxidation of sugar alcohols by *Acetobacter suboxydans*. J Am Chem Soc. 1938;60:1201-1203.
36. Herweg E, Schöpping M, Rohr K, et al. Production of the potential sweetener 5-ketofructose from fructose in fed-batch cultivation with *Gluconobacter oxydans*. Bioresour Technol. 2018;259:164–172.
37. Höppner A, Schomburg D, Niefind K. 2013. Enzyme-substrate complexes of the quinate/shikimate dehydrogenase from Corynebacterium glutamicum enable new insights in substrate and cofactor binding, specificity, and discrimination. Biol Chem 394:1505-16.
38. Hoffmann JJ, Hövels M,Kosciow K, et al. Synthesis of the alternative sweetener 5-ketofructose from sucrose by fructose dehydrogenase and invertase producing *Gluconobacter* strains. J Biotechnol. 2020;307: 164–174.
39. Kawai S, Goda-Tsutsumi M, Yakushi T, Kano K, Matsushita K. 2013. Heterologous overexpression and characterization of a flavoprotein-cytochrome c complex fructose dehydrogenase of *Gluconobacter japonicus* NBRC3260. Appl Environ Microbiol 79:1654-60.
40. Krissinel E, Henrick K. 2007. Inference of macromolecular assemblies from crystalline state. J Mol Biol 372:774-97.
41. Krissinel E, Henrick K. 2004. Secondary-structure matching (SSM), a new tool for fast protein structure alignment in three dimensions. Acta Crystallogr D Biol Crystallogr 60:2256-68.
42. Kubota T, Tanaka Y, Hiraga K, Inui M, Yukawa H. 2013. Characterization of shikimate dehydrogenase homologues of *Corynebacterium glutamicum.* Appl Microbiol Biotechnol 97:8139-49.
43. Kovach ME, Elzer PH, Hill DS, Robertson GT, Farris MA, Roop RM, 2nd, Peterson KM. 1995. Four new derivatives of the broad-host-range cloning vector pBBR1MCS, carrying different antibiotic-resistance cassettes. Gene 166:175-6.
44. Kostner D, Peters B, Mientus M, Liebl W, Ehrenreich A. 2013. Importance of codB for new codA-based markerless gene deletion in *Gluconobacter* strains. Appl Microbiol Biotechnol 97:8341-9.

45. Kabsch W. 2010. XDS. Acta Crystallogr D Biol Crystallogr 66:125-32.
Evans P. 2006. Scaling and assessment of data quality. Acta Crystallogr D Biol Crystallogr 62:72-82.
46. Kulhánek M. Microbial Dehydrogenations of Monosaccharides. In: Neidleman SL, editor. Adv Appl Microbiol. Vol. 34: Academic Press; 1989. p. 141-182.
47. Krajewski V, Simic P, Mouncey NJ, Bringer S, Sahm H, Bott M. 2010. Metabolic engineering of *Gluconobacter oxydans* for improved growth rate and growth yield on glucose by elimination of gluconate formation. Appl Environ Microbiol 76:4369-76.
48. Lin X, Liu S, Xie G, Chen J, Li P, Chen J. Enhancement of 1,3-Dihydroxyacetone Production from *Gluconobacter oxydans* by Combined Mutagenesis. J. Microbiol. Biotechnol. 2016;26:1908-1917.
49. Liu DF, Ai GM, Zheng QX, Liu C, Jiang CY, Liu LX, Zhang B, Liu YM, Yang C, Liu SJ. 2014. Metabolic flux responses to genetic modification for shikimic acid production by Bacillus subtilis strains. Microb Cell Fact 13:40.
50. Lindner HA, Nadeau G, Matte A, Michel G, Menard R, Cygler M. 2005. Site-directed mutagenesis of the active site region in the quinate/shikimate 5-dehydrogenase YdiB of *Escherichia coli*. J Biol Chem 280:7162-9.
51. Moonmangmee D, Adachi O, Ano Y, Shinagawa E, Toyama H, Theeragool G, Lotong N, Matsushita K. 2000. Isolation and characterization of thermotolerant *Gluconobacter* strains catalyzing oxidative fermentation at higher temperatures. Biosci Biotechnol Biochem 64:2306-15.
52. Moonmangmee D, Adachi O, Ano Y, et al. Isolation and characterization of thermotolerant *Gluconobacter* strains catalyzing oxidative fermentation at higher temperatures. Biosci Biotechnol Biochem. 2000;64:2306-2315.
53. Moonmangmee D, Fujii Y, Toyama H, et al. Purification and characterization of membrane-bound quinoprotein cyclic alcohol dehydrogenase from *Gluconobacter frateurii* CHM 9. Biosci Biotechnol Biochem. 2001;65:2763-2772.
54. Matsushita K, Fujii Y, Ano Y, Toyama H, Shinjoh M, Tomiyama N, Miyazaki T, Sugisawa T, Hoshino T, Adachi O. 2003. 5-keto-D-gluconate production is catalyzed by a quinoprotein glycerol dehydrogenase, major polyol dehydrogenase, in *Gluconobacter* species. Appl Environ Microbiol 69:1959-66.
55. Matsushita K, Fujii Y, Ano Y, et al. 5-keto-D-gluconate production is catalyzed by a quinoprotein glycerol dehydrogenase, major polyol dehydrogenase, in *Gluconobacter* species. Appl Environ Microbiol. 2003;69:1959-1966.
56. Matsushita K, Toyama H, Adachi O. 1994. Respiratory chains and bioenergetics of acetic acid bacteria, p 247-301. In Rose AH, Tempest DW (ed), Adv Microb Physiol, vol 36. Academic Press, London.
57. Matsushita K, Toyama H, Tonouchi N, Okamoto-Kainuma A. 2016. Acetic acid bacteria. Springer Tokyo publisher.
58. Matsushita, K., Nagatani, Y., Shinagawa, E., Adachi, O., Ameyama, M. (1991) Reconstitution of the ethanol oxidase respiratory chain in membranes of quinoprotein alcohol dehydrogenase-deficient *Gluconobacter suboxydans* subsp. alpha strains. *J Bacteriol* 173, 3440-3445
59. Matsumoto N, Hattori H, Matsutani M, Matayoshi C, Toyama H, Kataoka N, Yakushi T, Matsushita K. 2018. A single-nucleotide insertion in a drug transporter gene induces a thermotolerance phenotype in *Gluconobacter frateurii* by increasing the NADPH/$NADP^+$ ratio via metabolic change. Appl Environ Microbiol 84:e00354-18.
60. Matsutani M, Yakushi T. Pyrroloquinoline quinone-dependent dehydrogenases of acetic acid bacteria. Appl Microbiol Biotechnol. 2018;102:9531-9540.
61. Matsutani M, Kawajiri E, Yakushi T, Adachi O, Matsushita K. (2013) Draft Genome Sequence of Dihydroxyacetone-Producing *Gluconobacter thailandicus* Strain NBRC 3255. Genome Announcement 1:e0011813.
62. Marmur J. A procedure for the isolation of deoxyribonucleic acid from micro-organisms. J Mol Biol. 1961;3:208-218.
63. Marx CJ, Lidstrom ME. Development of improved versatile broad-host-range vectors for use in methylotrophs and other Gram-negative bacteria. Microbiology. 2001;147:2065-2075.
64. Mientus M, Kostner D, Peters B, et al. Characterization of membrane-bound dehydrogenases of *Gluconobacter oxydans* 621H using a new system for their functional expression. Appl Microbiol Biotechnol. 2017;101:3189-3200.
65. Miyazaki T, Tomiyama N, Shinjoh M, et al. Molecular cloning and functional expression of D-sorbitol dehydrogenase from *Gluconobacter suboxydans* IFO3255, which requires

pyrroloquinoline quinone and hydrophobic protein SldB for activity development in *E. coli*. Biosci Biotechnol Biochem. 2002;66:262-270.
66. McNicholas S, Potterton E, Wilson KS, Noble ME. 2011. Presenting your structures: the CCP4mg molecular-graphics software. Acta Crystallogr D Biol Crystallogr 67:386-94.
67. Murshudov GN, Skubák P, Lebedev AA, Pannu NS, Steiner RA, Nicholls RA, Winn MD, Long F, Vagin AA. 2011. REFMAC5 for the refinement of macromolecular crystal structures. Acta Crystallogr D Biol Crystallogr 67:355-67.
68. Marx CJ, Lidstrom ME. 2001. Development of improved versatile broad-host-range vectors for use in methylotrophs and other Gram-negative bacteria. Microbiology 147:2065-2075.
69. Marmur J. 1961. A procedure for the isolation of deoxyribonucleic acid from micro-organisms. J Mol Biol 3:208-218.
70. Michel G, Roszak AW, Sauvé V, Maclean J, Matte A, Coggins JR, Cygler M, Lapthorn AJ. 2003. Structures of shikimate dehydrogenase AroE and its Paralog YdiB. A common structural framework for different activities. J Biol Chem 278:19463-72.
71. Mowshowitz S, Avigad G, Englard S. 5-Keto- 155 D-fructose: formation and utilization in the course of D-fructose assimilation by *Gluconobacter cerinus*. J Biol Chem. 1974;118:1051–1058.
72. Prust C, Hoffmeister M, Liesegang H, Wiezer A, Fricke WF, Ehrenreich A, Gottschalk G, Deppenmeier U. 2005. Complete genome sequence of the acetic acid bacterium *Gluconobacter oxydans*. Nat Biotechnol 23:195-200. Epub 2005 Jan 23.
73. Peek J, Lee J, Hu S, Senisterra G, Christendat D. 2011. Structural and mechanistic analysis of a novel class of shikimate dehydrogenases: evidence for a conserved catalytic mechanism in the shikimate dehydrogenase family. Biochemistry 50:8616-27.
74. Peek J, Garcia C, Lee J, Christendat D. 2013. Insights into the function of RifI2: structural and biochemical investigation of a new shikimate dehydrogenase family protein. Biochim Biophys Acta 1834:516-23.
75. Padyana AK, Burley SK. 2003. Crystal structure of shikimate 5-dehydrogenase (SDH) bound to NADP: insights into function and evolution. Structure 11:1005-13.
76. Pappenberger G, Hohmann H-P. Industrial Production of L-Ascorbic Acid (Vitamin C) and D-Isoascorbic Acid. In: Zorn H, Czermak P, editors. Biotechnology of Food and Feed Additives. Advances in Biochemical Engineering/Biotechnology. Vol. 143: Springer Berlin Heidelberg; 2014. p. 143-188.
77. Peters B, Mientus M, Kostner D, et al. Expression of membrane-bound dehydrogenases from a mother of vinegar metagenome in *Gluconobacter oxydans*. Appl Microbiol Biotechnol. 2017;101:7901-7912.
78. Peters B, Mientus M, Kostner D, et al. Characterization of membrane-bound dehydrogenases from *Gluconobacter oxydans* 621H via whole-cell activity assays using multideletion strains. Appl Microbiol Biotechnol. 2013;97:6397-6412.
79. Peek J, Christendat D. 2015. The shikimate dehydrogenase family: functional diversity within a conserved structural and mechanistic framework. Arch Biochem Biophys 566:85-99.
80. Regula G., Rudolf B., Luis F. G., Ulrich B., Bernhard E. (2001). The dihydroxyacetone kinase of *Escheria coli* utilizes a phosphoprotein instead of ATP as phosphoryl donor. European molecular biology. 20, 10, 2480-2486.
81. Richhardt J, Bringer S, Bott M. 2012. Mutational analysis of the pentose phosphate and Entner-Doudoroff pathways in *Gluconobacter oxydans* reveals improved growth of a Δedd Δeda mutant on mannitol. Appl Environ Microbiol 78:6975-86.
82. Richhardt J, Luchterhand B, Bringer S, Büchs J, Bott M. 2013. Evidence for a key role of cytochrome bo3 oxidase in respiratory energy metabolism of *Gluconobacter oxydans*. J Bacteriol 195:4210-20.
83. Rosaria C., Alexandra F., Laura M. I., Mario P. (2018). Dihydroxyacetone: an update insight into an important bioproduct. ChemistryOpen. 7, 233-236.
84. Singh S, Stavrinides J, Christendat D, Guttman DS. 2008. A phylogenomic analysis of the shikimate dehydrogenases reveals broadscale functional diversification and identifies one functionally distinct subclass. Mol Biol Evol 25:2221-32.
85. Singh S, Korolev S, Koroleva O, Zarembinski T, Collart F, Joachimiak A, Christendat D. 2005. Crystal structure of a novel shikimate dehydrogenase from *Haemophilus influenzae*. J Biol Chem 280:17101-8.
86. Schoepe J, Niefind K, Schomburg D. 2008. 1.6 angstroms structure of an NAD -dependent quinate dehydrogenase from *Corynebacterium glutamicum*. Acta Crystallogr D Biol Crystallogr D64:803-9.

87. Siemen A, Kosciow K, Schweiger P, Deppenmeier U. 2018. Production of 5-ketofructose from fructose or sucrose using genetically modified *Gluconobacter oxydans* strains. Appl Microbiol Biotechnol 102:1699-1710.
88. Siebold, C., Arnold, I., Garcia-Alles, L.F., Baumann, U., Erni, B. (2003) Crystal structure of the *Citrobacter freundii* dihydroxyacetone kinase reveals an eight-stranded alpha-helical barrel ATP-binding domain. J Biol Chem 278, 48236-48244
89. Studier FW, Moffatt BA. 1986. Use of bacteriophage T7 RNA polymerase to direct selective high-level expression of cloned genes. J Mol Biol 189:113-30.
90. Studier FW. 1991. Use of bacteriophage T7 lysozyme to improve an inducible T7 expression system. J Mol Biol 219:37-44.
91. Schüttelkopf AW, van Aalten DM. 2004. PRODRG: a tool for high-throughput crystallography of protein-ligand complexes. Acta Crystallogr D Biol Crystallogr 60:1355-63.
92. Stecher G, Tamura K, Kumar S. 2020. Molecular Evolutionary Genetics Analysis (MEGA) for macOS. Mol Biol Evol 37:1237-1239.
93. Stark MJ. 1987. Multicopy expression vectors carrying the lac repressor gene for regulated high-level expression of genes in *Escherichia coli*. Gene 51:255-67.
94. Schweiger P, Gross H, Deppenmeier U. 2010. Characterization of two aldo-keto reductases from *Gluconobacter oxydans* 621H capable of regio- and stereoselective alpha-ketocarbonyl reduction. Appl Microbiol Biotechnol 87:1415-26.
95. Soemphol W, Saichana N, Yakushi T, et al. Characterization of genes involved in D-sorbitol oxidation in thermotolerant *Gluconobacter frateurii*. Biosci Biotechnol Biochem. 2012;76:1497-1505.
96. Terada O, Suzuki S, Kinoshita S. 1961. Formation of 5-dehydrofructose by members of Acetobacter. Part III. Characterization of the unknown substance. . J Agric Chem Soc Jpn 35:178-182.
97. Tamura K, Dudley J, Nei M, Kumar S. 2007. MEGA4: Molecular Evolutionary Genetics Analysis (MEGA) software version 4.0. Mol Biol Evol 24:1596-9.
98. Xi L., Sha L., Guangrong X., Jing C., Penghua L., Jianhua C. (2016). Enhancement of 1,3-dihydroxyacetone production from *Gluconobacter oxydans* by combined mutagenesis. J. Microbiol. Biotechnol., 26(11), 1980-1917.
99. Yamada Y, Aida K, Uemura T. 1967. Enzymatic studies on the oxidation of sugar and sugar alcohol. II. Purification and properties of NADPH-linked 5-ketofructose reductase. J Biochem 61:803-11.
100. Yakushi T, Komatsu K, Matsutani M, et al. Improved heterologous expression of the membrane-bound quinoprotein quinate dehydrogenase from *Gluconobacter oxydans*. Protein Expr Purif. 2018a;145:100-107.
101. Yakushi T, Matsushita K. Alcohol dehydrogenase of acetic acid bacteria: structure, mode of action, and applications in biotechnology. Appl Microbiol Biotechnol. 2010;86:1257-1265.
102. Yakushi T, Terada Y, Ozaki S, Kataoka N, Akakabe Y, Adachi O, Matsutani M, Matsushita K. 2018. Aldopentoses as new substrates for the membrane-bound, pyrroloquinoline quinone-dependent glycerol (polyol) dehydrogenase of *Gluconobacter* sp. Appl Microbiol Biotechnol 102:3159-3171.
103. Yang X-P, Wei L-J, Lin J-P, et al. Membrane-bound pyrroloquinoline quinone-dependent dehydrogenase in *Gluconobacter oxydans* M5, responsible for production of 6-(2-hydroxyethyl) amino-6-deoxy-L-sorbose. Appl Environ Microbiol. 2008;74:5250.
104. Yorimitsu T, Mimaki A, Yakushi T, Homma M. 2003. The conserved charged residues of the C-terminal region of FliG, a rotor component of the Na -driven flagellar motor. J Mol Biol 334:567-83 Vagin A, Teplyakov A. 1997. MOLREP: an Automated Program for Molecular Replacement. J Appl Crystallogr 30:1022-1025.
105. Yu P L., Yang S, Cong T, Hua L, Xiao J Z, Kui Q J, Gang W. (2013). Efficient production of dihydroxyacetone from biodiesel-derived crude glycerol by newly isolated *Gluconobacter frateurii*, Bioresource Technology, 142, 384-389.
106. Wang X, Lv M, Zhang L, et al. Efficient bioconversion of 2,3-butanediol into acetoin using *Gluconobacter oxydans* DSM 2003. Biotechnol Biofuels. 2013;6:155.
107. Wyrobnik D, Wyrobnik I, Silcoff E. 2009. Agent for reducing the useable calorie content of food and for therapeutic reduction of weight, in particular for use in the case.
108. Winn MD, Ballard CC, Cowtan KD, Dodson EJ, Emsley P, Evans PR, Keegan RM, Krissinel EB, Leslie AGW, McCoy A, McNicholas SJ, Murshudov GN, Pannu NS, Potterton EA, Powell HR, Read RJ, Vagin A, Wilson KS. 2011. Overview of the CCP4 suite and current developments. Acta Crystallographica Section D 67:235-242.

109. Zahid N, Deppenmeier U. 2016. Role of mannitol dehydrogenases in osmoprotection of *Gluconobacter oxydans*. Appl Microbiol Biotechnol 100:9967-9978.

LIST OF PUBLICATIONS

Chapter 2

1. Osao Adachi, **Thuy M. Nguyen**, Roque A. Hours, Naoya Kataoka, Kazunobu Matsushita, Yoshihiko Akakabe and Toshiharu Yakushi, 2019, 5-Keto-D-fructose production from sugar alcohol by isolated wild strain *Gluconobacter frateurii* CHM 43
   Bioscience,Biotechnology,Biochemistry - Vol. 84, No. 8, 1745–1747

Chapter 3

1. **Thuy Minh Nguyen**, Kotone Naoki, Naoya Kataoka, Minenosuke Matsutani, Yoshitaka Ano, Osao Adachi, Kazunobu Matsushita, and Toshiharu Yakushi, 2021, Characterization of a cryptic, pyrroloquinoline quinone- dependent dehydrogenase of *Gluconobacter* sp. strain CHM43
   Bioscience,Biotechnology,Biochemistry – In press

Chapter 4

1. Naoya Kataoka, Kaori Hirata, Minenosuke Matsutani, Yoshitaka Ano, **Thuy Minh Nguyen**, Osao Adachi, Kazunobu Matsushita, and Toshiharu Yakushi, 2021, Three ATP-dependent phosphorylating enzymes in the first committed step of dihydroxyacetone metabolism in *Gluconobacter thailandicus* NBRC3255

   Applied Microbiology and Biotechnology – Vol. 105, 1227-1236